Aligned Fibrillar Collagen Matrices for Tissue Engineering

Dissertation

Zur Erlangung des Akademischen Grades

Doktor-Ingenieur

(Dr.-Ing.)

vorgelegt der
Fakultät Maschinenwesen
der Technischen Universität Dresden
von

Babette Lanfer (M.Sc.)
geboren am 10.5.1979 in Stuttgart

eingereicht am 2.12.2009
verteidigt am 21.4.2010

Gutachter:
Prof. Dr.rer.nat.habil. Thomas Bley, TU Dresden
Prof. Dr.rer.nat. Carsten Werner, TU Dresden

Contents

Danksagung iii

Nomenclature iv

Abstract v

1 Introduction 1

2 Fundamentals 3

2.1 The extracellular matrix - a biomolecular scaffold . . . 3

2.1.1 Collagens . . . 4

2.1.2 Proteoglycans . . . 6

2.2 Cell-matrix interactions . . . 7

2.2.1 Biochemical signals . . . 7

2.2.2 Mechanical signals . . . 8

2.2.3 Structural signals . . . 8

2.3 Approaches to engineer aligned extracellular matrix structures . . . 9

2.3.1 Topographically and chemically patterned surfaces . . . 10

2.3.2 Electrospun fibers . . . 10

2.3.3 Reconstitution of extracellular matrix . . . 11

2.3.4 Guidance conduits . . . 12

2.4 Cellular response to aligned structural cues . . . 13

2.4.1 Cellular response in general . . . 13

2.4.2 Mesenchymal stem and progenitor cells . . . 14

2.4.3 Neural stem and progenitor cells . . . 16

3 Objectives 19

4 General Discussion 20

4.1 Aligned collagen matrices obtained by shear flow deposition . . . 20

4.1.1 Alignment mechanism . . . 21

4.1.2 Functionalization with heparin . . . 23

4.2 Mesenchymal stem and progenitor cells cultured on aligned collagen matrices . . . 24

4.3 Human neural stem cells cultured on aligned collagen matrices . . . 25

4.4 Cellulose hollow fiber membranes coated with aligned collagen for spinal cord regeneration . . . 27

5 Summary and Outlook **28**

Bibliography **30**

Appendices **42**

Danksagung

Die vorliegende Dissertation wurde am Leibniz-Institut für Polymerforschung Dresden e.V. in der Arbeitsgruppe Biofunktionelle Polymermaterialien am Max Bergmann Zentrum für Biomaterialien angefertigt.

Herzlich bedanken möchte ich mich bei Herrn Prof. Dr. Thomas Bley für die Ermöglichung und Betreuung der Promotion und die konstruktiven Hinweise bei der Anfertigung dieser Arbeit.

Mein besonderer Dank gilt Herrn Prof. Dr. Carsten Werner für seine wissenschaftliche Unterstützung und Förderung, sein stetes Interesse am Fortgang der Arbeit, die motivierenden Gespräche und das freundschaftliche Arbeitsklima.

Für die anregenden Diskussionen, wertvollen Hinweise sowie hilfreichen Kritiken zum erfolgreichen Fortgang der Arbeit möchte ich mich herzlich bei Herrn Dr. Uwe Freudenberg bedanken.

Herrn Dr. Philipp Seib danke ich besonders für die sehr gute fachliche Betreuung bei der Durchführung der Zellversuche und die nützlichen Ratschläge zum Manuskript.

Für seinen großen Beitrag bei der Entwicklung des Versuchsaufbaus und seine stete Hilfsbereitschaft danke ich Herrn Dr. Ralf Zimmermann. Herrn Dr. Tilo Pompe danke ich für die fachlichen Anregungen und hilfreichen Kritiken zum erfolgreichen Fortgang der Arbeit.

Meinen Kollegen und Mitarbeitern des Forschungsbereich Biofunktionelle Polymermaterialien möchte ich ganz herzlich für die gute Zusammenarbeit und für ihren Beitrag zum Entstehen und Gelingen der vorliegenden Arbeit danken. Insbesondere bedanke ich mich bei Frau Milauscha Grimmer für die fachkundige Einweisung in die Präparation der Kollagengele und ihren Beitrag zur Entwicklung der orientierten Kollagenmatrices, bei Frau Yvonne Müller für ihren Beitrag bei der Beschichtung der Zellulosekapillaren und bei Herrn Martin Kaufmann und Herrn Lars Renner für die hilfreichen Tipps und Tricks bei der konfokalen Mikroskopie. Mein Dank gilt auch Frau Martina Franke und Frau Marina Prewitz für ihre Hilfe bei der Durchführung der Zellversuche, Herrn Dimitar Stamov für die Charakterisierung der Kollagenmatrices durch Rasterkraftmikroskopie und Frau Tina Lenk für die HPLC Untersuchungen.

Für die angenehme und freundschaftliche Atmosphäre in der Arbeitsgruppe danke ich David Sebinger, Marion Fischer, Marina Prewitz, Andreas Ofenbauer, Uwe Freudenberg, Martin Kaufmann, Dimitar Stamov und meinen ehemaligen Arbeitskollegen Lars Renner und Philipp Seib.

Abschließend möchte ich mich bei meiner Familie, bei meinen Freunden und ganz besonders bei meinem Freund Martin für ihre Unterstützung und Motivation während der Anfertigung dieser Arbeit bedanken.

Nomenclature

3D Three - Dimensional

CFUs Colony-Forming Unit-Fibroblasts

CNS Central Nervous System

ECM Extracellular Matrix

EGF Epidermal Growth Factor

FGF Fibroblast Growth Factor

GAGs Glycosaminoglycans

GFAP Glial Fibrillary Acid Protein

GlcA Glucuronic Acid

GlcNAc N-Acetylglucosamine

MSC Mesenchymal Stem Cell

NSCs Neural Stem Cells

PA Peptide-Amphiphile

PDMS Polydimethylsiloxane

PEMA Poly(ethylene alt maleic anhydride)

PLA Poly Lactic Acid

PLGA Poly (Lactic-Coglutamic) Acid

PLLA Poly(L-lactic acid)

PNS Peripheral Nervous System

POMA Poly(octadecene alt maleic anhydride)

PS Polystyrene

RGD Arginine-Glycine-Asparate

Abstract

The desire for repair of tissue defects and injury is the major need prompting research into tissue engineering. Engineering of anisotropic tissues requires production of ordered substrates that orient cells preferentially and support cell viability and differentiation. Towards this goal, this thesis investigated methodologies to align extracellular matrix structures *in vitro* to guide stem/progenitor cell behaviour for tissue regeneration. Aligned collagen fibrils were deposited on planar substrates from collagen solutions streaming through a microfluidic channel system. Collagen solution concentration, degree of gelation, shear rate and pre-coating of the substrate were demonstrated to determine the orientation and density of the immobilized fibrils. The degree of collagen fibril orientation increased with increasing flow rates of the solution while the matrix density increased at higher collagen solution concentrations and on hydrophobic polymer pre-coatings. Additionally, the length of the immobilized collagen fibrils increased with increasing solution concentration and gelation time. Aligned collagen matrices were refined by incorporating the glycosaminoglycan heparin to study multiple extracellular matrix components in a single system. Multilineage (osteogenic/adipogenic/chondrogenic) differentiation of mesenchymal stem and progenitor cells was maintained by the aligned structures. Most noticeable was the observation that during osteogenesis, aligned collagen substrates choreographed ordered matrix mineralization. Likewise, myotube assembly of C2C12 cells was profoundly influenced by aligned topographic features resulting in enhanced myotube organization and length. Neurites from neural stem cells were highly oriented in the direction of the underlying fibrils. Neurite outgrowth was enhanced on aligned collagen compared to non-aligned collagen or poly-D-lysine substrates, while neural differentiation and cell survival were not influenced by the type of substrate. Using the new method to align collagen type I, the interior walls of cellulose hollow fiber membranes were coated with longitudinally aligned collagen fibrils to fabricate an advanced guidance conduit for nerve regeneration. First cell culture experiments showed that the tubes coated with aligned collagen supported viability and adherence of spinal cord-derived neurospheres. Together, these results demonstrate the feasibility of aligned collagen matrices as a versatile platform to control cell behaviour towards tissue regeneration. Ultimately, the new method to align collagen fibrils and to coat hollow membranes may become an integral component of tissue engineering, working synergistically with other emerging techniques to promote functional tissue replacements.

1 Introduction

Tissue loss and organ failure resulting from traumatic or non-traumatic destruction give rise to morbidity and mortality and impose immense pressure on current health care budgets. On an annual basis, many millions of patients undergo surgery for tissue reconstruction in order to repair, replace, maintain or augment the functions of the affected tissues or organs [1]. To this end, a wide variety of tissues or organs have been traditionally harvested from a donor site and implanted into the patient. Current treatment modalities include tissue transfer from a healthy body site to the affected site in the same individual or tissue transplantation from one individual to another. Alternatively, replacement with mechanical devices such as artificial hip prostheses, heart valves or stents have significantly improved patient outcomes [2]. Although these strategies have made great progress in the field of medicine they have a number of limiting factors. The lack of donor tissue availability results in a discrepancy between the number of patients needing transplants and available organs. Every year, over 80.000 patients in U.S. are waiting for tissue and organ transplantation [2]. This striking gap between donor supply and demand is predicted to widen year by year and to further worsen in course of the ageing of the baby-boomer generation. The need for additional surgery to harvest the graft and the possibility of donor site morbidity are further drawbacks of organ or tissue transplantation. Tissue or organ replacement with mechanical devices is limited by an increased risk of infection and thromboembolism.

Therefore, great efforts have been made to develop strategies to overcome the limitations of traditional therapies and to increase the accessibility and long-term viability of tissue implants. As a potential solution the concept of tissue engineering has emerged. It is *"an interdisciplinary field that applies the principles of engineering and life sciences toward the development of biological substitutes that restore, maintain, or improve tissue function or a whole organ"* [3]. The tissue engineering approach involves the use of scaffolding material that serves as environment for the cultivation of cells that have been harvested from the patient or donor(s). Thus, engineered constructs can be introduced into the patient's body. There are a number of examples where tissue engineering strategies have been successfully applied in humans including engineered skin equivalents being in clinical use since 1997 [4]. A growing arsenal of tissue substitutes for cartilage, bone, blood vessel and pancreas are approved and in a recent seminal study, seven patients benefited from tissue engineered bladders [5].

The rationale behind artificial scaffold design comes from the natural template, the extracellular matrix (ECM). In native tissues, the extracellular matrix forms the cellular microenvironment that is crucial for cell fate decisions and tissue growth. Thus, a tissue engineering scaffold needs to take on this instructive role to some degree in order to choreograph cell behavior and tissue development. Towards this goal, both biologically derived and synthetic materials have been

extensively explored [4]. Synthetic materials offer the advantages of high reproducibility and control over material properties. However, problems may occur such as little control over cell behavior and tissue response *in vivo* [6]. Thus, latest research has spurred the development of synthetic materials equipped with molecular cues mimicking certain aspects of structure or function of natural extracellular microenvironment to overcome these limitations [7].

Despite these research efforts, biologically derived/ natural materials are frequently the material of choice due to their inherent biological recognition including the presentation of receptor-binding ligands and susceptibility to cell-triggered proteolytic degradation and remodeling. For example, following a top-down approach, many decellularized ECM products have found clinical use due to its inherent bioactivity sufficient to induce regeneration. Decellularized intestinal submucosa of pigs is routinely used as skin substitutes in reconstructive surgery (an example being Oasis Wound Matrix, Healthpoint [4]). Last year a 30-year old women benefited from the first tissue engineering tracheal segment and confirmed this approach as a further development towards whole organ-tissue engineering [8]. Here, the scaffold was a decellularized human donor trachea that was seeded with the patient's own cells after biopsy. The decellullarization protocol solved the problem of tissue rejection so that the patient required no immuno-suppressive drugs.

In addition to intact acellular tissues, a great deal of research has focused on the use of isolated, dissociated ECM components/biopolymers to be reconstituted and self-assembled *in vitro*, which can be modified to serve as appropriate scaffolding. In contrast to decellularized scaffolding material, this bottom-up alternative offers the advantage to study effects of single or multiple components on cell behavior in one system. Collagen specifically has received great attention in biomaterial research being the most abundant protein in mammals assembling into frequently anisotropic three-dimensional fibrillar arrays specific to each tissue. However, when collagen type I is reconstituted in vitro it looses its natural anisotropic three-dimensional architecture assembling into a randomly oriented fibrillar network. So far, there is a lack of studies that have set out to systematically investigate the alignment of collagen fibrils *in vitro*. A reconstituted aligned collagen scaffold that more closely mimics the *in vivo* situation and that allows multi-component binding of e.g. proteoglycans would provide the means for well-designed cell culture experiments leading to a detailed understanding of cell-matrix interactions. Thus, the aim of this study was to establish a robust technique to align native collagen type I and to examine the biological impact of such substrates on stem and progenitor cells. However, to understand the scope of this study there is the need to have background knowledge to construct aligned substrates which are described in the following chapter.

2 Fundamentals

The scaffold is one of the key factors for successful tissue engineering. *In vivo*, cells derive a vast wealth of information from their surrounding ECM, the material which surrounds and separates them within tissues. A tissue engineering scaffold must take on this instructive role to some degree in order to maintain cell viability and control cell behavior. Certainly, the characteristics of a scaffold vary according to the tissue types where the scaffold is to be applied. Nonetheless, clues for how to construct bioactive artificial scaffolds come from the naturally bioactive scaffolds. In the following section the role of native ECM as ideal scaffold and its components (with emphasis on those relevant for this study) will be described.

2.1 The extracellular matrix - a biomolecular scaffold

The ECM represents the secreted product of resident cells within each tissue and organ (Figure 2.1). It is an intricate network of structural and functional molecules, namely proteins, glycosaminoglycans (GAGs) , glycoproteins and small molecules, organized in a three-dimensional architecture that is unique to each tissue [9, 10]. The ECM provides the structural support and mechanical strength required for proper function of each tissue and serves as a conduit for information exchange between adjacent cells and between cells and the ECM itself. The ECM plays a key role in a wide variety of processes related to cell differentiation, tissue formation and homeostasis by providing attachment sites for cell surface receptors and feedback-controlled reservoirs for signaling factors [9]. The components of the ECM can be roughly divided into two main classes of molecules (i) the fibrous and adhesion proteins and (ii) the proteoglycans. Fibrous and adhesion proteins like collagen, fibronectin, laminin and elastin impart structure and mechanical stability to the ECM and offer structurally defined and chemically specific cell adhesion sites. The second class of molecules are proteoglycans that are glycoproteins in a heavily glycosylated state. These set of macromolecules are defined by a common type of post-translational modification: the GAGs which are usually covalently bound to the protein core (except hyaluron).

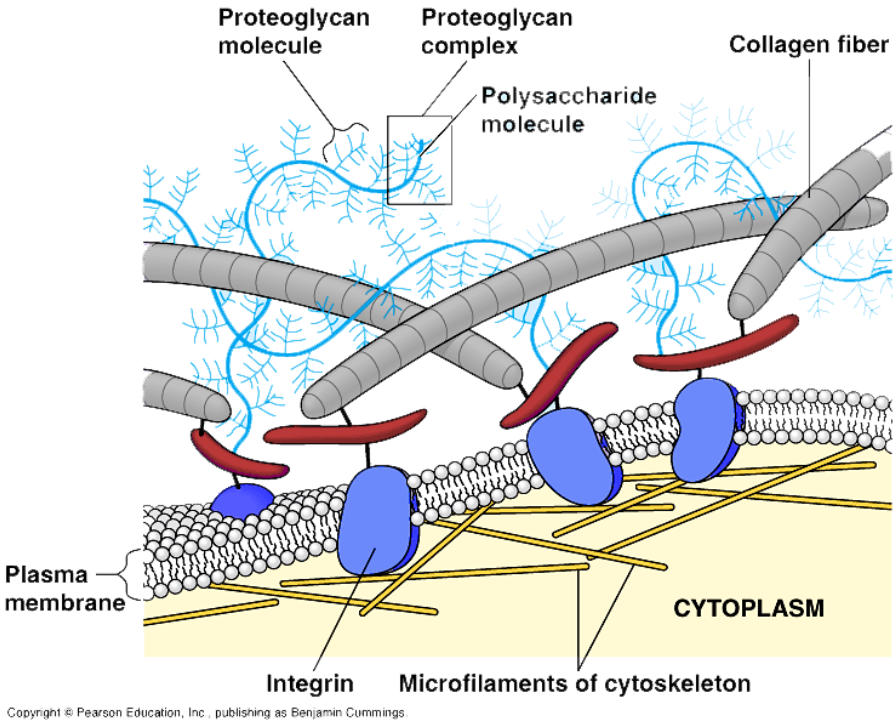

Figure 2.1: The extracellular matrix as natural scaffold consisting of structural proteins and proteoglycans. Adapted from ref. [11].

The common GAGs include the galactosaminoglycans, chondroitin sulfate and dermatan sulfate and the glycosaminoglycans heparan sulfate, heparin, and keratan sulfate. Proteoglycans have a net negative charge that attracts water molecules, keeping the ECM and resident cells hydrated. Proteoglycans support cell adhesion and help to trap and store growth factors within the ECM. The division of the ECM into structural and functional components is difficult since many of the introduced molecules have both structural and functional roles in health and disease. The ECM is in a state of dynamic reciprocity and will change in response to environmental cues. Thus, the ultimate decision of a cell to differentiate, proliferate, migrate or apoptose is a coordinated response to molecular interactions with the ECM molecules. This involves a highly bidirectional flow of information between cells and their ECM including ECM degradation, synthetization and reorganization [7]. In the following section collagen type I as major fibrous protein and heparan/heparan sulfate as important proteoglycans will be explained.

2.1.1 Collagens

Collagen is the most abundant protein within the mammalian ECM. Greater than 90% weight of the ECM from most tissues and organs is represented by collagen [12]. Almost thirty distinct types of collagen have been identified each with a unique biologic function. The collagen familiy can be categorized into different subfamilies of fibrillar (e.g. type I, II, III, V, XI ...), network-forming (type IV, VIII, X ...), fibril-associated (IX, XII, XIV ...), transmembrane (e.g. XIII, XVII) and multiple collagens (e.g. XV, XVIII) according to their supramolecular assembly [13]. Collagen type I, II, III, and V are the main types that make up the essential part of

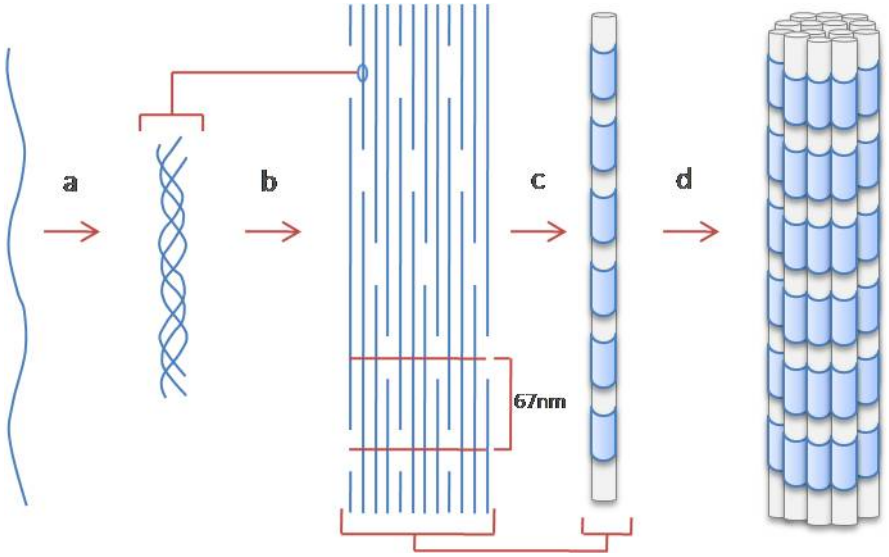

Figure 2.2: Collagen type I fibril formation. Three polypeptide chains form a triple helix (a) and aggregate to build collagen fibrils (b) exhibiting a regular banding pattern with a perioditiy of 67nm (d). Many fibrils running together in a tough bundle form the collagen fiber (d).

collagen in bone, cartilage, tendon, skin, and muscle. Collagen type I is the major structural protein present in tissue and provides the necessary strength to accommodate the uniaxial and multiaxial mechanical loading to which these tissue are commonly subjected. The primary feature of a typical collagen molecule I is its long, stiff, triple-stranded helical structure (1.5 x 300 nm2) made of two identical α1(I)-chains and one α2(I)-chain which contain the sequence repeat (G-X-Y)n, X being frequently proline and Y hydroxyproline (Figure 2.2a). These repeats allow the formation of a triple helix which is the characteristic feature of the collagen superfamily [13].

Current models describe the formation of collagen fibrils as a self-assembly process in which collagen monomers laterally aggregate to form fibrils [14, 15, 16] (Figure 2.2b). These insoluble fibrils are intermediate in length, have diameters of 10-300 nm exhibit regular band patterns with a periodicity of 67 nm (Figure 2.2c). This banding pattern results from collagen fibril assembly in a quasi-crystalline structure. Many fibrils running together in a tough bundle form the so-called collagen fiber (Figure 2.2d).

In vivo, collagen type I assembles into three-dimensional (3D) () tissue-specific architectures which perform different functions. Frequently, collagen fibrils run parallel to each other, in an oriented fashion. In tendons and ligaments for example, collagen fibrils are oriented longitudinally as parallel bundles to support the great tensile stress exerted on the tissue [17]. The organic part of bone is mainly constructed by collagen type I fibrils in elaborate 3D arrays [18]. Lamellar bone is filled with many collagen fibrils parallel to other fibrils in the same layer. The fibrils run in opposite direction in alternating layers, much like plywood, assisting in the bone's ability to resist torsion forces. The human dermis consists predominantly of type I collagen which exists in the form of loosely interwoven, large, wavy, randomly oriented bundles and within each bundle the collagen is packed together closely [19]. The stroma of the cornea which constitutes approx-

imately 90% of the corneal volume is mainly comprised of type I and V collagens existing in parallel-organized fibrils that are further arranged in lamellae. Here the fibrils impart the desired tensile strength and the 3D architecture of the thin collagen fibrils is believed to contribute to cornea transparency [20]. The endoneurium of peripheral nerves surrounding individual axons and their Schwann cell sheaths is composed predominantly of oriented collagen fibers [21].

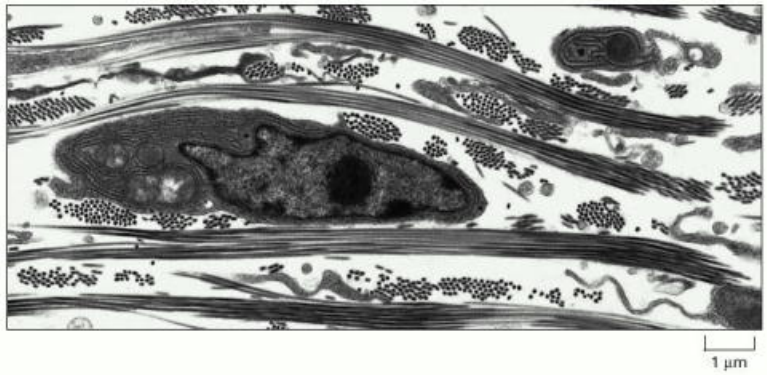

Figure 2.3: Electron micrograph of a fibroblast surrounded by collagen fibrils in the connective tissue of embryonic chick skin. Collagen fibrils are organized in bundles; some bundles are oriented longitudinally, whereas others are seen in cross-section. Adapted from ref.[22].

2.1.2 Proteoglycans

Besides structural proteins, the ECM consists of proteoglycans. Within this group, heparin and heparin sulfate play an important role by regulating cellular functions and extracellular matrix assemblies. Heparin and heparan sulfate are both members of the GAG family of carbohydrates and both consist of a variably sulfated repeating dissacharide unit. Within heparan sulfate the most frequent disaccharide unit is composed of a glucuronic acid (GlcA) linked to N-acetylglucosamine (GlcNAc) typically making up around 50% of the total disaccharide units. Heparin, in comparison, contains IdoA(2S)-GlcNS(6S) which makes up 85% of heparins from beef lung and about 75% of those from porcine intestinal mucosa. Numerous growth factors and cytokines bind to heparin and heparan sulfates and moreover need their presence for being biologically active [9]. Fibroblast growth factor (FGF) () for example requires the presence of heparan sulfate on the cell surface or in the adjacent extracellular matrix or in the form of exogeneously added heparan sulfate, heparin or heparan sulfate proteoglycans [23] for high affinity binding to their tyrosine kinase receptors. Several other growth factors including heparin binding epidermal growth factor show strong dependence on heparin for their biological function [24]. Furthermore heparin and heparan sulfate are involved in the regulation of ECM assembly and structure binding to large, mulitdomain ECM proteins like collagen containing heparin binding sites [9]. The immobilization of diffusible molecules on the cell surface or the extracellular matrix presents another important function of heparin and heparan sulfate like for instance the latter is known to both store and release FGFs in the ECM [25]. Cell surface heparan sulfate is also known to immobilize both lipoproteins and the enzymes that act on these lipoproteins such as lipoptrotein lipase and hepatic triglyceride lipase [26].

2.2 Cell-matrix interactions

The integration of cell sources, scaffolds and bioactive materials drives the success of tissue engineering applications. Constructing a substitute for tissue repair, therefore, requires a clear understanding of cell-cell interactions and cell-biomaterials/scaffold interactions. *In vivo*, cellular functions such as cell adhesion, proliferation, migration, differentiation and death are essentially controlled by the surrounding ECM [27]. The mechanical, biomolecular/chemical and structural properties of the ECM are consequently crucial for the selection of cells at interfaces and the formation of tissues. Chemical cues, for the most part, comprise biomolecules available for binding to cell membrane receptors which are involved in cell adhesion, polarity, migration, proliferation, and differentiation. Physical characteristics, on the other hand, govern tensile strength of tissue, cushioning (as in cartilage), filter functions (as in kidney), formation of boundaries between and within tissues and the storage of growth factors, cytokines and chemokines [28]. In general, it is difficult to make a clear distinction between biomolecular and physical cues since assemblies often unify both characteristics. Nevertheless, biochemical, mechanical and structural influences will be discussed separately as they form the basis for successful engineering of articular cell microenvironment.

2.2.1 Biochemical signals

Biochemical signals can be transmitted via cell surface receptors reacting to specific ligand molecules. For example, the ECM can be remodeled in response to biomolecular signals transmitted by ECM receptors such as integrins, other laminin receptors and syndecans. Most of the ECM biomolecules contain multiple active sites to interact with different receptors depending on the particular activities. Additionally, ECM molecules may bind specifically to other biomolecules of the ECM resulting in supramolecular assemblies. Multiple specific interactions between fibronectin and collagen result in the formation of fibrils of collagen I, co-fibrils of collagen I GAGs, or meshwork-like networks of fibronectin fibrils [28]. The deposition of collagen type I requires integrin-mediated assembly of fibronectin into fibrils tethered to the cell surface [29]. These examples show the interrelationship of both biomolecular and physical characteristics of the ECM. Another mechanism based on biomolecular interactions by which the ECM is remodeled involves the proteolytic cleavage of ECM components. For example, matrix metalloproteinases convert structural molecules to signaling molecules by releasing small bioactive peptides, release growth factors stored within the ECM and degrade matrix proteins directly. To maintain tissue homeostasis, protease activity must be under exquisite control during development and in adult tissues [30]. The interactions between growth factors and ECM regulate cell behavior in various ways. For instance, the direct binding of growth factors to the ECM can affect the local concentration as well as the biological activity of growth factors [31]. On the other hand, various growth factors regulate the transcription, translation, and post-translational modification of ECM macromolecules [32]. The binding of growth factors to the ECM is regulated by the GAG side chains. Specifically, the presence of basic amino acid clusters within regions of α-helical structure of growth factors seems to mediate the binding to the negatively charged

heparin sulfate side chains of proteoglycans [33]. Fibroblast growth factor (FGF), for example, degrades less when bound to ECM when compared to free FGF [34]. Finally other means of signaling involve the formation of gradients like stromal cell-derived factor-1 for the homing of circulating stem cells or spatial concentration gradients mediated by ECM biopolymers .

2.2.2 Mechanical signals

Physical cues of ECM refer to the mechanical and structural signals acting upon the embedded cell. Most of the mechanical interactions between the cell and the ECM are integrin-mediated cell adhesion since integrins connect mechanical components from the cytoskeleton with mechanical components of the ECM. The cells can deform and rearrange the ECM by means of tensile forces [35]. Additionally, cells react to the rigidity of the ECM in a highly sensitive manner. For example, fibroblasts prefer a tissue with a Young's modulus higher than 3 kPa [36], whereas neurons, in contrast, naturally prefer rather soft surfaces with a Young's modulus of 0.1 - 1 kPa [37]. Recently, important facts were reported how substrate stiffness impacts cell differentiation. Breast epithelial cells, for example, differentiated into tubules only when they were cultured on a rather soft collagen matrix, whereas on rigid matrices they did not [38]. An important work done by the Discher laboratory [39, 40, 41] showed that substrate elasticity regulated mesenchymal stem cells (MSCs) (besides other cell types) lineage commitment in response to substrate compliance. Polymer gels with varied elasticity could regulate MSC differentiation towards neurons, myoblasts, and osteoblasts under identical serum conditions. Here, rather soft matrices that mimicked brain were neurogenic, stiffer matrices that mimicked muscle were myogenic, and comparatively rigid matrices that mimic collagenous bone proved osteogenic. The influence of physical signal on cell behavior was also observed for cells being exposed to mechanical stress. Active mechanical stimulation of cells results in changes of their cytoskeleton that can have an influence on cell differentiation. The influence of static and dynamic mechanical stress on osteoblast differentiation was also demonstrated in mechanically stressed 3D collagen matrices [42].

2.2.3 Structural signals

So far it has been discussed how the ECM biochemically and mechanically interacts with cells. However, it is of crucial importance how and in which pattern mechanical and biomolecular cues are presented. One of the most investigated cell-matrix interactions is the effect of surface topography on cellular behavior. The effect of surface topography on the development, motility, differentiation, orientation, and alignment of cells was first reported by Harrison [43] in 1912, and termed as "Contact Guidance" by Weiss [44] in 1945 for the ability of an underlying substrate to direct or modify the response of cells. Weiss showed in his studies that nerve fibers regenerating from explants cultured in plasma clots tend to follow a course dictated by fibrin micelles orientated in the direction of stress within the clot. Following these early seminal studies, many studies have addressed and expand on this observation (reviewed in ref. [45]). For example, oriented collagen fibrils have been shown to induce contact guidance of dermal cells of

the dermal papillae in developing embryonic chick skin [46], as well as fibroblasts in the posterior stroma of the developing chick cornea [47] and neural crest cells on the surface of axolotl neural tubes [48].

An important work by Ingber and co-workers [49, 50] demonstrated that adherent endothelial cells could be switched from proliferation to apoptosis or vasculogenesis by micropatterning a planar surface with islands of adhesive ECM proteins. It was shown that increased cell death occurred when cells adopted a rounded shape (as result of decreasing size of patterned island) when compared to a spread cell morphology that was independent of the type of matrix protein or antibody integrin used to mediate adhesion. Thus, cell shape per se appears to be the critical determinant that switched cells between life and death and between proliferation and quiescence [50]. The mechanism by which cells transduce changes in cell geometry into different biochemical responses is attributed to the specialized cytoskeletal structure, or focal adhesion complex, that forms intracellular at the site of integrin binding. This molecular bridge mechanically couples integrins, and hence ECM, to the actin cytoskeleton. By doing so, focal adhesion evoke chemical signals and thereby adjust downstream signaling [51, 52, 53].

Stem cell differentiation was also shown to be affected by structural cues in several reports. The seminal study by Chan and co-workers demonstrated that different sizes of patterned fibronectin islands influenced cell shape that in turn regulated the commitment of human mesenchymal stem cells into a adipocytic or osteoblastic fate [54]. Additionally, there is substantial evidence from studies on planar substrates using patterned surface chemistry and topography to suggest that feature sizes in the sub-micron range in particular affect cell behavior. In particular, the nanoscale nature of ECM consisting of various nanoscaled fibers and molecules has a two-fold benefit for cells: a high specific surface area and a better structural/mechanical support. For instance, osteoblasts cultured on carbon nanofibers showed increased adhesion, proliferation, alkaline phosphatase activity, and ECM secretion when fiber diameter was reduced to the range of 60–200 nm [55].

These *in vivo* and *in vitro* examples demonstrate how extrinsic factors from the surrounding ECM regulate cell fate. Hence, a tissue engineering material substrate/scaffold need to exhibit features that ensure cell viability and control cell behavior. Specifically, recent biomaterial research has progressed towards the incorporation of nanoscale detail and anisotropic cues observed in real tissues [4]. There has been great interest to design systems that provide chemical-physical cues in biologically relevant manner to mimic the aligned architectures found *in vivo*. To better understand the scope of this thesis, it is important to have a basic understanding of the techniques used to generate aligned ECM structures.

2.3 Approaches to engineer aligned extracellular matrix structures

The anisotropic structural composition of ECM in many tissues fulfills important biomechanical functions related to the overall structural integrity and mechanical property of a tissue and impacts crucial cell functions. However, when cultivating cells on standard tissue culture ware they lose their native organization and adopt random distributions that do not resemble physiologi-

cal tissue architecture. Thus, different approaches were followed to create aligned biomaterials to induce alignment of cells ranging from micro- and nanostructuring of surfaces with aligned grooves/ridges, chemical patterning of lines or stripes, electrospinning aligned nanofibers and the reconstitution of aligned ECM assemblies.

2.3.1 Topographically and chemically patterned surfaces

Structured 2D surfaces consisting of arrays of aligned micro- or nanostructures have been developed to examine the effect of anisotropic topographies on cell behavior. For cell culture assays mainly basic structures like lines, grooves or ridges were designed using techniques developed in the microelectronics industry such as electron beam or ion beam lithographies [56, 57] with synthetic materials including polystyrene (PS) or polydimethylsiloxane (PDMS) . Another approach involved the fabrication of chemically patterned surfaces that result from the spatial organization and immobilization of biological molecules in controllable size and position. Frequently, ECM molecules are used including fibronectin, vitronectin, laminin, and collagens or their constitutional motifs such as arginine-glycine-asparate (RGD) peptides [58]. Biologically active (protein adsorbing, biofouling) or inactive (protein repellent, nonfouling) patterns can be produced by altered surface chemistry, so that selectively adsorbed proteins in turn effect cell behavior. Micropatterning techniques include photolithography, microcontact printing and microfluidic and stencil patterning [59, 60, 58]. In various efforts to mimic the nanaoscale structural composition of ECM more closely various new nanopatterning techniques have recently been developed and reviewed elsewhere [58].

2.3.2 Electrospun fibers

In the past few years, considerable efforts have been taken for the processing of aligned fibrous scaffolds with structural features similar to the ECM. Micro- and nanofibrous scaffolds were produced by self-assembling processes of individual, preexisting components into an ordered structure like peptide-amphiphile (PA) nanofibers or by phase separation using e.g. Poly(L-lactic acid) (PLLA). Although phase separation and self-assembly give rise to micro and nanfibrous scaffolds, difficulties were encountered in controlling the fiber orientation. Thus, electrospinning has lately gained increased attention as it allows the production of randomly and aligned oriented fibers [61, 62]. In electrospinning an electrical charge is used to form fibers ranging from micron (30 mm) to submicron (50 nm) range similar to the features of natural ECM. Mostly synthetic polymers including the most prominent as polycaprolactone, poly lactic acid (PLA), poly (lactic-coglutamic) acid (PLGA), or polycaprolactone (PCL) [63] can be used for electrospinning. Additionally, biopolymers like collagen type I have been shown to be electrospun into nanofibers [62]. Alignment of electrospun fibers can be induced for example by a rotating plate with a sharping edge as collector. Lately, increased attention has been drawn to the generation of electrospun nanofibers as being specifically crucial for cell behavior and fate, resembling ECM with its nanostructural features. Although several studies have reported the biocompatibility and ideality of electrospun polymers as tissue scaffolds [64], major drawbacks such as low poros-

ity, weak mechanical properties, and lack of biological activity to cells, limit the applications of electrospinning nanofibers in tissue engineering.

2.3.3 Reconstitution of extracellular matrix

As discussed in the previous section scaffolds to mimic aligned *in vivo* structures can be readily produced from mainly synthetic polymers. With man-made materials many different kind of geometries and structures can be created allowing precise control over the final micro and nanostructure by varying chemistry and processing technique. However, little control over cell behavior and tissue response *in vivo* is provided so that recent efforts have focused on adding biological cues to generate materials for a specific cell type and/or tissue [6]. Additionally, as already mentioned above, materials exhibiting structures on the nanoscale were found to be crucial for cell behavior due to the larger surface areas for example to adsorb proteins presenting many more binding sites to cell membrane receptors (e.g. integrins) [65]. Hence combining nanoscale features with biomolecular cues into a single material is likely to prove most rewarding. This can be achieved by building scaffolds from naturally derived biopolymers that are isolated and dissociated from natural tissue. Using this principle, ECM assemblies can be built-up in the lab that closely resemble *in vivo* ECM structures. Many natural biopolymers are assembled in multiple steps from the bottom up. The most prominent examples are collagen and fibrin gels, which have found wide applications in tissue engineering applications and regenerative medicine [66]. These constructs have nanoscale structures and borrow their binding sites from the ECM biopolymers providing innate informational guidance. Collagen type I is the most studied *in vitro* assembled ECM component owing to its abundance in all kinds of tissues and for the relatively easy access and reconstitution. *In vitro* fibrillogenesis of collagen type I is a straightforward example of entropy-driven protein self-assembly/polymerization [16]. In early experiments collagen type I was demonstrated to be easily extracted from tissues in dilute acidic solutions or high-salt buffers by enzymatic fragmentation and reconstituted into fibrils by neutralizing and/or warming the solution to 37°C [67]. The spontaneous self-assembly of monomeric collagen was referred to the entropy gain upon binding of collagen molecules. Hydrophobic interactions between collagen monomers were implied to be the major force for fibrillogenesis. Further, water clusters bridging recognition sites on opposing helices have been identified as the driving force for fibril formation [68][69]. The precipitated fibrils resemble those found in tissues both morphologically and functionally exhibiting the characteristic 67nm banding pattern. However, when collagen type I is reconstituted *in vitro* it does not assemble into ordered arrays as seen in connective tissue but rather arrange in a loose non-oriented network of fibrils. Therefore, engineering efforts have focused on generating aligned collagen matrices (summarized in Table 2.1). Different approaches were followed including inclining a surface during collagen polymerization (drainage technique) [70], the use of a strong magnetic field [71], electrical gradients [72], a combination of fluid flow and magnetic fields [73], or the flow through a microfluidic channel [74].

However, the production of aligned collagen matrices still requires complex technical equipment or lacks broad application to cell biology due to the limited size of the area covered or the rather artificial characteristics of ‘‘non-native’’ matrices. Importantly, none of the above-mentioned

techniques enables collagen fibril alignment, density and morphology to be varied to adopt the very versatile structures found in tissues.

Table 2.1: Methods to align collagen type I matrices

Resultant matrices	Alignment method	Reference
Aligned collagen gel	Drainage	[70]
Aligned collagen gel	Electrical gradients	[72]
Aligned collagen gel	External magnets	[71, 75]
Aligned collagen gel with magnetic beads	Magnetic beads and external magnets	[73]
Flat microribbons	Hydrodynamic flow and mica surface	[76, 77]
Aligned collagen gel	Microfluidic channel (<10µm width)	[74]

2.3.4 Guidance conduits

Physical guidance is a vital component for nervous tissue regeneration. Repair of nerve injury requires tubular guidance structures that reconnect nerves to the distal targets. Therefore, in recent years, so called guidance tubes or conduits have been developed to serve as bridging materials for defects in the peripheral or central nervous system. These guidance channels have been predominately produced as hollow tubes mainly from synthetic materials. When these constructs were implanted, the body generated an oriented fibrin matrix to support axonal regeneration [21]. Thus, in order to mimic the natural repair in the body, in recent studies longitudinally aligned fibers or channels have been inserted in the nerve conduits. By doing so, the conduits enhanced nerve regeneration and enabled shorter regeneration times. For instance, the integration of polyamide filaments or polylactic acid into nerve guidance conduits improved nerve regeneration[21]. The diameters of these filaments were in most cases in the micrometer range. However, only recently, the importance of nanofibers for nerve regeneration has been demonstrated. For example, under differentiation condition rat neural stem cells showed a 40% increase in oligodendrocyte differentiation on 283-nm electrospun fibers and 20% increase in neuronal differentiation on 749-nm fibers, in comparison to tissue culture polystyrene surface [78]. Thus, current and future research focuses on guidance cues on the nanoscale. Since nerve guidance conduits are mainly produced from synthetic materials recent studies aimed at incorporating biochemical cues. Specifically, since trophic support is required to enable entire nerve regeneration specifically over larger distances [79]. Biochemical cues can be realized by the incorporation of growth/neurotrophic factors, cells, and ECM molecules such as collagen, laminin, and fibronectin. Various advanced approaches came up in the last years to create complex guidance channels and to combine multiple stimuli into a single therapy. For example, extruded or spun fibers of collagen have been placed within the lumen of conduits. Matsumoto et al. [80] showed that poly(glycolic acid)-collagen conduits filled with collagen fibers permitted regeneration over 80mm defect lengths in dogs. This study suggested that the internal collagen

fibers indeed enhanced axonal elongation.

2.4 Cellular response to aligned structural cues

2.4.1 Cellular response in general

Besides the tissue scaffold, the appropriate use of specific cells and the control of cell-matrix interactions is crucial for the success of tissue engineering. As already discussed in section 2.2, cell proliferation, function, migration, and death are dictated by cell-matrix interactions. Cells interact with their environment through receptors present on their surfaces. For anchorage-dependent cells, the degree of attachment determines and influences the function and the proliferation of the cells. For a cell to attach on a surface, several proteins, receptors and ligands interact together in a complex manner. The signal transduction from the cell exterior to the cytoplasm is mediated by receptors, which are linked to the extracellular matrix of the cells. Thus, a clear understanding and control of cell-surface interactions is an essential means to induce the functioning of a cell and crucial for the success of tissue engineering applications and regenerative therapies.

In the body cells are frequently oriented in aligned arrays of collagen fibrils imparting mechanical strength and structural integrity to the tissue. In addition to its function as structural support aligned collagen structures are believed to increase the efficiency of the cell interactions and impact cell behavior. Thus, extensive studies have been conducted to investigate the influence of aligned topographical features on cellular behaviors and activities [81]. Aligned topographical cues were shown to alter cell morphology from randomly oriented cell shapes towards an anisotropic morphology [81]. Contact guidance was observed on various substrates containing ridges, grooves, chemical patterns of ECM molecules and growth factors and aligned collagen gels with cell types including endothelial cells, fibroblast, neural cells [82, 83]. Cell behavior and functionality was also shown to be effectively influenced by aligned topographical cues. The alignment of electrospun nanofibers increased proliferation of rabbit conjunctiva fibroblasts [84] and promoted endothelialization using human coronary artery endothelial cells [85]. *In vitro* and *in vivo* studies using human monocytes showed that aligned electrospun scaffolds minimized host response, enhanced tissue-scaffold integration, and elicited a thinner fibrous capsule after implantation when compared to a randomly oriented scaffold [86].

These examples highlight how aligned structural cues influence the behavior and function of already differentiated and committed cell types. However, oriented features can also have crucial impact on stem cell differentiation. Besides specialized cells that are an important source for tissue engineering, the use of stem/progenitor cells are of particular interest in the advent of tissue engineering and regenerative medicine owing to their enormous potential in producing a variety of cells and tissues with diverse functions [87]. It was discovered that bone marrow harbors two populations of stem cells: hematopoietic stem cells, which are responsible for the formation of blood cells [88] and mesenchymal stem cells (MSCs) [89], which are responsible for the formation of bone cells, for example. In 1992, Reynolds and Weiss were the first to isolate neural stem cells (NSCs) that are capable to generate the main phenotypes of the nervous system.

The following chapter gives an overview of the current knowledge of mesenchymal and neural stem cells and their response to aligned topographical cues.

2.4.2 Mesenchymal stem and progenitor cells

The definition of an MSC still presents a challenge since neither MSCs' origin is clearly proved nor are specific phenotype markers established to identify MSCs from the heterogeneous bone marrow-derived population [90]. Therefore various synonyms can be found in literature including bone marrow stromal (stem) cells, bone marrow progenitor cells, multipotent adult progenitor cells, bone marrow stromal fibroblasts, bone marrow mesenchymal progenitor cells and many more [91]. For the purpose of this thesis those cells will be nominated as mesenchymal stem cells (MSCs). MSCs differentiate into a variety of connective tissue lineages, including bone, cartilage and adipose [92](Figure 2.4), making them promising candidates for regenerative medicine. Already in the late 1960s Friedenstein et al. [89] described an adherent, fibroblast-like cell population which have the ability to regenerate the essentials of normal bone as colony-forming unit-fibroblasts (CFUs) . The term mesenchymal stem cell (MSC) was coined by Caplan in 1991 [93] to describe bone-marrow-derived stromal cells. It is well documented that MSCs are capable of differentiating into bone [94], cartilage [95], muscle [96], marrow stroma [97], tendon and ligament [98], fat [99], and a variety of other connective tissues [100]. Bioactive factors localized in the cell micro-environment or added to the culture environment of *in vitro* cultivated cells initiate and control the differentiation of MSCs involving multi-step lineages. Since multipotent MSCs can be easily harvested from the donor site MSC transplantation is considered as a promising approach to improve several tissue functions of mesenchymal origin. In various tissue engineering applications MSCs have been utilized in order to support specific tissue organization and function including cartilage, myocardium, liver, nerve, spinal cord and derma [101, 102, 103, 104, 105]. However, the differentiation of human MSCs along the myogenic lineage has previously been controversial. While it was reported that murine MSCs were successfully differentiated into skeletal myoblasts and cardiomyocytes [106, 107], conflicting results have been published with respect to MSCs from other species including human [108, 109]. Alternatively, mouse-derived C2C12 myoblasts can serve as an experimentally tractable model system for investigating the molecular basis of skeletal muscle cell specification and development. C2C12 cells were originally obtained by Yaffe and Saxel (1977) through selective serial passage of myoblasts cultured from the thigh muscle of C3H mice 70 h after a crush injury. These cells were shown to be capable of differentiation so that they are a useful model to study the differentiation of non-muscle cells to skeletal muscle cells.

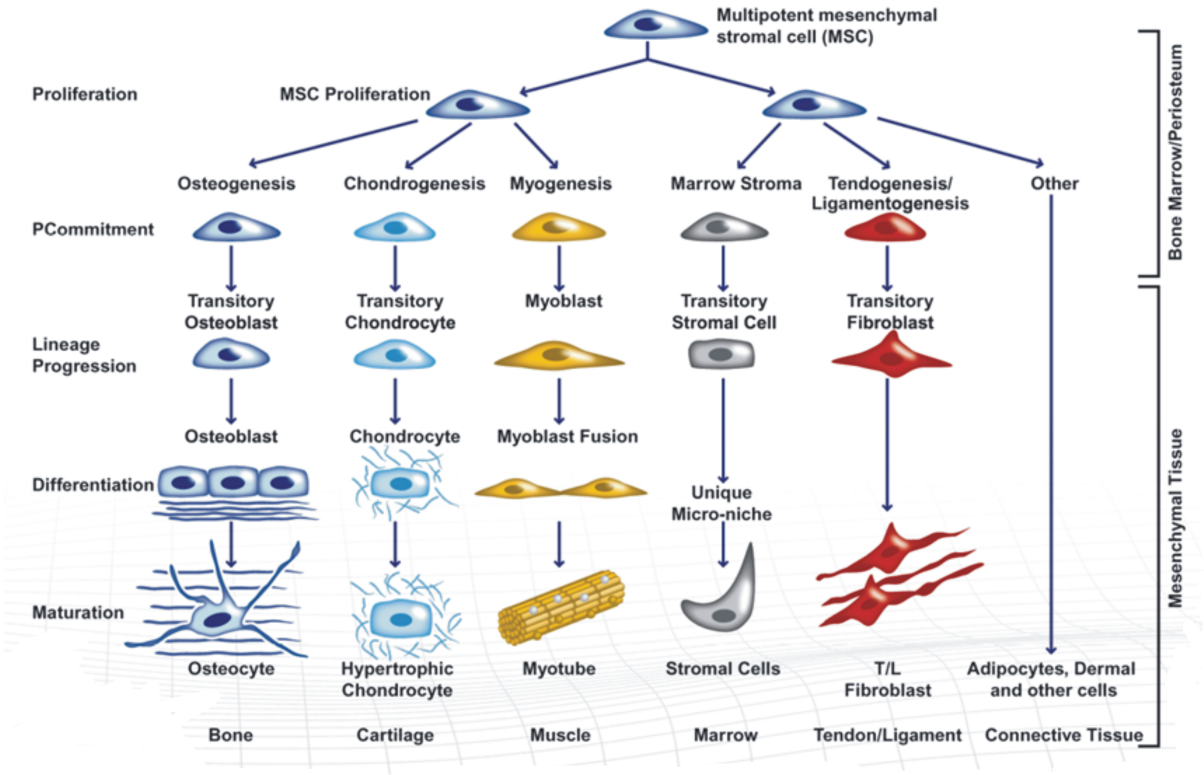

Figure 2.4: Differentiation of bone-marrow derived mesenchymal stem cells. Adapted from ref. [110]

It has been shown that structural cues can have crucial impact on stem cell differentation [111]. Since many mesenchyme-derived tissues contain anisotropic collagenous architectures including bone, muscle or cartilage, it has been proposed that aligned ECM structures in particular could guide and support the differentiation of resident mesenchymal stem and progenitor cells. In this context, MSCs are specifically interesting since they are adherent cells that show robust differentiation into fat, cartilage and bone. MSCs contribute to highly organized tissue architectures (e.g. bone, cartilage) so that aligned ECM may be critically important for their differentiation. One of the major challenges associated with the use of MSCs is to provide appropriate cellular environment cues that regulate cell growth and subsequent tissue formation. Once MSCs are isolated from their natural environment, they start to lose their phenotype and differentiated functions [112]. Thus, it is a special challenge to maintain cell phenotypic expression and differentiated function while supporting proliferation under laboratory conditions. It was shown in several studies that changes in cell shape themselves can alter the differentiation of precommitted mesenchymal lineages [113, 114, 115]. Cell spreading for instance has been demonstrated to increase osteoblast differentiation in preosteoblastic progenitors [114, 115]. However, little is known about whether cell shape affects earlier development stages such as the commitment of MSCs. In this context, MSC differentiation behavior has been the objective of extensive research efforts. Many studies have addressed the effect of cellular environment cues to support and maintain MSC differentiation and the influence of topographical cues on MSC fate. Recent

findings are summarized in Table 2.2. These studies demonstrate that cell shape which is influenced by topography drives stem cell commitment specifically when substrates have features on the nanoscale. Additionally, aligned features seem to influence chondrogenic and neuronal differentiation of human MSCs.

Table 2.2: Effect of topographical cues on MSCs

Topographical features	**Observed effect**	**Reference**
Chemically patterned islands (1024µm^{2}or 10000µm^2)	Size of pattern induces either adipogenic or osteogenic differentiation	[54]
Ordered nanopitches (120nm)	Induction of osteogenic differentiation	[116]
Nanotubular-shaped titanium oxide surface structures (30-100nm)	Induction of osteogenic differentiation	[117]
Aligned electrospun nanofibers (500nm)	Enhanced chondrogenic differentiation	[118]
Aligned nanopatterns (350nm width)	Induction of differentiation into neuronal lineage	[119]

2.4.3 Neural stem and progenitor cells

Neural stem cells (NSCs) can be defined as cells that are capable to generate neural tissue, possess the ability for self-renewal, and can differentiate into all major cell types of nervous tissue such as neurons and glia cells [120]. NSCs can be derived from the fetal or adult brain for example the subventricular zone or the hippocampus or a larger variety of structures in the developing brain and proliferated in culture. Alternatively, embryonic stem cells can be extracted, proliferated and differentiated into neural precursor cells (Figure 2.5). Early reports demonstrated the dissection of stem-like cells from embryonic mammalian central nervous system (CNS) [121, 122] and the peripheral nervous system (PNS) [123]. Subsequently many regions of the embryonic CNS could be identified to yield stem cells and studies also reported the isolation of NSCs from adult brain [124, 125]. Additionally, NSCs have been found in some non-neurogenic regions including the spinal cord [120]. Some of these findings however are still discussed controversially in literature [126, 127].

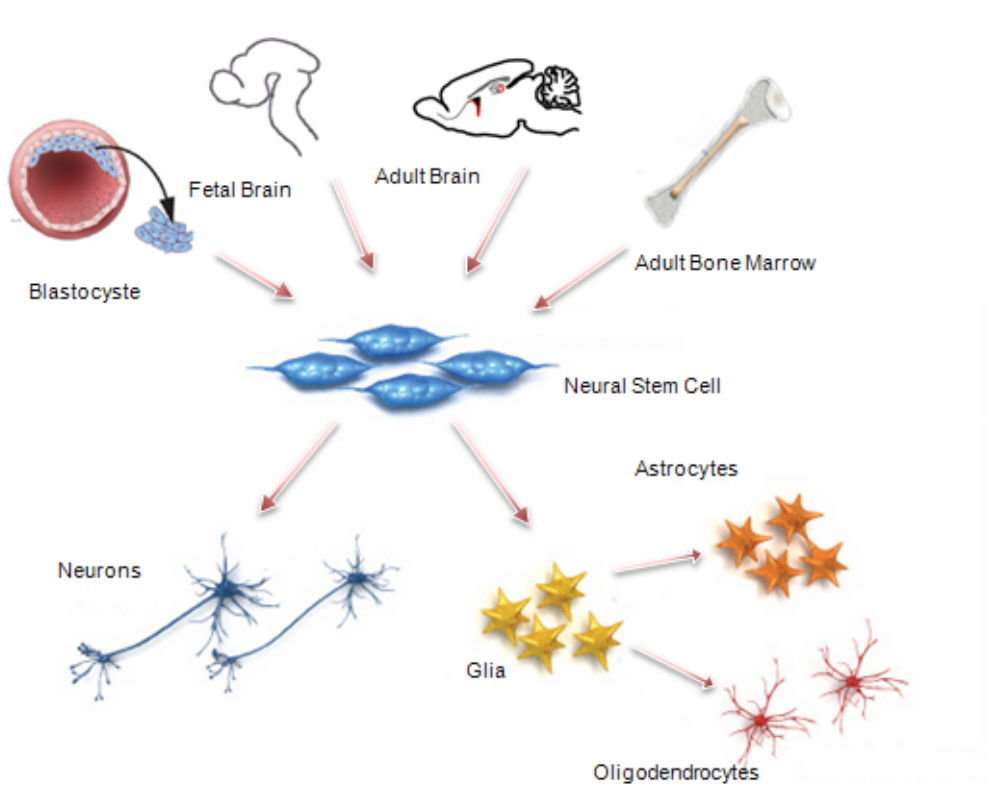

Figure 2.5: Neural stem cell - origin and differentiation. Adapted from ref. [128]

Usually, NSCs are isolated *in vitro* by disaggregating the brain tissue and exposing the dissociated cells to mitogens such as FGF-2 or epidermal growth factor (EGF) in medium on a planar surface as binding substrate. During expansion brain-derived neural stem cells usually grow as floating aggregates called "neurospheres". After some proliferation, differentiation is induced by withdrawing the mitogens or by exposing the cells to another factor that initiates differentiation into a distinct lineage. Subsequently, cellular fate is determined by staining with antibodies directed against antigens specific for neurons (TUJ1), astrocytes (glial fibrillary acid protein - (GFAP), and oligodendrocytes (GalC) [120].

Recovery of diseased nervous tissue has become a major goal for regenerative therapeutic approaches. Neuronal repair is, however, severely hampered by inappropriate neurite outgrowth and synaptic integration of regenerating or grafted neurons [21]. Since autologous nerve grafts are insufficient regarding nerve cell regeneration and result in loss of sensory function there is an urgent need to develop bioartificial materials that improve nerve regeneration and function. Materials containing aligned guidance structures have been introduced to replace the need for nerve autografts and profoundly affect the guidance, neurite length and differentiation of neural cells (recent findings summarized in Table 2.4). In this context, ECM components are of great importance mainly collagen, laminin, and fibronectin as well as matrix-bound trophic factors. This holds true, considering the improved nerve regeneration as result of recent efforts to functionalize synthetic materials with ECM components (see Table 2.4). Collagen type I is of special interest since it has been shown to favor neuronal rather than glial growth [21]. In peripheral nerves, the endoneurium surrounding the axons with Schwann cell sheets is predominately com-

posed of orientated collagen fibers. Thus, the nanoscale spatial organization of collagen fibrils as major constituents of ECM is believed to be crucial for neurite guidance in neural development and repair. Moreover, it is now clear from a growing body of evidence that neurite growth strongly depends on substrate topography, including dimension and density of guidance cues [129].

Table 2.4: Effect of aligned topographies on neural progenitor cells and neurons.

Cell type	**Topographical features**	**Observed effect**	**References**
Rat hippocampal progenitor cell	Aligned micropatterns PS coated with laminin in coculture with astrocytes	Enhanced neuronal differentiation	[65]
Rat Schwann cells	Aligned fibronectin fibers	Enhanced cell migration	[130]
Rat dorsal root ganglia	Aligned astrocyte monolayers	Increased neurite length	[131]
Chick dorsal root ganglia /mice sciatic nerve	Aligned collagen gel	Increased nerve regeneration	[132, 133]
Rat dorsal root ganglia	Aligned nanofibers (poly-L-lactate); aligned microgrooves coated with laminin	Increased neurite length	[134];[135]
Chick sympathetic ganglia	Aligned micropatterns	Increased neurite length	[136]

3 Objectives

Aligned ECM biopolymer assemblies offer valuable options for advanced cell culture technology and tissue engineering. Specifically, a material system which provides multiple extracellular components to study cell-matrix interactions also in a 3D environment is of great interest. Thus, in an effort to develop a method to create aligned collagen type I matrices for tissue engineering, the following key questions need to be addressed within this thesis:

- Is it possible to deposit and align collagen fibrils from streaming collagen solutions onto planar substrates? How do process-relevant parameters such as flow rate, substrate pre-coatings, collagen concentration and gelation time influence structural characteristics of the resultant matrices? (Chapter 4.1, Appendix A).

- Does the glycosaminoglycan heparin bind to the reconstituted aligned collagen matrices? (Chapter 4.1.2, Appendix B).

- Is there an impact of aligned collagen fibrils on orientation and functionality of stem cells being relevant in tissue engineering such as neural and mesenchymal stem and progenitor cells ? How do aligned structural topographies influence cell differentiation ? (Chapter 4.2, 4.3, Appendix B).

- Is it possible to coat cellulose hollow fiber membranes with aligned collagen matrices obtained by shear flow deposition? Is this model suitable to study spinal cord derived neurospheres? (Chapter 4.4, Appendix D).

4 General Discussion

4.1 Aligned collagen matrices obtained by shear flow deposition

This section refers to the following publication (see Appendix A):

Lanfer B., Freudenberg U., Zimmermann R., Stamov D., Körber V., Werner C. Aligned fibrillar collagen matrices obtained by shear flow deposition. *Biomaterials* 29 (2008) 3888–3895.

In the frame of this work a novel method to orient collagen type I fibrils has been developed to mimic aligned collagen type I fibrils found *in vivo* (Appendix A). As discussed in section 2.3.3, several approaches have aimed to reconstitute aligned collagen scaffolds. However, individual drawbacks have hampered their broad application to cell biology. For instance, shear flow has been used as tool to align collagen molecules/fibrils, however the channel width limited the aligned areas to a maximum of 100µm. Importantly, none of these methods allowed the generation of aligned matrices containing collagen fibrils of varying length and density. The novel method developed within this thesis involves a mircrofluidic setup that allows both orientation and collagen fibril morphology to be controlled. Collagen fibrils can be aligned and deposited on a planar substrate by streaming a collagen solution through a microfluidic channel. In order to vary the characteristics of the collagen matrices, this new setup allows to change and control the hydrodynamic flow (shear rate), the applied collagen solution, and the precoating of the substrate (hydrophobicity, reactivity, charging). Collagen solution concentrations correlate well with fibril orientation, length and density of the matrices. Higher collagen concentrations resulted in greater density of matrices, longer fibrils and higher orientation. Hence, morphology and density of the collagen matrices mirrors the different states of collagen fibril formation as a concentration-dependent process. On the other side the new method enabled the generation of collagen matrices with long and highly aligned fibrils at low density. Here, collagen solutions containing individual long collagen fibrils were used. Thus, the collagen solution concentration can be used as parameter to adjust length, density and orientation of collagen fibrils. Further, the hydrophobicity of the substrates affected the density of the resultant matrices. Surface-modified substrates spin-coated with thin films of copolymers of poly(octadecene alt maleic anhydride) (POMA) and poly(ethylene alt maleic anhydride) (PEMA) [137] influenced the density of the resultant matrices. The hydrophobic POMA surface gave rise to the highest surface coverage.

The higher coverage of collagen on POMA-coated substrates may be explained by the capability of the long alkyl chains of POMA to mediate hydrophobic interactions between collagen and the substrate surface. The hydrophilic gel-like structure of PEMA [137] and the smooth and unswollen glass surface apparently do not favor adsorption of the hydrophobic collagen. Additionally, increased shear rates resulted in better orientation of collagen fibrils whereas the fibril density was slightly reduced. Taken together, this method allows both density and collagen fibril orientation to be controlled by varying the applied solution, hydrodynamic flow (shear rate) and pre-coating of the substrate (hydrophobicity, reactivity, charging).

4.1.1 Alignment mechanism

Although shear flow has been used as tool to align collagen molecules/fibrils [74], little is known about the dynamics of collagen self-assembly and fibrils under the influence of shear stress. In order to get an insight into the underlying mechanism of fibril alignment the behavior of a rod-like particle in a shear flow was considered and compared to the results obtained. Our results revealed that an increase of fibril length in response to increasing collagen solution concentration is related to an increase in fibril alignment. Alignment was further increased when collagen solution containing already developed collagen fibrils was deposited on the substrate. The resultant matrices consisted of long, highly aligned, and individual collagen fibrils. Additionally, it was shown for this system that lowering the flow rate decreases fibril alignment. These results indicate that the alignment of collagen fibrils strongly depends on collagen fibril length and applied flow rate, which might point at the underlying mechanism of a 'mechanical alignment'. "Prealignment" phenomena related to liquid crystal ordering in collagen *in vitro* systems have been reported in literature. Nematic, precholesteric and cholesteric phases are observed with highly concentrated collagen solutions (5 mg/ml-40 mg/ml) [138, 139]. However, due to the comparatively high concentrations necessary for liquid crystal formation and the low concentrations (typically between 0.2 mg/ml and 5 mg/ml) of collagen solutions [140, 141] commonly required for fibrillogenesis, these phenomena are not considered to occur in our experiments. Additionally, viscosity only slightly influences fibril alignment since the matrices which showed the highest degrees of alignment were generated with solutions of low viscosity. Thus, prealignment effects in the form of liquid crystal formation prior to fibril formation, and viscosity appear to play a minor role in this system. This implies, that the formation of longer fibrils (besides the flow rate) rather critically determines alignment. The orientation of a rodlike particle can be described by a spherical coordinate system (Figure 4.1). In a simple shear flow, ellipsoidal particles align most of the time in the direction of flow, however their orientation can change by 180° in a "tumbling" motion. This effect was first described by Jefferey [45], who calculated the motion of a single ellipsoid in a shear flow independent of fluid and particle inertia. Motion of an ellipsoid in an unbounded simple shear flow is given by the following equations.

$$\tan\theta = \frac{Cr_e}{\left(r_e^2\cos^2\phi + \sin^2\phi\right)^{\frac{1}{2}}} \tag{4.1}$$

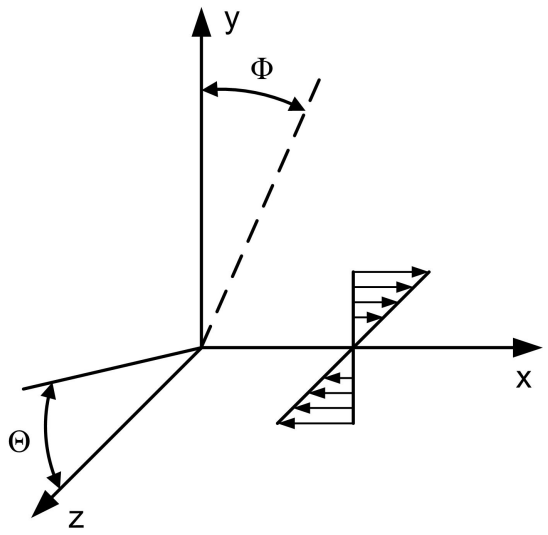

Figure 4.1: Spherical coordinate system

$$\tan\phi = r_e \tan\left(\frac{2\pi t}{T} + \kappa\right) \tag{4.2}$$

Angles ϕ and θ describe the fiber orientation with respect to the flow direction (see Figure 2), r_e is the effective aspect ratio of the particle (length/diameter), C is the orbit constant, and κ is the initial value of ϕ. The spheroid will rotate with a period

$$T = \frac{2\pi}{\gamma}\left(r_e + r_e^{-1}\right) \tag{4.3}$$

where γ is the shear rate in the y-direction. The particle is aligned with the vorticity axis for $C = 0$ and located in the xy-plane for C approaching infinity. The motion of a fiber near a wall (at distances smaller than a half fiber length) has been reported to result in smaller angular velocities of the particles and larger periods between fiber rotation [142, 143, 144, 145], however Moses et al. [146] claim shorter periods of rotation. In regions closer to the wall (less than half a fiber length), fibers follow a "pole vaulting" motion or a "springy rotation" during which the mass center of the fiber moves away from the wall [144, 147]. As fiber flexibility increases, the rotation changes towards snake and helix rotation and coil formation [147]. Fibers perform a "rolling-sliding motion" perpendicular to the flow direction as described by Holm et al. [148]. With increasing aspect ratio and distance to the wall, the number of perpendicularly oriented fibers decreases. Near the wall, fibers with a particle aspect ratio (length/diameter of particle) of $rp = 40$ stayed aligned with the flow direction whereas those of $rp = 10$ moved towards an orientation perpendicular to the flow direction [149]. Fibers in a shear flow perform a periodically tumbling motion. This motion was observed in a low Reynolds number regime for pulp fibers that reveal rigidities in the same range as collagen fibrils (pulp fibers: 5.4 GPa [150], collagen fibers: 5.5 GPa [151]. Thus, in our system, it is likely that the collagen fibrils interact with the wall during the tumbling motion. If one end of the fibril attaches to the surface, the remaining part can be aligned by the streaming fluid in a position of low hydrodynamic resistance, i.e. parallel

to the flow direction. However, due to additional interaction of the fibril with the surface, not all fibrils align parallel to the flow. The greater alignment of longer fibrils is consistent with the results of Holm et al. [148]: the number of fibers aligning in flow direction in the near wall region is higher for higher aspect ratios [152]. Since aspect ratios of the fibrils in our system are comparable to those of [152], inertia effects may additionally contribute to the increase of fibril alignment with increasing length. Thus, it can be concluded that fibril alignment is dependent on (i) the flow rate (which influences the shear stress/force in the system (tubing and channel)), (ii) the length of the fibrils, and to a lesser degree (iii) the viscosity of the solution (which also influences shear force, but in a much lower order than flow rate).

4.1.2 Functionalization with heparin

This section refers to parts of the following publication (see Appendix B):

Lanfer B., Seib F.P., Freudenberg U., Stamov D., Bley T., Bornhäuser M., Werner, C. The growth and differentiation of mesenchymal stem and progenitor cells cultured on aligned collagen matri*ces. Biomaterials* 30 (2009) 5950–5958.

It was the aim of this study to develop cell culture substrates/scaffolds that mimic extracellular matrix structures, specifically the anisotropic morphology found *in vivo*. Collagen type I was the material of choice due to its abundance, its importance for maintaining tissue integrity and its ability to interact with nearly 50 different molecules including almost all natural proteoglycans [153]. However, single component systems do not fully mirror the functional and structural complexity of the natural microenvironment. Besides providing adhesion sites and structural and mechanical stability the ECM allows the presentation of matrix-bound growth factors which in turn trigger important cellular functions. The functionality of collagen fibrils in terms of coupling, release and presence of growth factors is known to be affected by proteoglycans [154]. GAGs like heparin are responsible for the attachment of a variety of growth factors and proteins. Hence, in an effort to (a) demonstrate the visibility of the applied methodology to study multiple ECM components in a single system, (b) mimic the broad variety of ECM structures found *in vivo* more closely, and (c) study the impact of multiple biochemical cues in the set-up, the aligned collagen matrices were refined by incorporating the GAG heparin (Appendix B). The aligned collagen matrices were first reconstituted, then a heparin/PBS solution was subsequently streamed across. As a result, heparin co-localized with the corresponding fibrillar matrices, indicating that this 1-step functionalization process decorated most of the collagen fibrils with heparin. Heparin immobilization was shown to be stable for 3 days when incubated with culture medium. As already discussed in the previous sections many studies have recently addressed the additional incorporation of biochemical cues into systems with topographical features. For example synthetic materials exhibiting aligned topographical features have been coated with relevant ECM components to enhance certain cellular functions and differentiation [65]. In

comparison, our setup enables the study of two naturally derived ECM components that mimic the structural and functional complexity of natural ECM more closely. The functionalization of heparin is especially relevant for future applications as it allows the binding of certain growth factors that are specific to the target cell type or tissue engineering application. Thus, the rapid functionalization with heparin enables the study of multiple biochemical and physical cues in a single set-up and provides a versatile cell culture platform that can be tailored as needed.

4.2 Mesenchymal stem and progenitor cells cultured on aligned collagen matrices

This section refers to the following publication:

Lanfer B., Seib F.P., Freudenberg U., Stamov D., Bley T., Bornhäuser M., Werner, C. The growth and differentiation of mesenchymal stem and progenitor cells cultured on aligned collagen matri*ces. Biomaterials* 30 (2009) 5950–5958.

The influence of aligned structural cues on cell morphology and proliferation has been demonstrated in a number of studies. However, little is known about stem cell behavior. Although the pioneering work of Mc Beath et al. has demonstrated the effect of topographically patterned islands of different sizes on MSC fate, the impact of aligned topographies remains rather unclear. Therefore, human MSCs were cultured on aligned collagen and collagen/heparin matrices and differentiated along the adipogenic, osteogenic and chondrogenic lineages (Appendix B). In order to study the ability of aligned collagen structures to both guide and support morphogenesis of skeletal muscle tissue, C2C12 myoblasts were used as a model system. MSCs reacted to the physical signals from the substrates as their cell morphology altered to resemble the anisotropic topographies of the aligned ECM structures. Additionally, the aligned matrices supported mulitlineage differentiation of MSCs.

Most noticeable was that mineralization was highly organized and orchestrated by the underlying ECM, which served as a nucleation network. This was clearly demonstrated by aligned ECM structures that resulted in aligned mineralized nodules, indicating that cell-matrix interactions are precisely controlled by the topographical features of the ECM substrate. Considering the hierarchical structure of bone, i.e. ordered mineralization and oriented collagen type I fibrils, directed mineralization is an important prerequisite for mimicking *in vivo* bone formation. Thus, our results are important for bone tissue engineering and emphasize that cells reciprocally interact with surrounding ECM by adapting cell behavior and function to changes in ECM structure and topography. Interestingly, the extent of osteogenic differentiation was not significantly affected by aligned and functionalized (with heparin) substrates. In addition, cells showed similar differentiation behavior either in the presence or absence of collagen. This was surprising, since

several studies demonstrated accelerated mineralization by collagen type I [155]. However, it is possible that a critical collagen concentration is necessary to achieve this effect.

Adipogenic differentiation was well supported by the aligned matrices and MSCs developed into mature adipocytes. Although there are indications in literature that heparin enhances adipogenesis [156], no such effect was observed in the present study. It is still open to debate whether the presence of collagen causes this discrepancy.

A monolayer culture of MSCs in chondrogenic differentiation medium was carried out to examine the ability of the substrates to support chondrogenesis. A recent study by Wise et al. [118] reported the stimulating effect of aligned electrospun nanofibers on chondrogenic differentiation. In our study the cells increased sulfated GAG (sGAG) content when cultured in chondrogenic differentiation medium on aligned substrates, however there were no significant differences when compared to non-aligned matrices. This general increase in sGAG content might be due to increasing proteoglycan synthesis, a marker of early chondrogenesis. However, considering that the standard *in vitro* pellet culture for chondrogenic differentiation of MSCs was not feasible in the present system due to technical limitations, and cellular condensation is a prerequisite for chondrogenesis, a monolayer culture has its obvious limitations. This might also explain the contrary results obtained by Wise et al..

C2C12 cells were used to investigate the influence of topographical features on myoblast differentiation and myotube fusion. Aligned collagen matrices gave rise to aligned and highly organized myotubes, choreographed by the underlying fibrillar structures. It appeared that longer myotubes formed on aligned matrices than on randomly aligned ones although it was not possible to quantify the length of the myotubes due to technical limitations. Extending the width of aligned matrices to enable measurement of whole myotube length will certainly allow the quantification in future experiments. Our results have been in line with recent studies showing that C2C12 myoblasts align into parallel arrays that fuse to form oriented and longer myotubes in response to aligned topographies [157, 158].

4.3 Human neural stem cells cultured on aligned collagen matrices

This section refers to the following publication (see Appendix C):

Lanfer B., Hermann A., Kirsch M., Freudenberg U., Reuner U., Werner, C and Storch A. Directed Growth of Adult Human White Matter Stem Cell-derived Neurons on Aligned Fibrillar Collagen. *Accepted for publication in Tissue Engineering Part A.*

In the field of neural tissue engineering several studies have investigated axonal outgrowth and

differentiation of neural stem cells on aligned scaffolds (see table 2.4). However, mainly synthetic materials have been studied so that the effect of aligned collagen matrices on NSCs remains to be investigated. Therefore, human neural stem cells [159] were cultured on aligned collagen matrices with varying structural characteristics (Appendix C). We chose an human adult model system for two reasons: (a) the high developmental potential of fetal or embryonic stem cell-derived neurons could potentially skew observed effects and (b) a human model system is closest to a clinical application since animal models often do not accurately represent the human situation. With regard to the design of a 3D nerve conduit, the ideal case would be the use of adult human dorsal root ganglia and/or spinal cord neurons. However, these cells cannot be isolated for *in vitro* use after being fully differentiated. Therefore, NSCs derived from white matter were used, currently being the exclusive source of NSCs besides the hippocampus.

We demonstrated for the first time that neurite outgrowth of adult human nerve cells, derived from white-matter neural stem cells, can be choreographed by aligned collagen matrices. Neurites on aligned collagen were highly oriented in the direction of the underlying fibrils, while neurites on non-aligned collagen or control surfaces did not exhibit a preferred direction, forming instead a web-like morphology. Thus, the aligned matrices served as guidance cues to direct neurite outgrowth. This was especially apparent for matrices containing long fibrils at high density. Although the best alignment of collagen fibers in our study was seen using long fibrils at low density, the best neurite orientation was achieved on long fibrils at high density. It appeared that the exact interplay of collagen fibril alignment, density and length critically determined the extent of neurite alignment. Thus, aligned collagen matrices of varying structural properties allowed us to gain new insights with regard to NSC axon sprouting and neurite path finding. Another important finding of this study was enhanced neurite outgrowth on aligned collagen compared to non-aligned collagen. Moreover, the mean neurite length on non-aligned collagen was still higher than on control substrates. Fibril alignment, however, did not seem to influence differentiation behavior in our system. Obviously, the synergistic effect of physical cues (aligned fibrils) and biochemical signals (collagen) is crucial for optimal neurite outgrowth. These results are consistent with recently published studies [135, 134] and confirm the importance of biochemical cues to be incorporated in artificial guidance scaffolds. Additionally, it has been reported that neuronal differentiation of adult rat hippocampal progenitor cells co-cultured with astrocytes is enhanced on aligned polystyrene microgrooves compared to substrates without a pattern [65]. However, their differentiation is not affected when cultured on aligned or non-aligned substrates without astrocytes. Thus, it is likely that the absence of astrocytes as supporting feeder layer is responsible for the differentiation behavior in our system.

4.4 Cellulose hollow fiber membranes coated with aligned collagen for spinal cord regeneration

The following section refers to Appendix D.

The previous examples have shown that the established methodology is well suited to examine the impact of aligned ECM features on human stem/progenitor cells. However, to translate these studies into *in vivo* models there is the need to construct scaffolds that mimic the 3D cellular microenvironment. In particular, engineering of nervous tissue and nerve regeneration requires guidance scaffolds or materials that ideally have tubular/cylindrical geometries. Thus, the last part of this thesis aimed at developing a protocol to coat the interior side of cellulose hollow fiber membranes with longitudinally aligned collagen matrices.

Within this study we could show that streaming of a collagen solution through cellulose hollow fiber membranes results in longitudinally aligned collagen matrices inside the tubes. The collagen matrices deposited in the hollow fiber membranes closely resemble those characterized on planar substrates regarding fibril length and density. Thus, it can be expected that the variation of process-relevant parameters such as collagen solution concentration results in changes of matrices' morphology such as fibril length and density. This would enable the fabrication of matrices with specific characteristics tunable to the cell type of interest. In order to go beyond a single component system we additionally functionalized the matrices with heparin. This is especially interesting for further experiments in which heparin can mediate growth factor binding and release.

In some cases, however, rather non-aligned fibril coils or the absence of collagen reduced the quality of the deposited matrices. Therefore, we chemically modified the cellulose surface in an effort to improve collagen binding. The quality of the resultant matrices in terms of consistency and fibrils alignment varied remarkably ranging from non-coated hollow fiber membranes to well-deposited matrices. Thus, it is not yet clear whether the technical setup, the modification process or the collagen solution as such is responsible for this variation of reproducibility. Further experiments are necessary to optimize the technical setup in order to rule out possible artefacts during the streaming process. Our first cell culture experiments showed that hollow fiber membranes coated with aligned collagen well supported viability and adherence of spinal cord-derived neurospheres. In further experiments the influence of aligned collagen yet needs to be elucidated. In addition, it would be of great interest to study human white matter NSCs in cellulose hollow fiber membranes in a further step towards clinical application.

5 Summary and Outlook

The aim of this thesis was the development of a method to produce aligned collagen matrices. *In vitro* systems that mimic the aligned physiological architecture are necessary to understand the role of spatial cues in regulating cell and tissue functions and to engineer tissue for therapeutic applications. Towards this goal, a bottom-up approach from nanoscale fibrillar collagen to the assembly of cell and tissue structure was followed. This approach comprised four complimentary studies to address the following complementary issues: (i) the development of a method to align collagen type I matrices and the functionalization with heparin, (ii) the investigation of MSC growth and differentiation on aligned collagen matrices, (iii) the investigation of NSC growth and differentiation on aligned collagen matrices, and (iv) the incorporation of aligned collagen matrices in 3D guidance channels to be used for tissue regeneration.

The first task was accomplished within a first study (Appendix A) in which a new method to align collagen type I matrices was successfully established. Using an easy to handle microfluidic system, collagen type I matrices were created resembling those found in natural ECM. In order to mimc the versatile structures found in ECM, the new method allows the variation of alignment, density and morphology of the collagen matrices. This can be achieved by adjustment of the process-relevant parameters like flow rate, substrate and solution concentration. Besides varying physical characteristics of the matrices, additional biochemical cues were incorporated by decorating the reconstituted collagen scaffold with heparin. Thus, the versatility of this method enables quick and easy preparation of fine-tuned collagen matrices and the study of multiple cues in one system. The biochemical and physical characteristics can be controlled by varying morphology, density and alignment of the matrices and by the functionalization with heparin. In particular, these well-defined matrices provide an opportunity to characterize and control cell adhesion, orientation and migration.

Based on task 1, the second and third task was accomplished by studying cell-matrix interactions and cellular response to the aligned ECM structures produced by shear flow deposition. In the second study (Appendix B) the effects of aligned collagen/heparin matrices on the growth and differentiation of MSCs was investigated. It was found that aligned ECM structures dictate cell orientation and directly impact differentiation outcome. The aligned ECM matrices supported and maintained differentiation of MSCs along the osteogenic, adipogenic and chondrogenic lineage. Aligned collagen culture substrates were found to orchestrate and direct ordered matrix mineralization during osteogenesis of human MSCs. Furthermore, myotube assembly of C2C12s

was profoundly influenced by topographic features and aligned collagen could enhance myotube organization and length.

In the third study (Appendix C), the growth and differentiation of NSCs cultured on aligned collagen were analyzed. The results demonstrated that aligned collagen matrices served as guidance cues to direct neurite outgrowth of human NSCs along aligned collagen fibrils without affecting cell fate decisions or survival. By mimicking the size and fashion of endoneurium collagen alignment, the optimal orientation, density and length of collagen fibrils was effective in guiding and promoting human NSC-derived neuronal extensions. The exact interplay of collagen fibril alignment, density and length was found to be crucial, thus proving the importance of the developed shear flow deposition method to produce aligned collagen matrices of varying structural properties. Furthermore, the alignment of collagen fibrils enhanced neurite outgrowth. Hence, topographical cues seem to influence axon outgrowth, but additional biochemical cues, here collagen type I, also affect the speed of axonal outgrowth.

Based on task 1, 2 and 3 the fourth task was performed by engineering a new tubular scaffold containing aligned collagen fibrils in order to mimic the cell 3D microenvironment more closely (Appendix D). The inner surface of cellulose hollow fiber membranes were coated with aligned collagen fibrils and functionalized with heparin in accordance to the streaming protocol developed in the first part of this thesis. Axolotl spheroids were successfully cultured in these tubes and preliminary results point at improved adhesion and polarization of these cells when compared to uncoated, control surfaces.

Three important conclusions can be drawn deduced from the tasks performed: (i) aligned matrices with varying biochemical and physical characteristics can be produced using microfluidic techniques, (ii) aligned collagen matrices (optionally functionalized with heparin) can guide and support stem cell alignment and differentiation, and (iii) the method for collagen alignment can be employed to produce more clinically relevant cylindrical scaffolds containing aligned collagen fibrils for 3D spheroid cell culture.

Together, the obtained results prove the applicability of the new method to versatile microfluidic channel geometries including hollow fiber membranes. In addition, a recent study by Saeidi et al. [160] recapitulated the formation of aligned collagen fibrils under shear-flow conditions. This group confirmed the feasibility of the new method to generate aligned collagen matrices using a commercially available perfusion chamber.

While the results of this thesis project are promising, they also demonstrate important areas where further research is required. Since aligned collagen matrices guide mesenchymal and neural stem cell behavior and function, this platform has the potential to possibly guide morphogenesis of other tissue types with anisotropic structure, e.g., cardiac muscle, cornea, blood vessel, tendon, and ligament. Thus, further culture of different cell types, for instance photoreceptor retina

cells or endothelial cells, would be beneficial to validate the advantages of this method. In such efforts, the immobilization of heparin could provide a means for growth factor presentation. Depending on the application of interest, binding and release of growth factors like nerve growth factor or vascular endothelial growth factor could yield crucial effects in cell culture experiments. The generation of gradients of growth factors along the matrices would offer valuable options for advanced cell culture technology. Additionally, other extracellular matrix components like fibrin could be employed using this approach to create aligned fiber matrices. Likewise, the incorporation of laminin in a multiple component approach is likely to prove rewarding for neural tissue engineering applications. With regard to future clinical applications the use of human cells within this study holds advantages. In an effort to push research towards clinical applications these cells could be tested in a clinically more relevant environment using coated cellulose hollow fiber membranes. In particular, considering the potential of the coated cellulose hollow fiber membranes to be used as nerve guidance conduit, the employment of human white-matter derived NSCs or other relevant cell types derived from the peripheral nervous system is highly intriguing. Likewise, further experiments involving axolotl neurospheres combined in one system with aligned collagen fibrils and relevant growth factors could provide new insights into regeneration mechanisms in general and pave the way to whole spinal cord regeneration.

Bibliography

[1] L. E. Niklason and R. Langer. Prospects for organ and tissue replacement. *JAMA*, 285(5):573–576, Feb 2001.

[2] J. R. Fuchs, B. A. Nasseri, and J. P. Vacanti. Tissue engineering: a 21st century solution to surgical reconstruction. *Ann Thorac Surg*, 72(2):577–591, Aug 2001.

[3] R. Langer and J. P. Vacanti. Tissue engineering. *Science*, 260(5110):920–926, May 1993.

[4] Elsie S Place, Nicholas D Evans, and Molly M Stevens. Complexity in biomaterials for tissue engineering. *Nat Mater*, 8(6):457–470, Jun 2009.

[5] Anthony Atala, Stuart B Bauer, Shay Soker, James J Yoo, and Alan B Retik. Tissue-engineered autologous bladders for patients needing cystoplasty. *Lancet*, 367(9518):1241–1246, Apr 2006.

[6] B.D. Ratner and S.J. Bryant. Biomaterials: where we have been and where we are going. *Annual Review Biomedical Engineering*, 6:41–75, 2004.

[7] M.P. Lutolf and J.A. Hubbell. Synthetic biomaterials as instructive extracellular microenvironments for morphogenesis in tissue engineering. *Nat Biotechnol*, 23(1):47–55, January 2005.

[8] Paolo Macchiarini, Philipp Jungebluth, Tetsuhiko Go, M. Adelaide Asnaghi, Louisa E Rees, Tristan A Cogan, Amanda Dodson, Jaume Martorell, Silvia Bellini, Pier Paolo Parnigotto, Sally C Dickinson, Anthony P Hollander, Sara Mantero, Maria Teresa Conconi, and Martin A Birchall. Clinical transplantation of a tissue-engineered airway. *Lancet*, 372(9655):2023–2030, Dec 2008.

[9] T. Kreis and R. Vale. *Extracellular Matrix and adhesion proteins.* Oxford University, 1993.

[10] P. Wassarman and J. Miner. *Extracellular Matrix in development and disease: advances in developmental biology*, volume 15. Elsevier, Amsterdam, 2005.

[11] Neil A. Campbell. *Biology.* Benjamin Cummings, 2004.

[12] M. van der Rest and R. Garrone. Collagen family of proteins. *FASEB J*, 5(13):2814–2823, Oct 1991.

[13] Sylvie Ricard-Blum and Florence Ruggiero. The collagen superfamily: from the extracellular matrix to the cell membrane. *Pathol Biol (Paris)*, 53(7):430–442, Sep 2005.

[14] J.P. Orgel, A. Miller, T.C. Irving, R.F. Fischetti, A.P. Hammersley, and T.J. Wess. The in situ supermolecular structure of type i collagen. *Structure*, 9(11):1061–1069, November 2001.

[15] D.J. Hulmes. Building collagen molecules, fibrils, and suprafibrillar structures. *J Struct.Biol*, 137(1-2):2–10, January 2002.

[16] Karl E Kadler, Adele Hill, and Elizabeth G Canty-Laird. Collagen fibrillogenesis: fibronectin, integrins, and minor collagens as organizers and nucleators. *Curr Opin Cell Biol*, 20(5):495–501, Oct 2008.

[17] S.P. Evanko and K.G. Vogel. Ultrastructure and proteoglycan composition in the developing fibrocartilaginous region of bovine tendon. *Matrix*, 10(6):420–436, Dec 1990.

[18] E.G. Canty and K.E. Kadler. Procollagen trafficking, processing and fibrillogenesis. *J Cell Sci*, 118(Pt 7):1341–1353, April 2005.

[19] Jeanette M Waller and Howard I Maibach. Age and skin structure and function, a quantitative approach (ii): protein, glycosaminoglycan, water, and lipid content and structure. *Skin Res Technol*, 12(3):145–154, Aug 2006.

[20] K. M. Meek, D. W. Leonard, C. J. Connon, S. Dennis, and S. Khan. Transparency, swelling and scarring in the corneal stroma. *Eye*, 17(8):927–936, Nov 2003.

[21] C.E. Schmidt and J.B. Leach. Neural tissue engineering: strategies for repair and regeneration. *Annu Rev Biomed Eng*, 5:293–347, 2003.

[22] B. Alberts. *Molecular Biology of the Cell*. Garland Publishing, 2004.

[23] D. Aviezer, E. Levy, M. Safran, C. Svahn, E. Buddecke, A. Schmidt, G. David, I. Vlodavsky, and A. Yayon. Differential structural requirements of heparin and heparan sulfate proteoglycans that promote binding of basic fibroblast growth factor to its receptor. *J Biol Chem*, 269(1):114–121, Jan 1994.

[24] G.R. Johnson and L. Wong. Heparan sulfate is essential to amphiregulin-induced mitogenic signaling by the epidermal growth factor receptor. *Journal of Biological Chemistry*, 269:27149–54, 1994.

[25] D. Moscatelli. Basic fibroblast growth factor (bfgf) dissociates rapidly from heparan sulfates but slowly from receptors. implications for mechanisms of bfgf release from pericellular matrix. *J Biol Chem*, 267(36):25803–25809, Dec 1992.

[26] A. Lookene, R. Savonen, and G. Olivecrona. Interaction of lipoproteins with heparan sulfate proteoglycans and with lipoprotein lipase. studies by surface plasmon resonance technique. *Biochemistry*, 36(17):5267–5275, Apr 1997.

[27] Francesco Rosso, Antonio Giordano, Manlio Barbarisi, and Alfonso Barbarisi. From cell-ecm interactions to tissue engineering. *J Cell Physiol*, 199(2):174–180, May 2004.

[28] C. Werner, T. Pompe, and K. Salchert. Modulating extracellular matrix at interfaces of polymeric materials. *Polymers For Regenerative Medicine*, pages 63–93, 2006.

[29] Jane Sottile and Denise C Hocking. Fibronectin polymerization regulates the composition and stability of extracellular matrix fibrils and cell-matrix adhesions. *Mol Biol Cell*, 13(10):3546–3559, Oct 2002.

[30] William P Daley, Sarah B Peters, and Melinda Larsen. Extracellular matrix dynamics in development and regenerative medicine. *J Cell Sci*, 121(Pt 3):255–264, Feb 2008.

[31] Jie Li, Yan-Ping Zhang, and Robert S Kirsner. Angiogenesis in wound repair: angiogenic growth factors and the extracellular matrix. *Microsc Res Tech*, 60(1):107–114, Jan 2003.

[32] Amy Rachfal and David Brigstock. Connective tissue growth factor (ctgf/ccn2) in hepatic fibrosis. *Hepatol Res*, 26(1):1–9, May 2003.

[33] M. T. Huhtala, O. T. Pentikäinen, and M. S. Johnson. A dimeric ternary complex of fgfr [correction of fgfr1], heparin and fgf-1 leads to an 'electrostatic sandwich' model for heparin binding. *Structure*, 7(6):699–709, Jun 1999.

[34] D. Moscatelli. Metabolism of receptor-bound and matrix-bound basic fibroblast growth factor by bovine capillary endothelial cells. *J Cell Biol*, 107(2):753–759, Aug 1988.

[35] D. Riveline, E. Zamir, N. Q. Balaban, U. S. Schwarz, T. Ishizaki, S. Narumiya, Z. Kam, B. Geiger, and A. D. Bershadsky. Focal contacts as mechanosensors: externally applied local mechanical force induces growth of focal contacts by an mdia1-dependent and rock-independent mechanism. *J Cell Biol*, 153(6):1175–1186, Jun 2001.

[36] Tony Yeung, Penelope C Georges, Lisa A Flanagan, Beatrice Marg, Miguelina Ortiz, Makoto Funaki, Nastaran Zahir, Wenyu Ming, Valerie Weaver, and Paul A Janmey. Effects of substrate stiffness on cell morphology, cytoskeletal structure, and adhesion. *Cell Motil Cytoskeleton*, 60(1):24–34, Jan 2005.

[37] Penelope C Georges, William J Miller, David F Meaney, Evelyn S Sawyer, and Paul A Janmey. Matrices with compliance comparable to that of brain tissue select neuronal over glial growth in mixed cortical cultures. *Biophys J*, 90(8):3012–3018, Apr 2006.

[38] Michele A Wozniak, Radhika Desai, Patricia A Solski, Channing J Der, and Patricia J Keely. Rock-generated contractility regulates breast epithelial cell differentiation in response to the physical properties of a three-dimensional collagen matrix. *J Cell Biol*, 163(3):583–595, Nov 2003.

[39] A. Engler, L. Bacakova, C. Newman, A. Hategan, M. Griffin, and D. Discher. Substrate compliance versus ligand density in cell on gel responses. *Biophys.J*, 86(1 Pt 1):617–628, January 2004.

[40] D. Discher, P. Janmey, and Y.L. Wang. Tissue cells feel and respond to the stiffness of their substrate. *Science*, 310(5751):1139–1143, Nov 2005.

[41] A.J. Engler, S. Sen, H.L. Sweeney, and D.E. Discher. Matrix elasticity directs stem cell lineage specification. *Cell*, 126(4):677–689, August 2006.

[42] O. Akhouayri, M. H. Lafage-Proust, A. Rattner, N. Laroche, A. Caillot-Augusseau, C. Alexandre, and L. Vico. Effects of static or dynamic mechanical stresses on osteoblast phenotype expression in three-dimensional contractile collagen gels. *J Cell Biochem*, 76(2):217–230, Dec 1999.

[43] R. G. Harrison. The cultivation of tissues in extraneous media as a method of morphogenetic study. *The Anatomical Record*, 6:182–93, 1912.

[44] P. Weiss. Experiments on cell and axon orientation in vitro: the role of colloidal exudates in tissue organization. *Journal of Experimental Zoology*, 100:353–386, 1945.

[45] A. S. Curtis and C. D. Wilkinson. Reactions of cells to topography. *J Biomater Sci Polym Ed*, 9(12):1313–1329, 1998.

[46] E.S. Stuart and A.A. Moscona. Embryonic morphogenesis: role of fibrous lattice in the development of feathers and feather patterns. *Science*, 157(3791):947–948, Aug 1967.

[47] J.B. Bard and K. Higginson. Fibroblast-collagen interactions in the formation of the secondary stroma of the chick cornea. *J Cell Biol*, 74(3):816–827, Sep 1977.

[48] J. Lofberg. Scanning and transmission electron microscopy of early neural crest cell migration and extracellular fiber systems in the amphibian embryo. *J. Ultrastruct. Res.*, 159:484, 1976.

[49] R. Singhvi, A. Kumar, G.P. Lopez, G.N. Stephanopoulos, D.I. Wang, G.M. Whitesides, and D.E. Ingber. Engineering cell shape and function. *Science*, 264(5159):696–698, Apr 1994.

[50] C.S. Chen, M. Mrksich, S. Huang, G.M. Whitesides, and D.E. Ingber. Geometric control of cell life and death. *Science*, 276(5317):1425–1428, May 1997.

[51] N. Wang, J.P. Butler, and D.E. Ingber. Mechanotransduction across the cell surface and through the cytoskeleton. *Science*, 260(5111):1124–1127, May 1993.

[52] D.E. Ingber. Tensegrity ii. how structural networks influence cellular information processing networks. *J Cell Sci*, 116(Pt 8):1397–1408, Apr 2003.

[53] D.E. Ingber. Tensegrity i. cell structure and hierarchical systems biology. *J Cell Sci*, 116(Pt 7):1157–1173, Apr 2003.

[54] R. McBeath, D.M. Pirone, C.M. Nelson, K. Bhadriraju, and C.S. Chen. Cell shape, cytoskeletal tension, and rhoa regulate stem cell lineage commitment. *Dev.Cell*, 6(4):483–495, April 2004.

[55] K.L. Elias, R.L. Price, and T.J. Webster. Enhanced functions of osteoblasts on nanometer diameter carbon fibers. *Biomaterials*, 23(15):3279–3287, August 2002.

[56] C. Vieu, F. Carcenac, A. Pepin, Y. Chen, M. Mejias, L. Lebib, A.and Manin-Ferlazzo, L. Couraud, and H. Launois. Electron beam lithography: Resolution limits and applications. *Applied Surface Science*, pages 111–117, 2000.

[57] E. Martínez, E. Engel, C. López-Iglesias, C. A. Mills, J. A. Planell, and J. Samitier. Focused ion beam/scanning electron microscopy characterization of cell behavior on polymer micro-/nanopatterned substrates: a study of cell-substrate interactions. *Micron*, 39(2):111–116, 2008.

[58] Jung Yul Lim and Henry J Donahue. Cell sensing and response to micro- and nanostructured surfaces produced by chemical and topographic patterning. *Tissue Eng*, 13(8):1879–1891, Aug 2007.

[59] C. S. Chen, M. Mrksich, S. Huang, G. M. Whitesides, and D. E. Ingber. Micropatterned surfaces for control of cell shape, position, and function. *Biotechnol Prog*, 14(3):356–363, 1998.

[60] A. Goessl, D.F. Bowen-Pope, and A.S. Hoffman. Control of shape and size of vascular

smooth muscle cells in vitro by plasma lithography. *Journal of Biomedical Materials Research*, 57:15–24, 2001.

[61] F. Yang, R. Murugan, S. Wang, and S. Ramakrishna. Electrospinning of nano/micro scale poly(l-lactic acid) aligned fibers and their potential in neural tissue engineering. *Biomaterials*, 26(15):2603–2610, May 2005.

[62] J.A. Matthews, G.E. Wnek, D.G. Simpson, and G.L. Bowlin. Electrospinning of collagen nanofibers. *Biomacromolecules*, 3(2):232–238, March 2002.

[63] C. Y. Xu, R. Inai, M. Kotaki, and S. Ramakrishna. Aligned biodegradable nanofibrous structure: a potential scaffold for blood vessel engineering. *Biomaterials*, 25(5):877–886, Feb 2004.

[64] Quynh P Pham, Upma Sharma, and Antonios G Mikos. Electrospinning of polymeric nanofibers for tissue engineering applications: a review. *Tissue Eng*, 12(5):1197–1211, May 2006.

[65] J.B. Recknor, D.S. Sakaguchi, and S.K. Mallapragada. Directed growth and selective differentiation of neural progenitor cells on micropatterned polymer substrates. *Biomaterials*, 27(22):4098–4108, August 2006.

[66] Robert A Brown and James B Phillips. Cell responses to biomimetic protein scaffolds used in tissue repair and engineering. *Int Rev Cytol*, 262:75–150, 2007.

[67] J. Gross and D. Kirk. The heat precipitation of collagen from neutral salt solutions: some rate-regulating factors. *J.Biol.Chem.*, 233(2):355–360, August 1958.

[68] K.E. Kadler, Y. Hojima, and D.J. Prockop. Assembly of collagen fibrils de novo by cleavage of the type i pc-collagen with procollagen c-proteinase. assay of critical concentration demonstrates that collagen self-assembly is a classical example of an entropy-driven process. *J Biol Chem.*, 262(32):15696–15701, November 1987.

[69] N. Kuznetsova, S.L. Chi, and S. Leikin. Sugars and polyols inhibit fibrillogenesis of type i collagen by disrupting hydrogen-bonded water bridges between the helices. *Biochemistry*, 37(34):11888–11895, August 1998.

[70] T. Elsdale and J. Bard. Collagen substrata for studies on cell behavior. *J Cell Biol*, 54(3):626–637, September 1972.

[71] J. Torbet and M.C. Ronziere. Magnetic alignment of collagen during self-assembly. *Biochem J*, 219(3):1057–1059, May 1984.

[72] H. B. Benjamin, E. Pawlowski, and A. B. Becker. Collagen as temporary dressing and blood vessel replacement. *Arch Surg*, 88:725–727, May 1964.

[73] C. Guo and L.J. Kaufman. Flow and magnetic field induced collagen alignment. *Biomaterials*, 28(6):1105–1114, February 2007.

[74] P. Lee, R. Lin, J. Moon, and L.P. Lee. Microfluidic alignment of collagen fibers for in vitro cell culture. *Biomed Microdevices.*, 8(1):35–41, March 2006.

[75] J. Torbet, M. Malbouyres, N. Builles, V. Justin, M. Roulet, O. Damour, A. Oldberg, F. Ruggiero, and D.J. Hulmes. Orthogonal scaffold of magnetically aligned collagen lamellae for corneal stroma reconstruction. *Biomaterials*, 28(29):4268–4276, October 2007.

[76] F. Jiang, K. Khairy, K. Poole, J. Howard, and D.J. Muller. Creating nanoscopic collagen matrices using atomic force microscopy. *Microsc.Res Tech.*, 64(5-6):435–440, August 2004.

[77] D.A. Cisneros, C. Hung, C.M. Franz, and D.J. Muller. Observing growth steps of collagen self-assembly by time-lapse high-resolution atomic force microscopy. *J Struct Biol*, 154(3):232–245, June 2006.

[78] Gregory T Christopherson, Hongjun Song, and Hai-Quan Mao. The influence of fiber diameter of electrospun substrates on neural stem cell differentiation and proliferation. *Biomaterials*, 30(4):556–564, Feb 2009.

[79] Xu Jiang, Shawn H Lim, Hai-Quan Mao, and Sing Yian Chew. Current applications and future perspectives of artificial nerve conduits. *Exp Neurol*, Sep 2009.

[80] K. Matsumoto, K. Ohnishi, T. Kiyotani, T. Sekine, H. Ueda, T. Nakamura, K. Endo, and Y. Shimizu. Peripheral nerve regeneration across an 80-mm gap bridged by a polyglycolic acid (pga)-collagen tube filled with laminin-coated collagen fibers: a histological and electrophysiological evaluation of regenerated nerves. *Brain Res*, 868(2):315–328, Jun 2000.

[81] R. Murugan and S. Ramakrishna. Design strategies of tissue engineering scaffolds with controlled fiber orientation. *Tissue Engineering*, 13(8):1845–1866, August 2007.

[82] A. S. Blawas and W. M. Reichert. Protein patterning. *Biomaterials*, 19(7-9):595–609, 1998.

[83] Mark-Anthony Bray, Sean P Sheehy, and Kevin Kit Parker. Sarcomere alignment is regulated by myocyte shape. *Cell Motil Cytoskeleton*, 65(8):641–651, Aug 2008.

[84] Shaoping Zhong, Wee Eong Teo, Xiao Zhu, Roger W Beuerman, Seeram Ramakrishna, and Lin Yue Lanry Yung. An aligned nanofibrous collagen scaffold by electrospinning and its effects on in vitro fibroblast culture. *J Biomed Mater Res A*, 79(3):456–463, Dec 2006.

[85] Wei He, Thomas Yong, Zu Wei Ma, Ryuji Inai, Wee Eong Teo, and Seeram Ramakrishna. Biodegradable polymer nanofiber mesh to maintain functions of endothelial cells. *Tissue Eng*, 12(9):2457–2466, Sep 2006.

[86] Haoqing Cao, Kevin McHugh, Sing Yian Chew, and James M Anderson. The topographical effect of electrospun nanofibrous scaffolds on the in vivo and in vitro foreign body reaction. *J Biomed Mater Res A*, Sep 2009.

[87] M. Karperien. *Tissue engineering*. Academic Press, 2008.

[88] A. J. Bekcer, E. A. McCulloch, and J. E. Till. Cytological demonstration of the clonal nature of spleen colonies derived from transplanted mouse marrow cells. *Nature*, 197:452–454, Feb 1963.

[89] A. J. Friedenstein, K. V. Petrakova, A. I. Kurolesova, and G. P. Frolova. Heterotopic of bone marrow.analysis of precursor cells for osteogenic and hematopoietic tissues. *Transplantation*, 6(2):230–247, Mar 1968.

[90] P. Bianco, M. Riminucci, S. Gronthos, and P. G. Robey. Bone marrow stromal stem cells: nature, biology, and potential applications. *Stem Cells*, 19(3):180–192, 2001.

[91] M. Dominici, K. Le Blanc, I. Mueller, I. Slaper-Cortenbach, Fc Marini, Ds Krause, Rj Deans, A. Keating, Dj Prockop, and Em Horwitz. Minimal criteria for defining multipotent mesenchymal stromal cells. the international society for cellular therapy position statement. *Cytotherapy*, 8(4):315–317, 2006.

[92] M.F. Pittenger, A.M. Mackay, S.C. Beck, R.K. Jaiswal, R. Douglas, J.D. Mosca, M.A. Moorman, D.W. Simonetti, S. Craig, and D.R. Marshak. Multilineage potential of adult human mesenchymal stem cells. *Science*, 284(5411):143–147, April 1999.

[93] A. I. Caplan. Mesenchymal stem cells. *J Orthop Res*, 9(5):641–650, Sep 1991.

[94] S. E. Haynesworth, J. Goshima, V. M. Goldberg, and A. I. Caplan. Characterization of cells with osteogenic potential from human marrow. *Bone*, 13(1):81–88, 1992.

[95] J. U. Yoo, T. S. Barthel, K. Nishimura, L. Solchaga, A. I. Caplan, V. M. Goldberg, and B. Johnstone. The chondrogenic potential of human bone-marrow-derived mesenchymal progenitor cells. *J Bone Joint Surg Am*, 80(12):1745–1757, Dec 1998.

[96] S. Wakitani, T. Saito, and A. I. Caplan. Myogenic cells derived from rat bone marrow mesenchymal stem cells exposed to 5-azacytidine. *Muscle Nerve*, 18(12):1417–1426, Dec 1995.

[97] M.K. Majumdar, M.A. Thiede, J.D. Mosca, M. Moorman, and S.L. Gerson. Phenotypic and functional comparison of cultures of marrow-derived mesenchymal stem cells (mscs) and stromal cells. *J.Cell Physiol*, 176(1):57–66, July 1998.

[98] R. G. Young, D. L. Butler, W. Weber, A. I. Caplan, S. L. Gordon, and D. J. Fink. Use of mesenchymal stem cells in a collagen matrix for achilles tendon repair. *J Orthop Res*, 16(4):406–413, Jul 1998.

[99] J. E. Dennis, A. Merriam, A. Awadallah, J. U. Yoo, B. Johnstone, and A. I. Caplan. A quadripotential mesenchymal progenitor cell isolated from the marrow of an adult mouse. *J Bone Miner Res*, 14(5):700–709, May 1999.

[100] Matus Studeny, Frank C Marini, Jennifer L Dembinski, Claudia Zompetta, Maria Cabreira-Hansen, Benjamin Nebiyou Bekele, Richard E Champlin, and Michael Andreeff. Mesenchymal stem cells: potential precursors for tumor stroma and targeted-delivery vehicles for anticancer agents. *J Natl Cancer Inst*, 96(21):1593–1603, Nov 2004.

[101] G. I. Im, D. Y. Kim, J. H. Shin, C. W. Hyun, and W. H. Cho. Repair of cartilage defect in the rabbit with cultured mesenchymal stem cells from bone marrow. *J Bone Joint Surg Br*, 83(2):289–294, Mar 2001.

[102] Donald Orlic, Jan Kajstura, Stefano Chimenti, David M Bodine, Annarosa Leri, and Piero Anversa. Bone marrow stem cells regenerate infarcted myocardium. *Pediatr Transplant*, 7 Suppl 3:86–88, 2003.

[103] Shuji Terai, Naoki Yamamoto, Kaoru Omori, Isao Sakaida, and Kiwamu Okita. A new cell therapy using bone marrow cells to repair damaged liver. *J Gastroenterol*, 37 Suppl 14:162–163, Nov 2002.

[104] M. Chopp, X. H. Zhang, Y. Li, L. Wang, J. Chen, D. Lu, M. Lu, and M. Rosenblum. Spinal

cord injury in rat: treatment with bone marrow stromal cell transplantation. *Neuroreport*, 11(13):3001–3005, Sep 2000.

[105] E. Mansilla, G. H. Marin, F. Sturla, H. E. Drago, M. A. Gil, E. Salas, M. C. Gardiner, G. Piccinelli, S. Bossi, E. Salas, L. Petrelli, G. Iorio, C. A. Ramos, and C. Soratti. Human mesenchymal stem cells are tolerized by mice and improve skin and spinal cord injuries. *Transplant Proc*, 37(1):292–294, 2005.

[106] S. Makino, K. Fukuda, S. Miyoshi, F. Konishi, H. Kodama, J. Pan, M. Sano, T. Takahashi, S. Hori, H. Abe, J. Hata, A. Umezawa, and S. Ogawa. Cardiomyocytes can be generated from marrow stromal cells in vitro. *J Clin Invest*, 103(5):697–705, Mar 1999.

[107] S. F. Konieczny and C. P. Emerson. 5-azacytidine induction of stable mesodermal stem cell lineages from 10t1/2 cells: evidence for regulatory genes controlling determination. *Cell*, 38(3):791–800, Oct 1984.

[108] B. Balana, C. Nicoletti, I. Zahanich, E.M. Graf, T. Christ, S. Boxberger, and U. Ravens. 5-azacytidine induces changes in electrophysiological properties of human mesenchymal stem cells. *Cell Research*, 16(12):949–960, December 2006.

[109] Y. Liu, J.A. Song, W.X. Liu, Y. Wan, X.C. Chen, and C.J. Hu. Growth and differentiation of rat bone marrow stromal cells: does 5-azacytidine trigger their cardiomyogenic differentiation? *Cardiovascular Research*, 58(2):460–468, May 2003.

[110] A. I. Caplan and S. P. Bruder. Mesenchymal stem cells: building blocks for molecular medicine in the 21st century. *Trends Mol Med*, 7(6):259–264, Jun 2001.

[111] E. Martínez, A. Lagunas, C. A. Mills, S. Rodríguez-Seguí, M. Estévez, S. Oberhansl, J. Comelles, and J. Samitier. Stem cell differentiation by functionalized micro- and nanostructured surfaces. *Nanomed*, 4(1):65–82, Jan 2009.

[112] A. Banfi, A. Muraglia, B. Dozin, M. Mastrogiacomo, R. Cancedda, and R. Quarto. Proliferation kinetics and differentiation potential of ex vivo expanded human bone marrow stromal cells: Implications for their use in cell therapy. *Exp Hematol*, 28(6):707–715, Jun 2000.

[113] B. M. Spiegelman and C. A. Ginty. Fibronectin modulation of cell shape and lipogenic gene expression in 3t3-adipocytes. *Cell*, 35(3 Pt 2):657–666, Dec 1983.

[114] R. S. Carvalho, J. L. Schaffer, and L. C. Gerstenfeld. Osteoblasts induce osteopontin expression in response to attachment on fibronectin: demonstration of a common role for integrin receptors in the signal transduction processes of cell attachment and mechanical stimulation. *J Cell Biochem*, 70(3):376–390, Sep 1998.

[115] Béatrice Thomas, Sylvie Thirion, Lydie Humbert, Lujian Tan, Mary B Goldring, Gilbert Bérézíat, and Francis Berenbaum. Differentiation regulates interleukin-1beta-induced cyclo-oxygenase-2 in human articular chondrocytes: role of p38 mitogen-activated protein kinase. *Biochem J*, 362(Pt 2):367–373, Mar 2002.

[116] M.J. Dalby, N. Gadegaard, R. Tare, A. Andar, M.O. Riehle, P. Herzyk, C.D. Wilkinson, and R.O. Oreffo. The control of human mesenchymal cell differentiation using nanoscale symmetry and disorder. *Nat.Mater.*, 6(12):997–1003, December 2007.

[117] S. Oh, K.S. Brammer, Y.S. Li, D. Teng, A.J. Engler, S. Chien, and S. Jin. Stem cell fate dictated solely by altered nanotube dimension. *Proc.Natl.Acad.Sci U.S.A*, 106(7):2130–2135, February 2009.

[118] J.K. Wise, A.L. Yarin, C.M. Megaridis, and M. Cho. Chondrogenic differentiation of human mesenchymal stem cells on oriented nanofibrous scaffolds: Engineering the superficial zone of articular cartilage. *Tissue Engineering Part A*, 15(4):913–921, April 2009.

[119] Evelyn K F Yim, Stella W Pang, and Kam W Leong. Synthetic nanostructures inducing differentiation of human mesenchymal stem cells into neuronal lineage. *Exp Cell Res*, 313(9):1820–1829, May 2007.

[120] F. H. Gage. Mammalian neural stem cells. *Science*, 287(5457):1433–1438, Feb 2000.

[121] E. Cattaneo and R. McKay. Proliferation and differentiation of neuronal stem cells regulated by nerve growth factor. *Nature*, 347(6295):762–765, Oct 1990.

[122] S. Temple. Division and differentiation of isolated cns blast cells in microculture. *Nature*, 340(6233):471–473, Aug 1989.

[123] D. L. Stemple and D. J. Anderson. Isolation of a stem cell for neurons and glia from the mammalian neural crest. *Cell*, 71(6):973–985, Dec 1992.

[124] C. Lois and A. Alvarez-Buylla. Proliferating subventricular zone cells in the adult mammalian forebrain can differentiate into neurons and glia. *Proc Natl Acad Sci U S A*, 90(5):2074–2077, Mar 1993.

[125] B. A. Reynolds and S. Weiss. Generation of neurons and astrocytes from isolated cells of the adult mammalian central nervous system. *Science*, 255(5052):1707–1710, Mar 1992.

[126] Elizabeth Gould and Charles G Gross. Neurogenesis in adult mammals: some progress and problems. *J Neurosci*, 22(3):619–623, Feb 2002.

[127] D. R. Kornack and P. Rakic. The generation, migration, and differentiation of olfactory neurons in the adult primate brain. *Proc Natl Acad Sci U S A*, 98(8):4752–4757, Apr 2001.

[128] Andreas Hermann. *In vitro neurogenesis of adult neural stem cells from bone marrow and brain*. PhD thesis, Universität Ulm, 2006.

[129] Xuejun Wen and Patrick A Tresco. Effect of filament diameter and extracellular matrix molecule precoating on neurite outgrowth and schwann cell behavior on multifilament entubulation bridging device in vitro. *J Biomed Mater Res A*, 76(3):626–637, Mar 2006.

[130] Z. Ahmed and R. A. Brown. Adhesion, alignment, and migration of cultured schwann cells on ultrathin fibronectin fibres. *Cell Motil Cytoskeleton*, 42(4):331–343, 1999.

[131] Roy Biran, Mark D Noble, and Patrick A Tresco. Directed nerve outgrowth is enhanced by engineered glial substrates. *Exp Neurol*, 184(1):141–152, Nov 2003.

[132] D. Ceballos, X. Navarro, N. Dubey, G. Wendelschafer-Crabb, W.R. Kennedy, and R.T. Tranquillo. Magnetically aligned collagen gel filling a collagen nerve guide improves peripheral nerve regeneration. *Exp Neurol.*, 158(2):290–300, August 1999.

[133] N. Dubey, P.C. Letourneau, and R.T. Tranquillo. Guided neurite elongation and schwann cell invasion into magnetically aligned collagen in simulated peripheral nerve regeneration. *Exp Neurol.*, 158(2):338–350, August 1999.

[134] Joseph M Corey, David Y Lin, Katherine B Mycek, Qiaoran Chen, Stanley Samuel, Eva L Feldman, and David C Martin. Aligned electrospun nanofibers specify the direction of dorsal root ganglia neurite growth. *J Biomed Mater Res A*, 83(3):636–645, Dec 2007.

[135] Cheryl Miller, Srdija Jeftinija, and Surya Mallapragada. Synergistic effects of physical and chemical guidance cues on neurite alignment and outgrowth on biodegradable polymer substrates. *Tissue Eng*, 8(3):367–378, Jul 2002.

[136] Jianming Li, Helen McNally, and Riyi Shi. Enhanced neurite alignment on micro-patterned poly-l-lactic acid films. *J Biomed Mater Res A*, 87(2):392–404, Nov 2008.

[137] T. Pompe, S. Zschoche, N. Herold, K. Salchert, M.F. Gouzy, C. Sperling, and C. Werner. Maleic anhydride copolymers–a versatile platform for molecular biosurface engineering. *Biomacromolecules*, 4(4):1072–1079, July 2003.

[138] M.M. Giraud-Guille. Liquid crystallinity in condensed type i collagen solutions. a clue to the packing of collagen in extracellular matrices. *J Mol.Biol*, 224(3):861–873, April 1992.

[139] R. Martin, J. Farjanel, D. Eichenberger, A. Colige, E. Kessler, D.J. Hulmes, and M.M. Giraud-Guille. Liquid crystalline ordering of procollagen as a determinant of three-dimensional extracellular matrix architecture. *J Mol Biol*, 301(1):11–17, August 2000.

[140] K. Salchert, U. Streller, T. Pompe, N. Herold, M. Grimmer, and C. Werner. In vitro reconstitution of fibrillar collagen type i assemblies at reactive polymer surfaces. *Biomacromolecules*, 5(4):1340–1350, July 2004.

[141] W.D. Comper and A. Veis. The mechanism of nucleation for in vitro collagen fibril formation. *Biopolymers*, 16(10):2113–2131, October 1977.

[142] T. Dabros. A singularity method for calculating hydrodynamic-forces and particle velocities in low-reynolds-number flows. *Journal of Fluid Mechanics*, 156(JUL):1–21, 1985.

[143] E. Gavze and M. Shapiro. Particles in a shear flow near a solid wall: Effect of nonsphericity on forces and velocities. *International Journal of Multiphase Flow*, 23(1):155–182, February 1997.

[144] C.A. Stover and C. Cohen. The motion of rodlike particles in the pressure-driven flow between 2 flat plates. *Rheologica Acta*, 29(3):192–203, May 1990.

[145] C. Pozrikidis. Orbiting motion of a freely suspended spheroid near a plane wall. *Journal of Fluid Mechanics*, 541:105–114, October 2005.

[146] K.B. Moses, S.G. Advani, and A. Reinhardt. Investigation of fiber motion near solid boundaries in simple shear flow. *Rheologica Acta*, 40(3):296–306, May 2001.

[147] O.L. Forgacs and S.G. Mason. Particle motions in sheared suspensions x. orbits of flexible threadlike particles. *Journal of Colloid Science*, 14:473–491, 1959.

[148] R. Holm and D. Soderberg. Shear influence on fibre orientation - dilute suspension in the near wall region. *Rheologica Acta*, 46(5):721–729, May 2007.

[149] A Carlsson. *Orientation of fibres in suspensions flowing over a solid surface.* Royal Institute of Technology, FTH Mechanics, Stockholm, 2007.

[150] B. Nilsson, L. Wagberg, and D. Gray. *Conformability of wet pulp fibres at small length scales.* Mid Sweden University, Sundsvall, 2000.

[151] L. Yang, K.O. van der Werf, B.F. Koopman, V. Subramaniam, M.L. Bennink, P.J. Dijkstra, and J. Feijen. Micromechanical bending of single collagen fibrils using atomic force microscopy. *J Biomed.Mater.Res.A*, 82(1):160–168, July 2007.

[152] G. Subramanian and D.L. Koch. Inertial effects on fibre motion in simple shear flow. *Journal of Fluid Mechanics*, 535:383–414, July 2005.

[153] Gloria A Di Lullo, Shawn M Sweeney, Jarmo Korkko, Leena Ala-Kokko, and James D San Antonio. Mapping the ligand-binding sites and disease-associated mutations on the most abundant protein in the human, type i collagen. *J Biol Chem*, 277(6):4223–4231, Feb 2002.

[154] H. Kresse and E. Schönherr. Proteoglycans of the extracellular matrix and growth control. *J Cell Physiol*, 189(3):266–274, Dec 2001.

[155] M.P. Lynch, J.L. Stein, G.S. Stein, and J.B. Lian. The influence of type i collagen on the development and maintenance of the osteoblast phenotype in primary and passaged rat calvarial osteoblasts: modification of expression of genes supporting cell growth, adhesion, and extracellular matrix mineralization. *Exp.Cell Res.*, 216(1):35–45, January 1995.

[156] W.J. Luo, H. Shitaye, M. Friedman, C.N. Bennett, J. Miller, O.A. MacDougald, and K.D. Hankenson. Disruption of cell-matrix interactions by heparin enhances mesenchymal progenitor adipocyte differentiation. *Experimental Cell Research*, 314(18):3382–3391, November 2008.

[157] N.F. Huang, S. Patel, R.G. Thakar, J. Wu, B.S. Hsiao, B. Chu, R.J. Lee, and S. Li. Myotube assembly on nanofibrous and micropatterned polymers. *Nano Letters*, 6(3):537–542, March 2006.

[158] M.T. Lam, S. Sim, X.Y. Zhu, and S. Takayama. The effect of continuous wavy micropatterns on silicone substrates on the alignment of skeletal muscle myoblasts and myotubes. *Biomaterials*, 27(24):4340–4347, August 2006.

[159] Marta C Nunes, Neeta Singh Roy, H. Michael Keyoung, Robert R Goodman, Guy McKhann, Li Jiang, Jian Kang, Maiken Nedergaard, and Steven A Goldman. Identification and isolation of multipotential neural progenitor cells from the subcortical white matter of the adult human brain. *Nat Med*, 9(4):439–447, Apr 2003.

[160] Nima Saeidi, Edward A Sander, and Jeffrey W Ruberti. Dynamic shear-influenced collagen self-assembly. *Biomaterials*, 30(34):6581–6592, Dec 2009.

Appendices

Appendix A:

Aligned fibrillar collagen matrices obtained by shear flow deposition

Lanfer B., Freudenberg U., Zimmermann R., Stamov D., Körber V., Werner C.
Leibniz Institute of Polymer Research, Max Bergmann Center of Biomaterials Dresden, Dresden
in *Biomaterials* 29 (2008) 3888-3895.

Abstract

Here we present a new technique to generate surface-bound collagen I fibril matrices with differing structural characteristics. Aligned collagen fibrils were deposited on planar substrates from collagen solutions streaming through a microfluidic channel system. Collagen solution concentration, degree of gelation, shear rate and pre-coating of the substrate were demonstrated to determine the orientation and density of the immobilized fibrils. The obtained matrices were imaged using confocal reflection microscopy and atomic force microscopy. Image analysis techniques were applied to evaluate collagen fibril orientation and coverage. As expected, the degree of collagen fibril orientation increased with increasing flow rates of the solution while the matrix density increased at higher collagen solution concentrations and on hydrophobic polymer pre-coatings. Additionally, length of the immobilized collagen fibrils increased with increasing solution concentration and gelation time.

1 Introduction

Collagen is the most abundant structural protein in mammals. To date, 28 different types of collagens [1] are known to be involved in shaping and maintaining the extracellular matrix (ECM) by forming fibrillar or other large-scale assemblies [2]. Collagen builds tissue-specific architecture that imparts mechanical strength and stability to the ECM and mediates cell attachment, morphology, proliferation and migration [3]. In order to better understand the *in vivo* function of collagen matrices it is of need to develop systems that mimic these structures *in vitro*. In this context it is of great interest to develop methods allowing for the variation and control of the morphology of collagen assemblies *in vitro* to adopt the very versatile structures found in tissues.

Collagen type I is the main collagen found in skin and bone and the major constituent of most ECM variants. Three left-handed supercoiled polypeptide chains (two α1(I) and one α2(I)) in a polyproline- II-like conformation form a right-handed triple helix, the collagen molecule, with a diameter of 1.5 nm and a length of 300 nm [2]. In an entropy-driven self-assembly process termed fibrillogenesis, collagen molecules form fibrils with diameters ranging from 20 nm to 70 nm [2, 4]. Turbidimetric analysis of fibril formation *in vitro* showed an initial lag phase followed by a growth phase with a sigmoidal increase in fibril formation rate [5]. It has been suggested that dimer and trimer formation takes place during the lag phase, while rapid lateral aggregation

involving five trimers (''microfibril'') occurs during the growth phase. Further growth occurs by linear and lateral addition of trimeric units to result in collagen fibril formation [6].

In vivo, collagen fibrils are arranged in complex three-dimensional arrays, often in an aligned manner, to fulfil certain biomechanical functions such as resisting high tensile forces in tendons. Collagens can be found as parallel fibre bundles in tendon and ligaments [7], as concentric waves in bone [8] or as orthogonal lattices in cornea [9]. The spatial organization of collagen fibres *in vivo* is believed to play an important role in directing cell behaviour and fate decisions. For example, it has been reported that fibroblasts align along oriented collagen fibril matrices via contact guidance [10, 11]. The direction of cell migration and the distribution of newly synthesized collagen are also determined by the alignment of collagen fibrils [12]. It is thus important that aligned collagen fibril matrices be created *in vitro* to investigate ECM structure and its influence on cell behaviour. However, this is problematic as reconstitution of collagen matrices *in vitro* results in isotropic structural networks containing arbitrarily oriented collagen fibrils [13].

Several approaches have been introduced to reconstitute aligned collagen matrices *in vitro*. Elsdale and Bard presented a technique that involved unidirectional draining of a supporting coverslip during gelation of a collagen solution [14]. Additionally, exposing a gelling collagen solution to a strong magnetic field aligns collagen fibrils due to the diamagnetic properties of collagen molecules [15, 16]. Guo and Kaufman [17] also made use of magnetic fields, but did so by adding magnetic beads to the collagen solution then aligning the gelling collagen solution by moving the beads towards their poles. Aligned collagen nanofibre matrices have also been produced by electrospinning [18] or use of a mica surface in combination with hydrodynamic flow [19]. Lastly, collagen fibril alignment has been observed in microfluidic channels (<100 mm width) as result of a short initial pressure-driven flow and subsequent static gelation of a collagen solution [20]. Despite the development of these methods [11, 16, 15, 17, 18, 19, 20], however, the production of aligned collagen matrices still requires complex technical equipment or lacks broad application to cell biology due to the limited size of the area covered or the rather artificial characteristics of ''non-native'' matrices. Importantly, none of the abovementioned techniques enables collagen fibril alignment, density and morphology to be varied.

Here we introduce a new technique using a microfluidic system to create well-aligned ''native'' collagen fibril matrices that cover large areas. This method allows both density and collagen fibril orientation to be controlled by varying the applied solution (gelation time, concentration), hydrodynamic flow (shear rate) and pre-coating of the substrate (hydrophobicity, reactivity, charging).

2 Materials and methods

2.1 Preparation of glass substrates/thin polymer films

For experiments with uncoated glass substrates, freshly cleaned 22 mm 22 mm glass coverslips (Menzel Gla¨ser, Braunschweig, Germany) were oxidized in a 1:1 mixture of aqueous ammonia solution (Acros Organics, Geel, Belgium) and hydrogen peroxide (Merck). For

thin film preparation, cleaned coverslips were functionalized by reaction with 3-aminopropyl-dimethylethoxy-silane (ABCR, Karlsruhe, Germany). Poly(octadecene-alt-maleic acid) (POMA; MW$\frac{1}{4}$ 30,000–50,000, Polysciences, Warrington, PA) and poly(ethylene-alt-maleic acid) (PEMA, MW$\frac{1}{4}$ 125,000, Aldrich, Munich, Germany) were dissolved in tetrahydrofuran (THF, Fluka, Deisenhofen, Germany) in a concentration of 0.08 wt% and 0.15 wt%, respectively, and spin coated (RC 5 Suess Microtec, Garching, Germany) onto the amine-modified coverslips at 4000 rpm for 30 s. Stable covalent binding of the polymer films was achieved by annealing at 120 C to form imide bonds with the amino-silane on the glass substrate [21]. The hydrophobicity of the surfaces (evaluated by the water contact angle) decreases in the following order: POMA (100)> PEMA (57)> Glass (<10) (previous measurements, see Ref. [21]).

2.2 Collagen solution

Bovine dermal collagen I solution (purified and pepsin-solubilized in 0.012 N HCl, PureCol, Inamed, Milmont Drive, USA) was brought to physiological pH by mixing eight parts of the acidic collagen solution (3.0 mg/ml) with one part of 10-fold concentrated phosphate buffered saline (PBS, Sigma, Steinheim, Germany) and one part 0.1 M NaOH. All components were kept in an ice bath before and after mixing. Appropriate volumes of chilled 1 PBS were added to adjust the final concentration of the collagen solution.

Time-dependent viscosity of the collagen solutions was measured with a rotational rheometer (Physica MCR 300, Anton Paar Germany GmbH, Ostfildern, Germany) using a double concentric cylinder measurement system equipped with a temperature unit that enables heating the sample up to 37 C. The initially chilled collagen solutions (0.2 mg/ml, 0.4 mg/ml, 0.8 mg/ml) were heated up to 37 C within 10 min and the viscosity was measured at every minute with an applied shear rate of 40 s1. Collagen solutions (0.8 mg/ml) showed a slight initial increase in viscosity (2.34–2.37 mPas) in the first 5 min. An increase was also observed for 0.4 mg/ml collagen solutions (1.41–1.44 mPas), however, it had longer time period. The viscosity subsequently decreased, reaching an end value of 1.28 mPas for 0.8 mg/ml and 1.05 mPas for 0.4 mg/ml collagen solutions after 60 min. Viscosity of 0.2 mg/ml collagen solutions showed a slight decrease (1.1–1 mPas) after 60 min (Fig. 1).

2.3 Microfluidic system

The microfluidic system used to deposit aligned collagen fibrils was fabricated by microcasting polydimethylsiloxane (PDMS) and sealed by a coverslip (see above). For detailed information concerning the technology, we refer the reader to Ref. [22]. Two parallel channels of 8 mm length, 1 mm width and 73.6 mm height were generated on one channel plate. In order to improve contact between PDMS and coverslip, additional channels were integrated into the PDMS portion of the channel plate and connected to a vacuum pump. The hydrodynamic flow (flow rate) of the collagen solutions in the micro-channels was controlled by a syringe pump (KDS, Holliston, USA) connected via polyether-ether-ketone (PEEK) tubing (diameter 750 mm, Nordantec, Bremerhaven, Germany) to external valves and to the channel plate.

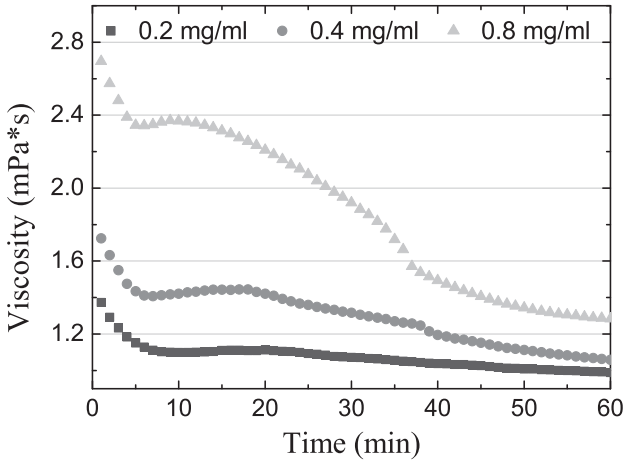

Figure 1: Time-dependent viscosity of differently concentrated collagen solutions at 37°C.

2.4 Flow conditions

Experiments were performed under conditions of laminar flow. In all experiments the Reynolds number (as a criterion for laminar flow) was smaller than 1. The following flow rates were applied: 0.45 ml/min, 4 ml/min, and 11 ml/min corresponding to wall shear rates of 8.3 s^{-1}, 73.8 s^{-1}, and 203.1 s^{-1}.

2.5 Deposition of collagen fibrils during fibril formation (Variant A)

The microfluidic system was placed in a CO2-free incubator (Sanyo, Bensenville, USA) at 37 C and the syringe pump was kept below 4 C in a cooled styrofoam box. The collagen solution was prepared at 4 C and drawn into chilled syringes (Roth, Karlsruhe, Germany), which were quickly installed into the syringe pump to avoid early fibrillogenesis. The streaming process was started immediately by pumping the chilled collagen solution from the cooled storage reservoir through the heated tubing. The length of the tubing leading to the microfluidic channel was varied according to the streaming time of the collagen solution through the heated tubing before entering the channel, defined here as conditioning time. Conditioning was followed by streaming through the microfluidic channel. In all experiments, a deposition time of 1 h was used. The sample was then rinsed with MilliQ and dried under a clean bench.

2.6 Deposition of fully developed collagen fibrils (Variant B)

The collagen solutionwas prepared at 4 C in a centrifuge tube (Roth, Karlsruhe, Germany), placed in a CO2-free incubator (Sanyo, Bensenville, USA) at 37 C, and allowed to form fibrils for 24 h. The resulting gels were homogenized for 4 min (T-8 Ultra Turrax) and centrifuged (Heraeus, Hanau, Germany) at 1000g for 6 min. The supernatant (∼2 ml) was drawn into a syringe that was subsequently installed into the syringe pump. The solution was then pumped for 1 h with flow rates of 0.45 ml/ min, 4 ml/min, and 11 ml/min through the microfluidic

channel. Afterwards the channel was rinsed with PBS for 20 min to flush away loose fibrils and the coated coverslip was removed from the PDMS channel plate. The sample was then rinsed and dried as described above. Experiments were carried out at room temperature.

2.7 Confocal reflection microscopy (CRM)

Confocal reflection microscopy (TCS SP, Leica, Bensheim, Germany) was performed at a wavelength of 488 nm (Ar laser) to visualize the unstained collagen fibrils. CRM pictures of the fibril matrices were obtained using a 40 oil immersion objective as previously described [23].

2.8 Atomic force microscopy (AFM)

Surface topography of the collagen matrices was investigated via intermittent contact scanning force microscopy with a PicoSPM (Molecular Imaging, Phoenix, AZ, United States) using silicon cantilevers (Tap300, BudgetSensors, Bulgaria) with a resonant frequency 300100 kHz, force constant 40 N/m and tip radius$<$ 10 nm.

2.9 Image analysis to quantify fibril alignment and coverage

The area covered with collagen fibrils and the degree of fibril alignment were quantified with NIH ImageJ 1.37v software. Three samples containing two channels with collagen fibrils were analyzed for each condition at three selected positions of the channel (inlet, middle, outlet). One sample contained a minimum coverage of 200 collagen fibrils. A threshold value of the reflection intensity was defined to isolate collagen fibrils from the background. By fitting an ellipse to the major axis of each collagen fibril, the angle of the fibrils to the flow direction was determined. The orientation of fibrils parallel to the flow direction corresponds to an angle of 0. The average orientation angle of the fibrils was calculated by taking the mean of the orientation angle of each fibril. The angular distribution of collagen fibrils was determined based on the relative frequency of fibril angles (classified into bins of 5 angles) of three samples and by a fit to a Gaussian the full-width half-maximum (FWHM). The coverage of collagen fibrils was calculated by taking the mean of area fractions of the fibrils as percentage of the total area. 2.10. Statistical analyses Data were analysed using GraphPad Instat 3.06, and the Student's t testwas used for inter-sample comparison. Multiple samples were evaluated by one-way ANOVA followed by Tukey's post hoc test to evaluate the statistical differences between all samples. The standard deviation (SD) of the data was assumed to be equal and normally distributed.

3 Results

The aim of this study was the formation of aligned collagen matrices with variable orientation, density, and morphology. The matrices were deposited from collagen solutions by means of a microfluidic system. In order to vary the characteristics of the collagen matrices two variants of the streaming experiment were applied.

Table 1: Influence of process-relevant parameters on angular distribution of collagen fibril matrices (FWHM) prepared according to Variants A and B.

Variant A	FWHM(°)	Variant B	FWHM(°)
Concentration		*Flow rate*	
0.2 mg/ml	41.4	0.45 μl/min	30.1
0.4 mg/ml	31.1	4 μl/min	16.3
0.8 mg/ml	30	11 μl/min	14.4
		Concentration	
		3±0.1μg/ml	14.4
		14±2.5μg/ml	17
		Substrate	
		POMA	14.4
		PEMA	18.1
		Glass	13.9

3.1 Deposition of collagen fibrils during fibril formation (Variant A)

To generate collagen matrices according to Variant A, three concentrations of collagen solution (0.2 mg/ml, 0.4 mg/ml and 0.8 mg/ml) were prepared and pumped with a flow rate of 11 μml/min through tempered tubing for 5 min before entering the channel. Fig. 2A shows CRM and AFM images of the resultant collagen matrices on POMA surfaces. Solutions with higher collagen concentrations produced significantly greater fibril coverage (6.9± 4.6% for 0.2 mg/ml, 29 ±5.7% for 0.4 mg/ml, 83± 4% for 0.8 mg/ml, at the middle position, Fig. 2B(i)). Visual inspection indicated that collagen matrices generated at a solution concentration of 0.2 mg/ml consisted of single, short and bent collagen fibrils (Fig. 2A). The length of these fibrils was increased at 0.4 mg/ ml collagen concentrations, and more so at 0.8 mg/ml (Fig. 2A). Higher solution concentration additionally increased collagen fibril orientation (FWHM 41.4° for 0.2 mg/ml, 31.1° for 0.4 mg/ml, 30° for 0.8 mg/ml, (Fig. 2B(ii), Table 1)). For 0.8 mg/ml matrices 47% of the collagen fibrils were within 5° of the channel axis.

In order to detect a possible connection between the conditioning time spent by the collagen solution in the tempered tubing before entering the channel and the morphology of the resultant collagen fibril matrices, streaming experiments were performed with 0.8 mg/ml collagen solutions using various lengths of tubing between the syringe and microfluidic channel. The length of the tubing was varied according to the calculated collagen solution conditioning times of 5 min, 10 min, and 30 min in the tempered tubing at a constant flow rate of 11 μl/min. Collagen matrices generated after 5 min of conditioning showed dense and aligned fibrillar matrices (Fig. 3) that consisted of long and short collagen fibrils. After 30 min, mainly long, aligned, and more individual collagen fibrils appeared (Fig. 3). Experimental reproducibility decreased as conditioning time increased due to the formation and adsorption of large fibril aggregates. Image analysis was not possible on matrices from solutions with 30 min conditioning time.

However, differences between the matrices in regard to morphology and structure were obvious by visual inspection. Short collagen fibrils had fibre aspect ratios (length/diameter of fibril) of

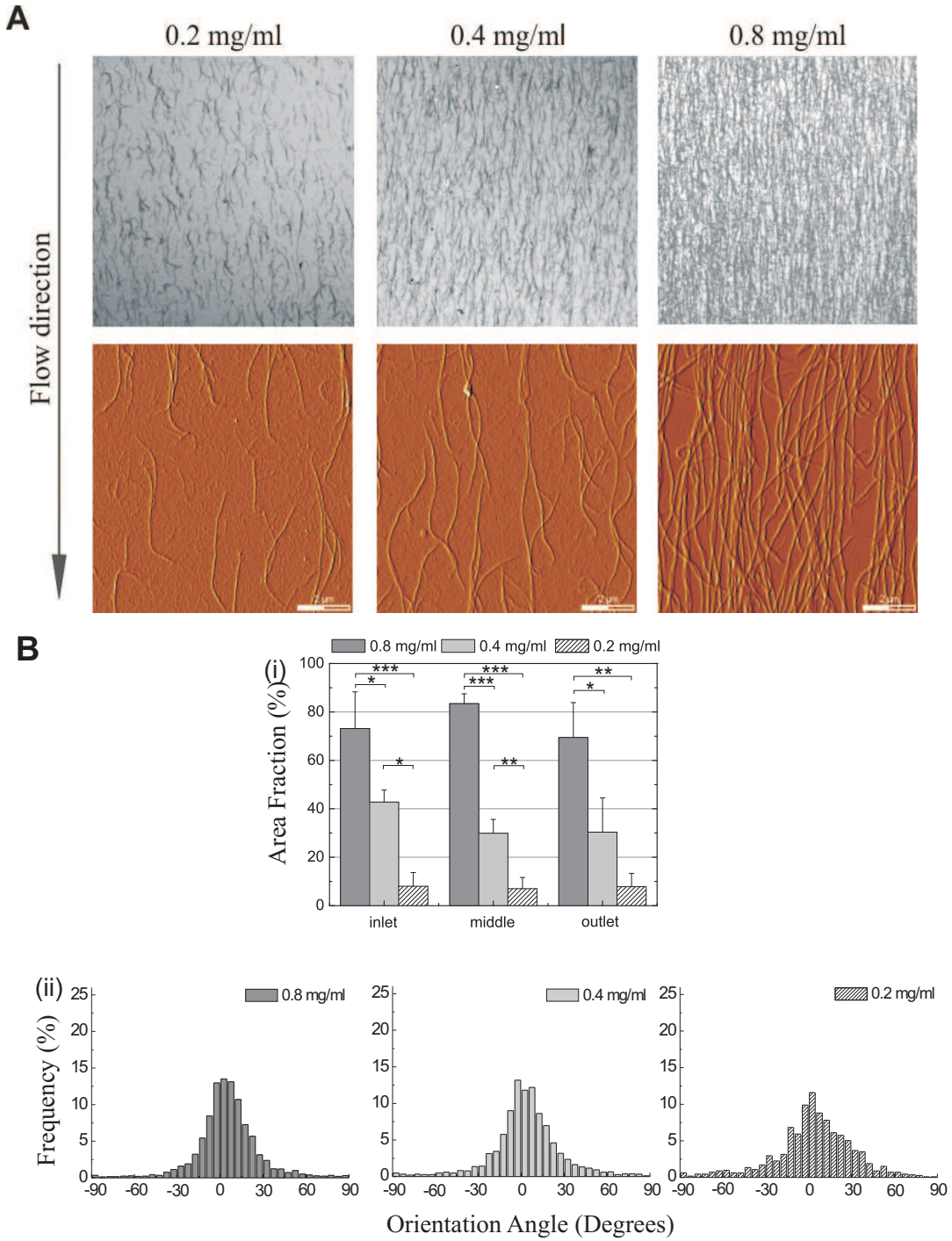

Figure 2: (A) CRM (first row) and AFM (second row) images of collagen fibril matrices prepared according to Variant A with varying concentrations 0.2 mg/ml, 0.4 mg/ml and 0.8 mg/ ml on POMA-coated substrate with a flow rate of 11 μl/min and conditioning time of 5 min. (B) Influence of varying collagen solution concentrations on the density and orientation of collagen fibril matrices produced according to Variant A (substrate POMA, flow rate 11 ml/min, conditioning time 5 min). (i) The relative area fraction (y-axis) of collagen fibril coverage at three different positions (x-axis) is plotted (n =3, $\pm$SD, *p $<$ 0.05, **p $<$ 0.01, ***p $<$ 0.001). (ii) Distribution of collagen fibre angles for the different concentrations at the middle position of the channel. The histograms show the relative frequency (y-axis) of fibre angles in 5° bins (x-axis) with 0° set as parallel to the channel axis.

r_p ~10-30, and longer ones r_p>40 (data not shown).

Streaming a chilled collagen solution through tempered tubings into a rectangular flow chamber was found to produce aligned collagen matrices with variable density, alignment and morphology. Higher collagen concentrations resulted in greater density of the matrices. The collagen concentration additionally affected the morphology of the deposited matrices: short and bent fibrils were obtained from lower concentrations and longer fibrils from higher concentrations. The alignment was influenced by both the preconditioning time as well as by the solution concentration. Longer preconditioning times (up to 30 min) as well as higher solution concentrations resulted in a higher degree of alignment of the deposited fibrils.

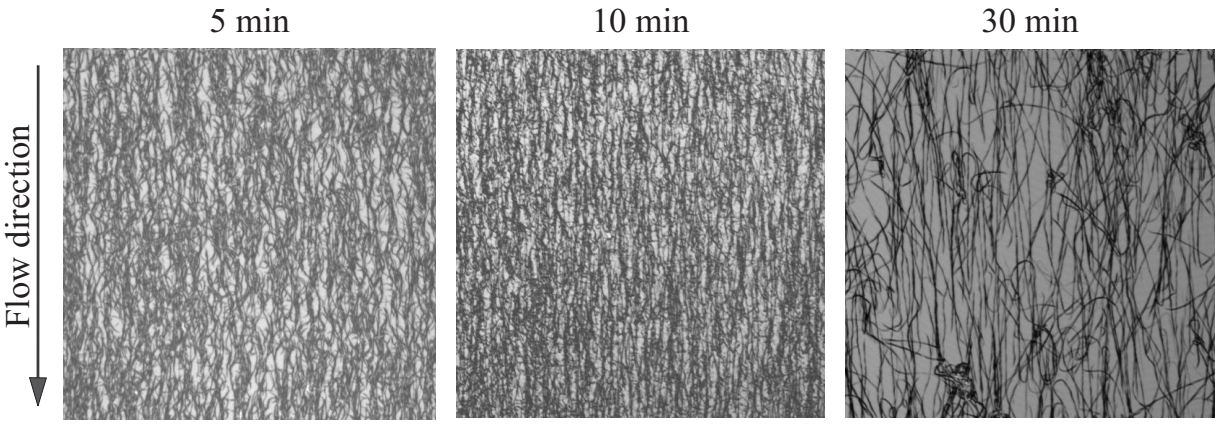

Figure 3: CRM images of collagen fibril matrices (Variant A) prepared from collagen solutions (0.8 mg/ml) pumped through heated tubing for varying conditioning time periods 5 min, 10 min, 30 min before entering the channel (on POMA surfaces, flow rate of 11 μl/min). Dimensions of images are 62.5x62.5 μm

3.2 Deposition of fully developed collagen fibrils (Variant B)

Variant B was developed to create highly aligned matrices of long ''mature'' collagen fibrils. Homogenization and centrifugation of collagen gels resulted in a low-concentrated supernatant containing individual long collagen fibrils. Subsequently, the preprocessed supernatant (3±0.1 mg/ml, determined by High Performance Liquid Chromatography (HPLC)) was pumped through the microfluidic channel. Fig. 4A shows CRM and AFM images of the resultant collagen matrices on POMA surfaces at a flowrate of 11 μl/ min. The flow rate of the system was initially adjusted to 11 μl/min since less fibril coverage across the width and length of the channel was observed at higher flow rates (data not shown). To further optimize orientation and coverage of the collagen matrices, flow rate in the streaming experiments was varied (11 μl/min, 4 μl/min and 0.45 μl/min) across the POMA-coated surfaces. The amount of adsorbed collagen fibrils increased significantly with decreasing flow rate, independently of channel position (17±8% for 11 ml/min, 38±10.3% for 4 ml/min and 65±3% for 0.45 μl/min, at inlet position, Fig. 4B(i)). However, at the lowest flow rate (0.45 μl/min), an increasing amount of non-aligned aggregates was observed at the channel inlet and outlet. The best alignment was achieved at 11 μl/ min (FWHM 14.4, Fig. 4B(iii), Table 1). The collagen fibrils (68%) were within 5° of the channel

axis. Parallel alignment of the fibrils was consistent across the entire length and width of the microfluidic channel (Fig. 4A and B(ii)), but collagen fibril coverage declined from the channel inlet to the outlet in all Variant B experiments (Figs. 4B(i), 5A(i) and B(i)). The generated collagen fibrils had fibre aspect ratios (length/diameter of fibril) of r_p>40 (data not shown).

In order to increase surface coverage, concentration of the collagen solutionwas increased. The collagen concentrations of the supernatant (after processing according to Variant A, see Section 2) used for the streaming experiments was 3±0.1 μg/ml and 14±2.5 μg/ml (determined by HPLC). At higher collagen solution concentration, the amount of adsorbed collagen fibrils increased independently of channel position (19±9% for 3± 0.1 μg/ml, 36±16.7% for 14±2.5 μg/ml, at inlet position), but orientation slightly decreased (FWHM 14.4°–17°) (Fig. 5A, Table 1). This decrease in alignment was attributed to an increase in aggregates of non-aligned collagen fibrils, not to alterations in collagen fibril orientation.

Influence of the substrate on coverage and orientation of the resulting fibril matrices was also systematically investigated. Streaming experiments with copolymer-coated glass coverslips (POMA and PEMA) and freshly cleaned glass coverslips were performed at a flow rate of 11 μl/min. On POMA-coated substrates, we detected substantially higher coverage (13.5±4.7%) in comparison to PEMA-coated (7±2.6%) and bare glass coverslips (6±1.5%) (at the inlet position, Fig. 5B(i)). The alignment of collagen fibrils on POMAcoated and glass substrates was higher than on PEMA-modified substrates (FWHM 14.4° for POMA; 18.1° for PEMA, 13.9° for glass, Fig. 5B(ii), Table 1). Solutions containing ''mature'' fibrils produced highly aligned collagen matrices. The fibril alignment was varied by the flow rate and the choice of the substrate. Highest degrees of alignment were determined on glass at a flow rate of 11 μl/min, lower flow rates resulted in less alignment. The fibril density was affected by the solution concentration and the substrate properties: Higher concentrations resulted in higher surface coverage; the hydrophobic POMA surface gave rise to the highest surface coverage.

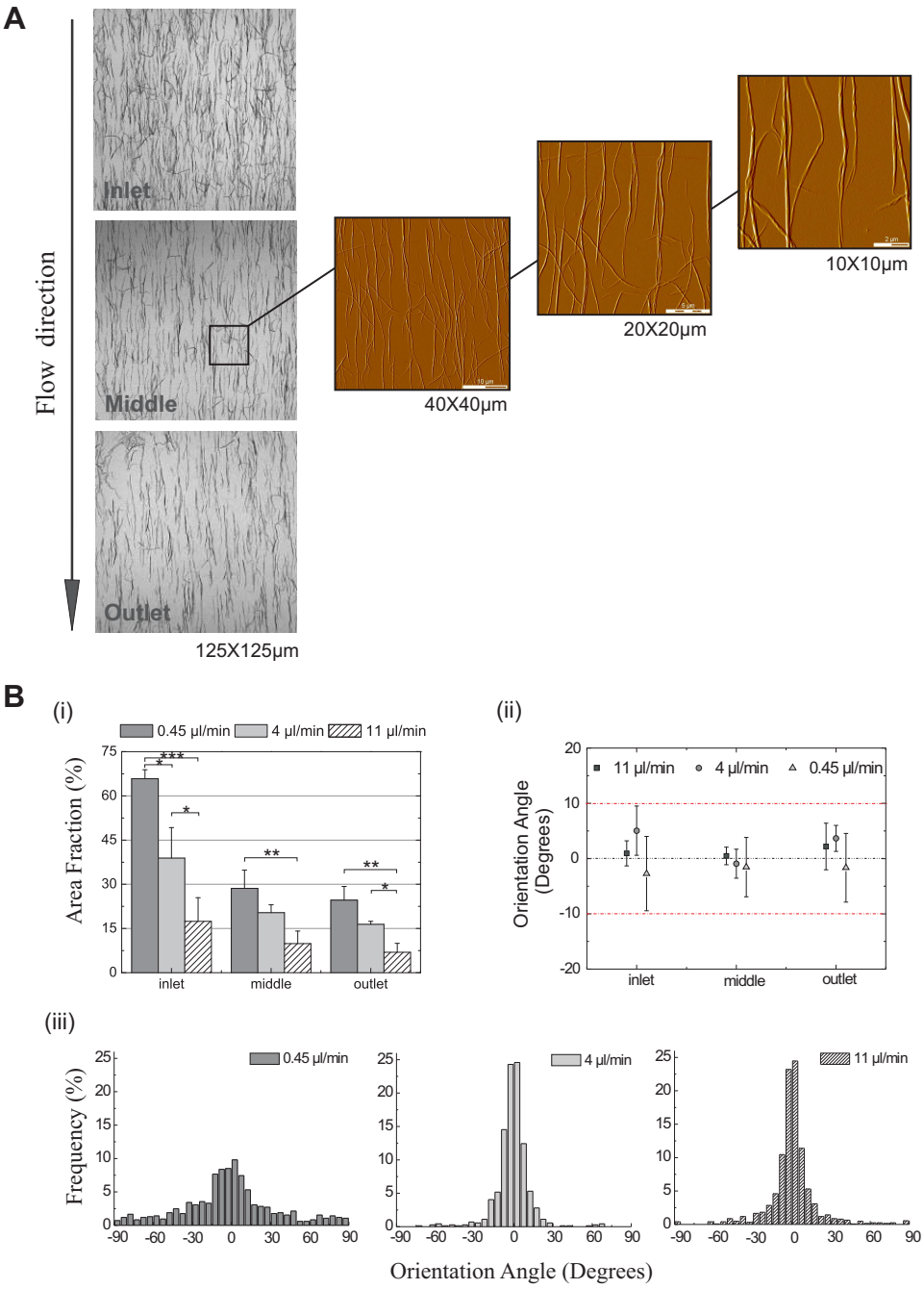

Figure 4: (A) CRM and AFM images of aligned collagen fibril matrices prepared according to Variant B (solution concentration 3± 0.1 μg/ml, substrate POMA, flow rate 11 μl/min) along the length (inlet, middle and outlet) of the microfluidic channel. (B) Influence of different flow rates on collagen fibril coverage and orientation of collagen matrices prepared according to Variant B (flow rate 11 μl/min, solution concentration: 3± 0.1 μg/ml, substrate POMA). (i) Collagen fibril coverage as area fraction in percentage at different channel positions for the different flow rates (n=3,±SD, *p $<$ 0.05, **p $<$ 0.01, ***p $<$ 0.001). (ii) Mean orientation angle of collagen fibrils along the channel length for the different flow rates (n=3,±SD). (iii) Distribution of collagen fibre angles for the different flow rates at the middle position of the channel. The histograms show the relative frequency (y-axis) of fibre angles in 5° bins (x-axis) with 0° set as parallel to the channel axis.

4 Discussion

The variation of gelation times and collagen concentrations allowed us to prepare aligned matrices consisting of collagen fibrils that show different degrees of fibril formation. Collagen fibrillogenesis is a multistep process whose dynamics depend on the starting concentration [24]. Higher starting concentrations of collagen is known to accelerate rate and number of fibrils formed [13]. This may explain the finding here that fibres formed at lower concentrations are shorter and reduced in number compared to those formed at higher starting concentrations (Variant A) (Fig. 2A). Turbidity measurements show that lag times for concentrations around 0.2 mg/ml exceed the conditioning time of 10 min [13]. Thus, it can be assumed that fibril formation does not take place under these conditions. However, it was reported that the lag time disappears when the neutralized collagen solution is kept at 4 C for longer than 5 min. Since we stored the collagen solution at 4°C up to 1 h before streaming (see Section 2 Variant A), it is likely that a lag time was not a factor. Thus, the fibrils in our experiments may have already begun to form in the chilled storage reservoir or while streaming through the tempered tubing. This was confirmed by the observation that longer and more isolated collagen fibrils are deposited on the substrate (see Fig. 3) as conditioning times increase while collagen solution concentration and flow rate are kept constant. Longer conditioning times allowed fibril formation to occur for a longer time period, hence the formation of longer fibrils.

Matrices consisting of long, highly aligned, and individual collagen fibrils were produced by streaming a collagen solution containing ''ready-made'' collagen fibrils (Variant B) (Fig. 4A). Since the collagen solution was allowed to gel for 24 h before streaming, it can be expected that the resultant matrices consist of collagen fibrils that were fully developed before they were deposited on the substrate.

4.1 Influence of flow rate and solution concentration

The significant increase in fibril coverage of matrices produced with initially cooled and neutralized collagen solutions at low starting concentrations (Variant A) (Fig. 2B(i)) can be directly attributed to the increase in monomer content and thus the amount of fibrils in the solution. Matrices generated according to Variant B also showed an increase of fibril coverage (Fig. 5A(i)) when solution concentration was increased. Appropriate adjustment of the flow rate enabled the generation of highly aligned matrices that were at the same time adjustable in density (Variant B, Fig. 4B). Thus, it was possible to influence collagen fibril coverage and alignment by adjusting the flow rate and collagen solution concentration. All matrices prepared according to Variant B exhibited a gradient of coverage along the channel, while the matrices prepared according to Variant A showed no such gradient (Figs. 2B(i), 4B(i) and 5A(i) and B(i)). A possible reason for this effect might be a depletion of collagen across the channel length [25], which was solely observable for Variant B matrices since very low-concentrated solutions were employed.

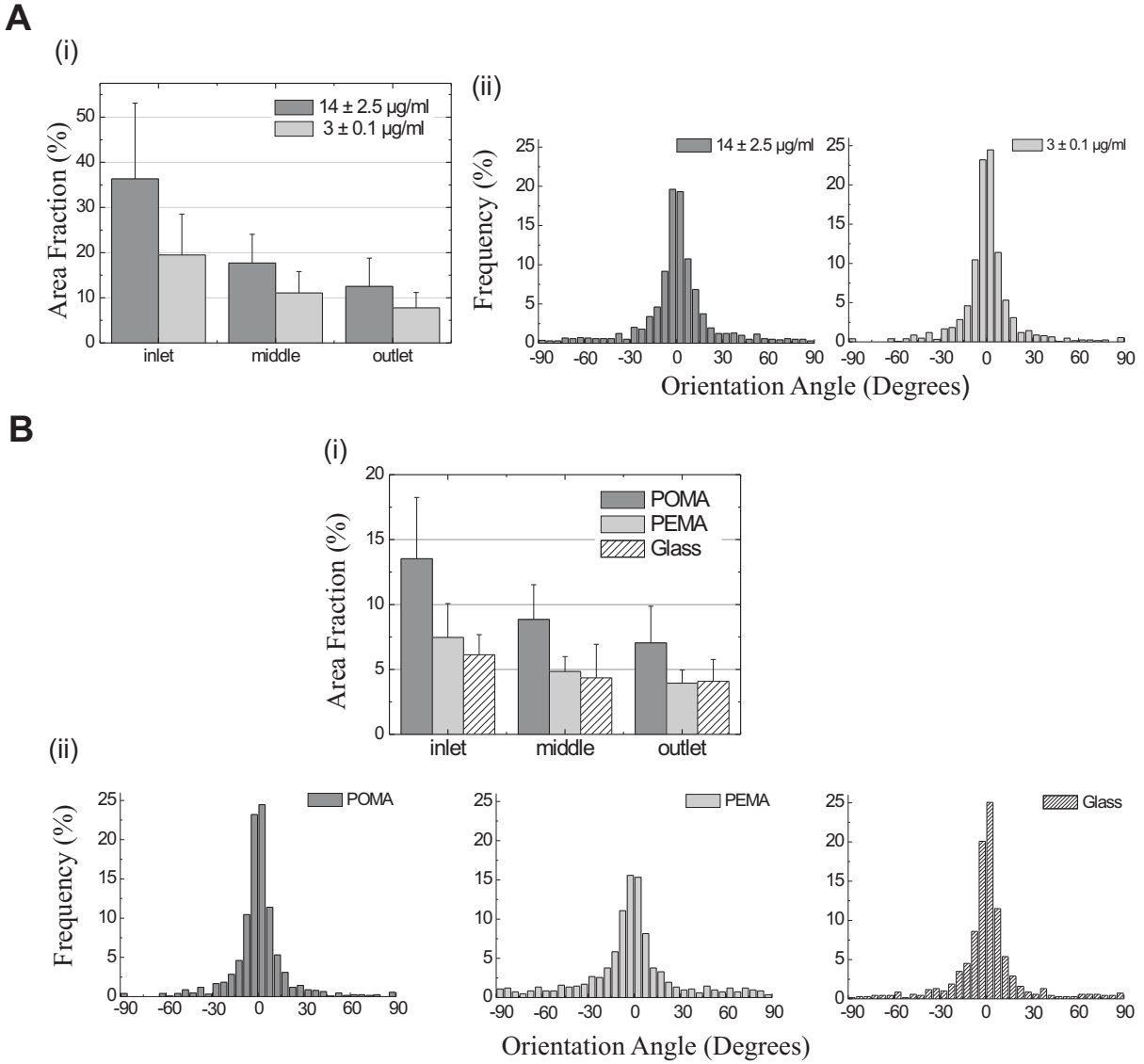

Figure 5: (A) Influence of the collagen solution concentration on density and orientation of collagen fibril matrices prepared according to Variant B (flow rate 11 μl/min, substrate POMA). (i) The relative area fraction (y-axis) of collagen fibrils coverage at three different positions (x-axis) at both concentrations is plotted (n=3,±SD). (ii) Distribution of collagen fibre angles for both concentrations at the middle position of the channel. The histograms show the relative frequency (y-axis) of fibre angles in 5° bins (x-axis) with 0 set as parallel to the channel axis. (B) Influence of substrate on density and orientation of collagen fibril matrices prepared according to Variant B (flow rate 11 μl/min, solution concentration: 3± 0.1 μg/ml). (i) The relative area fraction (y-axis) of collagen fibrils coverage for the three substrates at three different positions (x-axis) is plotted (n=3,±SD), SD). (ii) Distribution of collagen fibre angles for the three substrates at the middle position of the channel. The histograms show the relative frequency (y-axis) of fibre angles in 5° bins (x-axis) with 0° set as parallel to the channel axis.

4.2 Influence of substrate

Experiments with substrates differing in the degree of hydrophobicity/ hydrophilicity (glass, POMA- and PEMA-coated glass) were performed and substantially higher coverage of collagen fibrils was achieved on POMA-modified surfaces than on PEMAmodified and bare glass slides (Fig. 5B(i)). Both copolymers POMA and PEMA consist of alternating units of maleic acids and alkyl chains. However, the co-monomer octadecene in POMA is large in comparison to the small ethylene residue in PEMA. Consequently, thin films of these copolymers show differences in hydrophobicity and structural characteristics ranging from a nearly non-swollen, hydrophobic film for POMA to highly swollen copolymer brushes for PEMA [21]. Covalent attachment of the collagen to the copolymers could be excluded, since the other co-monomers of both POMA and PEMA were in the non-reactive diacid form. The higher coverage of collagen on POMA-coated substrates may be explained by the capability of the long alkyl chains of POMA to mediate hydrophobic interactions between collagen and the substrate surface. The hydrophilic gel-like structure of PEMA and the smooth and unswollen glass surface apparently do not favor adsorption of the hydrophobic collagen. Moreover, the swollen and uneven gel-like structure of PEMA possibly impedes collagen fibril alignment. This may explain the slight decrease in alignment seen on PEMA surfaces (Fig. 5B(ii), Table 1) compared to the hard and even surfaces of POMA and glass.

4.3 Possible mechanism of fibril alignment

Because ‘‘prealignment’’ effects [26] appear to play a minor role in this system and as viscosity only slightly influences fibril alignment – matrices produced according to Variant B showed the highest degrees of alignment despite of the low viscosity of the utilized solutions – the formation of longer fibrils (besides the flow rate) seems to critically determine alignment (Figs. 2A and B(ii), 3 and 4A and B(iii), Table 1) pointing at the underlying mechanism of a ‘mechanical alignment’. Fibres in a simple shear flowalign most of the time in the direction of flow, however, their orientation can change by 180 in a ‘‘tumbling’’ motion [27]. This motion was observed in a low Reynolds number regime for pulp fibres that reveal rigidities in the same range as collagen fibrils (pulp fibres: 5.4 Gpa [28], collagen fibres: 5.5 Gpa [29]). Thus, in our system, it is likely that the collagen fibrils interact with the wall during the tumbling motion. If one end of the fibril attaches to the surface, the remaining part can be aligned by the streaming fluid in a position of low hydrodynamic resistance, i.e. parallel to the flow direction. However, due to additional interaction of the fibril with the surface, not all fibrils align parallel to the flow. Near the wall, the number of fibres aligning in flow direction was reported to be higher for higher aspect ratios ($r_p >$ 40) [30, 31]. Since aspect ratios of the long fibrils in our system are comparable to those of Ref. [30], inertia effects may contribute to the increase of fibril alignment with increasing length. Thus, it can be concluded that fibril alignment is dependent on (i) the flow rate (which influences the shear stress/force in the system (tubing and channel)), (ii) the length of the fibrils, and to a lesser degree (iii) the viscosity of the solution (which also influences shear force, but in a much lower order than flow rate).

4.4 Comparison to other methods and potential benefits

Collagen alignment was homogeneous for the entire width and almost the whole length of the channel covering an area of several square millimeters. This is an major advantage of this method compared to collagen gels produced by microfluidic alignment in thin streaming channels [20] allowing only a small area (channel widths <30 mm) to be coated with consistently aligned fibres. This method limits the use for cell culture studies since the average cell diameter is in the same magnitude as the covered area. Our matrices showed greater fibril alignment for an area 100-fold bigger in width. Highest alignment was achieved with 68% and 47% of the collagen fibrils within 5 of the channel axis for Variant B and Variant A, respectively. In comparison, Lee et al. reported 40% of the collagen fibrils to be within 5° of the channel axis whereas for increasing channel width this percentage decreased. Our data thus indicate that our method produces highly aligned matrices that are of comparable or better quality to those obtained by other current techniques. To our knowledge it has not been demonstrated that any of the above techniques can give rise to aligned collagen matrices tuneable in morphology. Since *in vivo* collagen fibril architecture varies from tissue to tissue and cellular fate decisions critically depend on the surrounding matrices [32, 33], cell biology experiments to investigate the effect of collagen fibril length and density on stem cell differentiation could be of great interest. For that aim, the formation of aligned collagen fibrils will be further elaborated to incorporate glycosaminoglycans like heparin and heparan sulphate [34] which mediate growth factor and protein binding [35]. The method is also currently applied in ongoing studies to create three-dimensional matrices through layer by layer deposition and for the coating of hollow tubular structures to be used as conduit in nerve repair.

5 Conclusion

Here we present a new technique to generate aligned fibrillar collagen matrices on different substrates. Using an easy to handle microfluidic system, we created collagen matrices of differing alignment, density and morphology. We demonstrated that the degree of fibril alignment can be increased by increasing flow rate and fibril length. Furthermore, matrix density can be varied and increased by using different collagen solution concentrations and surface-modified substrates. Additionally, the matrix morphology is tuneable by varying gelation time and collagen concentration. The versatility of this method enables quick and easy preparation of fine-tuned collagen matrices that can be applied in advanced cell biology and tissue engineering researches. In particular, these welldefined matrices provide an opportunity to characterize and control cell adhesion, orientation and migration. In this context, we are currently applying the surface-engineered substrates described here to guide neurite outgrowth and elongation *in vitro*.

References

[1] K.E. Kadler, C. Baldock, J. Bella, and R.P. Boot-Handford. Collagens at a glance. *J Cell Sci.*, 120(Pt 12):1955–1958, June 2007.

[2] K.E. Kadler, D.F. Holmes, J.A. Trotter, and J.A. Chapman. Collagen fibril formation. *Biochem J*, 316 (Pt 1):1–11, May 1996.

[3] Frederick Grinnell. Fibroblast biology in three-dimensional collagen matrices. *Trends Cell Biol*, 13(5):264–269, May 2003.

[4] V. Ottani, D. Martini, M. Franchi, A. Ruggeri, and M. Raspanti. Hierarchical structures in fibrillar collagens. *Micron.*, 33(7-8):587–596, 2002.

[5] G.C. Wood. The formation of fibrils from collagen solutions. 2. a mechanism of collagen-fibril formation. *Biochem.J.*, 75:598–605, June 1960.

[6] F.H. Silver. Type i collagen fibrillogenesis in vitro. additional evidence for the assembly mechanism. *J Biol Chem*, 256(10):4973–4977, May 1981.

[7] D.H. ELLIOTT. Structure and function of mammalian tendon. *Biological Reviews of the Cambridge Philosophical Society*, 40(3):392–&, 1965.

[8] S. Weiner and W. Traub. Bone structure: from angstroms to microns. *FASEB J*, 6(3):879–885, February 1992.

[9] D.F. Holmes, C.J. Gilpin, C. Baldock, U. Ziese, A.J. Koster, and K.E. Kadler. Corneal collagen fibril structure in three dimensions: Structural insights into fibril assembly, mechanical properties, and tissue organization. *Proc Natl Acad Sci U S A*, 98(13):7307–7312, June 2001.

[10] T.R. Elsdale. Parallel orientation of fibroblasts in vitro. *Exp Cell Res*, 51(2-3):439–450, August 1968.

[11] S. Guido and R.T. Tranquillo. A methodology for the systematic and quantitative study of cell contact guidance in oriented collagen gels. correlation of fibroblast orientation and gel birefringence. *J Cell Sci*, 105 (Pt 2):317–331, June 1993.

[12] N. Matsumoto, S. Horibe, N. Nakamura, T. Senda, K. Shino, and T. Ochi. Effect of alignment of the transplanted graft extracellular matrix on cellular repopulation and newly synthesized collagen. *Arch.Orthop.Trauma Surg.*, 117(4-5):215–221, 1998.

[13] K. Salchert, U. Streller, T. Pompe, N. Herold, M. Grimmer, and C. Werner. In vitro reconstitution of fibrillar collagen type i assemblies at reactive polymer surfaces. *Biomacromolecules*, 5(4):1340–1350, July 2004.

[14] T. Elsdale and J. Bard. Collagen substrata for studies on cell behavior. *J Cell Biol*, 54(3):626–637, September 1972.

[15] J. Torbet, M. Malbouyres, N. Builles, V. Justin, M. Roulet, O. Damour, A. Oldberg, F. Ruggiero, and D.J. Hulmes. Orthogonal scaffold of magnetically aligned collagen lamellae for corneal stroma reconstruction. *Biomaterials*, 28(29):4268–4276, October 2007.

[16] J. Torbet and M.C. Ronziere. Magnetic alignment of collagen during self-assembly. *Biochem J*, 219(3):1057–1059, May 1984.

[17] C. Guo and L.J. Kaufman. Flow and magnetic field induced collagen alignment. *Biomaterials*, 28(6):1105–1114, February 2007.

[18] B.M. Baker and R.L. Mauck. The effect of nanofiber alignment on the maturation of engineered meniscus constructs. *Biomaterials*, 28(11):1967–1977, April 2007.

[19] D.A. Cisneros, J. Friedrichs, A. Taubenberger, C.M. Franz, and D.J. Muller. Creating ultrathin nanoscopic collagen matrices for biological and biotechnological applications. *Small*, 3(6):956–963, June 2007.

[20] P. Lee, R. Lin, J. Moon, and L.P. Lee. Microfluidic alignment of collagen fibers for in vitro cell culture. *Biomed Microdevices.*, 8(1):35–41, March 2006.

[21] T. Pompe, S. Zschoche, N. Herold, K. Salchert, M.F. Gouzy, C. Sperling, and C. Werner. Maleic anhydride copolymers–a versatile platform for molecular biosurface engineering. *Biomacromolecules*, 4(4):1072–1079, July 2003.

[22] F.U. Gast, P.S. Dittrich, P. Schwille, M. Weigel, M. Mertig, J. Opitz, U. Queitsch, S. Diez, B. Lincoln, F. Wottawah, S. Schinkinger, J. Guck, J. Kaes, J. Smolinski, K. Salchert, C. Werner, C. Duschl, M.S. Jaeger, K. Uhlig, P. Geggier, and S. Howitz. The microscopy cell (miccell), a versatile modular flowthrough system for cell biology, biomaterial research, and nanotechnology. *Microfluid Nanofluid*, pages 21–36, 2006.

[23] S.L. Voytik-Harbin, B. Rajwa, and J.P. Robinson. Three-dimensional imaging of extracellular matrix and extracellular matrix-cell interactions. *Methods in Cell Biology, Vol 63*, 63:583–+, 2001.

[24] R.A. Gelman, D.C. Poppke, and K.A. Piez. Collagen fibril formation in vitro. the role of the nonhelical terminal regions. *J.Biol.Chem.*, 254(22):11741–11745, November 1979.

[25] W. Norde and E. Rouwendal. Streaming potential measurements as a tool to study protein adsorption-kinetics. *Journal of Colloid and Interface Science*, 139(1):169–176, October 1990.

[26] M.M. Giraud-Guille. Liquid crystallinity in condensed type i collagen solutions. a clue to the packing of collagen in extracellular matrices. *J Mol.Biol*, 224(3):861–873, April 1992.

[27] G.B. Jeffery. The motion of ellipsoidal particles in a viscous fluid. *Proceedings of the Royal Society of London Series A-Containing Papers of A Mathematical and Physical Character*, 102(715):161–179, November 1922.

[28] B. Nilsson, L. Wagberg, and D. Gray. *Conformability of wet pulp fibres at small length scales*. Mid Sweden University, Sundsvall, 2000.

[29] L. Yang, K.O. van der Werf, B.F. Koopman, V. Subramaniam, M.L. Bennink, P.J. Dijkstra, and J. Feijen. Micromechanical bending of single collagen fibrils using atomic force microscopy. *J Biomed.Mater.Res.A*, 82(1):160–168, July 2007.

[30] G. Subramanian and D.L. Koch. Inertial effects on fibre motion in simple shear flow. *Journal of Fluid Mechanics*, 535:383–414, July 2005.

[31] A Carlsson. *Orientation of fibres in suspensions flowing over a solid surface*. Royal Institute of Technology, FTH Mechanics, Stockholm, 2007.

[32] F. Yang, R. Murugan, S. Wang, and S. Ramakrishna. Electrospinning of nano/micro scale poly(l-lactic acid) aligned fibers and their potential in neural tissue engineering. *Biomaterials*, 26(15):2603–2610, May 2005.

[33] A. Rajnicek, S. Britland, and C. McCaig. Contact guidance of cns neurites on grooved quartz: influence of groove dimensions, neuronal age and cell type. *J.Cell Sci.*, 110 (Pt 23):2905–2913, December 1997.

[34] D. Stamov, M. Grimmer, K. Salchert, T. Pompe, and C. Werner. Heparin intercalation into reconstituted collagen i fibrils: Impact on growth kinetics and morphology. *Biomaterials*, 29(1):1–14, January 2008.

[35] B. Casu and U. Lindahl. Structure and biological interactions of heparin and heparan sulfate. *Adv.Carbohydr.Chem.Biochem.*, 57:159–206, 2001.

Appendix B:

The growth and differentiation of mesenchymal stem and progenitor cells cultured on aligned collagen matrices

Lanfer B.[a,b], Seib F.P.[a,b,c], Freudenberg U.[a,b], Stamov D.[a], Bley T.[d], Bornhäuser M.[b,c], Werner C.[a,b]

[a]Leibniz Institute of Polymer Research, Max Bergmann Center of Biomaterials Dresden, Hohe Street 6, Dresden 01069, Germany

[b]Technische Universität Dresden, Center for Regenerative Therapies, Tatzberg 47, 01307 Dresden, Germany

[c]University Hospital Carl Gustav Carus, Technische Universität Dresden, Fetscher Street. 74, Dresden 01307, Germany

[d]Technische Universität Dresden, Institute of Food Technology and Bioprocess Engineering, Bergstraße 120, 01069 Dresden, Germany

in *Biomaterials* 30 (2009) 5950-5958.

Abstract

Cell-matrix interactions are paramount for the successful repair and regeneration of damaged and diseased tissue. Since many tissues have an anisotropic architecture, it has been proposed that aligned extracellular matrix (ECM) structures in particular could guide and support the differentiation of resident mesenchymal stem and progenitor cells (MSCs). We therefore created aligned collagen type I structures using a microfluidic set-up with the aim to assess their impact on MSC growth and differentiation. In addition, we refined our aligned collagen matrices by incorporating the glycosaminoglycan (GAG) heparin to demonstrate the versatility of the applied methodology to study multiple ECM components in a single system. Our reconstituted, aligned ECM structures maintained and allowed multilineage (osteogenic/ adipogenic/chondrogenic) differentiation of MSCs. Most noticeable was the observation that during osteogenesis, aligned collagen substrates choreographed ordered matrix mineralization. Likewise, myotube assembly of C2C12 cells was profoundly influenced by aligned topographic features resulting in enhanced myotube organization and length. Our results shed light on the regulation of MSCs through directional ECM structures and demonstrate the versatility of these cell culture platforms for guiding the morphogenesis of tissue types with anisotropic structures.

1 Introduction

A fundamental requirement for recapitulating tissue architecture is to control cell-matrix interactions [1]. Achieving this goal by mimicking native cellular microenvironments is a priority for a number of scientific disciplines, including tissue engineering. The extracellular matrix (ECM) microenvironment is composed of a variety of structural components, including collagen, fibrin and elastin, arranged in complex architectures that are in part tissuespecific. For example, collagen is found as parallel fiber bundles in tendons and ligaments [2], as concentric waves in bone [3] and as oriented fibrils in the superficial zone of articular cartilage [4]. This spatial organization imparts mechanical strength to the tissue and impacts cellular function, including adhesion, orientation, proliferation and differentiation [5, 6, 7].

Frequently, tissue-specific cellular functions are assessed outside their native (ECM) microenvironment by cultivating cells on standard tissue culture ware. By doing so, they lose their native organization and adopt random distributions that do not resemble physiological tissue architecture. Thus there is a need to design systems that provide chemical–physical cues in a biologically relevant manner. Although collagen is applied to tissue culture substrates to yield non-fibrillar or randomly oriented fibrillar networks, native tissues frequently have aligned collagen structures. To overcome this limitation, we recently developed a method to create aligned collagen type I matrices *in vitro* [8]. Collagen type I fibrils are deposited and aligned on planar substrates by means of shear flowdeposition in a microfluidic channel. Although a number of other methodologies have been explored to generate oriented collagen substrates [9, 10, 11, 12], our technique is unique as it permits the formation of a highly aligned, native collagen matrix. Density and morphology can be tuned by adjusting microfluidic flow rate and collagen solution concentration.

Mesenchymal stem cells (MSCs) have been at the forefront of tissue engineering as they are readily isolated from adult donors, expanded *in vitro* and show robust differentiation into fat, cartilage and bone [13, 14, 15, 16]. Since MSCs contribute to highly organized tissue architectures (e.g. bone, cartilage), aligned ECM may be critically important for their differentiation. While aligned and patterned biomaterial scaffolds have been used to study the influence of geometric signals on neural stem cells [17, 18], fibroblasts [19], myoblasts [20] and MSCs [21, 22, 23], there are no reported studies employing aligned ECM matrices to guide and support multilineage mesenchymal differentiation. Therefore, in an effort to better understand the spatial and biochemical cues regulating cell behavior, we examined the ability of our aligned ECM structures to guide and support the differentiation of mesenchymal stem and progenitor cells into specific lineages. In addition, we refined our aligned collagen matrices by incorporating the glycosaminoglycan (GAG) heparin to (a) demonstrate the visibility of the applied methodology to study multiple ECM components in a single system, (b) mimic the broad variety of ECM structures found *in vivo* more closely, and (c) study the impact of multiple biochemical cues in our set-up.

2 Materials and methods

2.1 Preparation of glass substrates and collagen solution

Surface activation of glass coverslips with Poly(octadecene-alt-maleic acid) (POMA; Polysciences, Warrington, PA) was performed as described elsewhere [8, 24]. To prepare the collagen solution, bovine dermal collagen I (purified and pepsinsolubilized in 0.012 N HCl, PureCol, Inamed, Milmont Drive, USA) was brought to physiological pH by mixing eight parts acidified collagen solution (3.0 mg/ml) with one part 10-fold concentrated phosphate buffered saline (PBS, Sigma, Steinheim, Germany) and one part 0.1 M NaOH. All components were kept on ice before and after mixing. Appropriate volumes of chilled 1xPBS were added to adjust the final concentration of the collagen solution.

2.2 2.2. Non-aligned ECM structures

To facilitate precise coating of collagen in designated areas, a silicone-based culture insert (Ibidi GmbH, Martinsried, Germany) consisting of two wells was placed onto a tempered POMA-coated glass slide [24]. A chilled non-fibrillar collagen solution (100 ml at 0.4 mg/ml) was placed in each well and kept in a CO2- free incubator at 37°C to initiate fibril formation. After 90 min, the resulting fibrillar collagen gel and the culture insert were removed from the surface leaving two 0.22 cm^2 rectangular areas covered with a thin collagen layer on the substrate. The modified surface was rinsed with PBS and stored in PBS until use. For collagen/ heparin surfaces, collagen fibril formation was performed as described above. After washing with PBS, a heparin (sodium salt from porcine intestinal mucosa, Fluka, Steinheim, Germany)/PBS solution (2 mg/ml) was placed (100 ml) into each well of the culture inset and allowed to equilibrate for 20 min before rinsing with PBS.

2.3 Aligned ECM structures and functionalization with heparin

Aligned collagen matrices were prepared using the microfluidic set-up described previously [8]. Aligned collagen heparin matrices were prepared analogously to the aligned collagen samples. Following the final PBS rinse, substrates were functionalized by streaming a heparin/PBS solution (2 mg/ml) through the channel for 20 min at 11 μl/min and subsequently washing with PBS. All samples were sterilized under UV light for 5 min.

2.4 Characterization of reconstituted ECM structures

After reconstitution, aligned and non-aligned collagen matrices were characterized by atomic force microscopy (AFM), confocal reflection microscopy (CRM) and laser scanning microscopy (LSM). For atomic force micrographs, the surface topography of air-dried collagen matrices was investigated via intermittent contact scanning force microscopy with a PicoSPM (Molecular Imaging, Phoenix, AZ, United States) using silicon cantilevers (Tap300, BudgetSensors, Bulgaria) with a resonant frequency of 300±100 kHz, force constant of 40 N/m and tip radius <10

nm. Confocal reflection microscopy (TCS SP 1/5, Leica, Bensheim, Germany) was performed at a wavelength of 488 nm (Ar laser) to visualize collagen fibrils, including heparin coated collagen fibrils, as described elsewhere [25]. CRM pictures of fibril matrices were obtained using a 63x oil immersion objective. Heparin deposited on collagen matrices was visualized using FITC-labeled heparin (Molecular Probes, Leiden, Netherlands). Fluorescent labeled and unlabeled polysaccharides were mixed at a ratio of 1:40 to yield an average concentration of 2.4 mg/ml in PBS. The surfaces were imaged using a confocal laser scanning microscope (TCS SP 1/5, Leica, Bensheim Germany) with a 63x oil immersion objective.

2.5 Cell culture

Human bone marrow-derived MSCs were isolated from healthy donors (male/ female, 22–25 years of age) after obtaining their informed consent. The cells were expanded and characterized as described previously [26]. The study was approved by the institutional review board of the Medical Faculty at the University Hospital Dresden. Cells were cultured in Dulbecco's modified essential medium (DMEM) (low glucose) supplemented with 10% fetal bovine serum (FBS), maintained in a humidified atmosphere of 5% CO_2 and subcultured when cells were approximately 80% confluent. The experiments were performed with low passage cells (<5) that were seeded at 5 x 10^3 cells/cm^2 on the various substrates unless indicated otherwise. C2C12 (mouse multipotent mesenchymal progenitors) were obtained from the American Type Culture Collection (Manassas, USA) and maintained as proliferating myoblasts in DMEM-high-glucose medium supplemented with 10% FBS with a seeding density of 5 x 10^3 cells/cm^2.

2.6 Cell viability and orientation analysis

MSCs were plated on substrates (5 x 10^3 cells/cm^2) and at days 2, 4 and 7, cells were incubated with fluorescein diacetate (FDA) and propidium iodide (PI) to stain viable and dead cells, respectively. Briefly, solutions of 100 mg/ml FDA and PI were prepared by dissolving the former in acetone and the latter in PBS (pH 7.4). A fresh working stock containing 100 ng/ml of FDA and 2 mg/ml of PI was prepared in PBS and added directly to the cell cultures (i.e. culture medium was not changed) at a 1:1 volume ratio. Samples were incubated for ∼2 min and visualized using a confocal laser scanning microscope with a 10x oil immersion objective. Images were taken from cells on the area covered with aligned collagen fibrils or the corresponding control area (5 mm x 1 mm) at the indicated time point. Using the image software NIH ImageJ 1.37v, a threshold value of the reflection intensity was defined to isolate cells frombackground. The orientation of each cell was determined by identifying its major axis with respect to the horizontal axis where the alignment direction corresponded to an angle of 0°. A histogram of the angular distribution of cells was plotted based on the relative frequency of orientation angles (classified into bins of 10° angles).

2.7 Differentiation studies

2.7.1 Osteogenic differentiation

MSCs were plated on respective substrates using DMEM (low glucose; Gibco) supplemented with 10% FBS as detailed above. After 7 days in culture, the medium was changed to DMEM+10% FBS supplemented with osteogenic supplement (100 mM ascorbic acid, 10 mM glycerophosphate and 100 nM dexamethasone). The supplemented medium and the respective control medium (DMEM+10% FBS) were replaced every 2–3 days. At week 3, von Kossa staining was used to stain matrix mineralization as detailed previously [26, 27] and visualized by light microscopy (Leica DMIL, Leica Microsystems GmbH, Wetzlar, Germany). Images of mineralization on aligned EC structures or the corresponding area (5 mm x 1 mm) on controls were taken. For quantification, a threshold value of the reflection intensity was defined to isolate mineralized nodules from background and the total mineralized area was calculated.

2.7.2 Adipogenic differentiation

MSCs were plated on respective substrates and allowed to establish themselves as described above. At day 7, cultures were switched to adipogenic medium (Mesencult supplemented with 10% adipogenic supplement from Stem Cell Technologies, Vancouver Canada). At week 3, lipid accumulation was quantified by Nile red staining as detailed elsewhere [28]. Briefly, cells were fixed in 1.5% glutaraldehyde for 5 min, washed with PBS and incubated for 30 min with Nile Red (100 ng/ml in PBS). Cell nuclei were stained with DAPI (100 ng/ml). Lipid vacuoles and cell nuclei were visualized using epi-fluorescent microscopy (Leica DM IRE2, Leica Microsystems, Wetzlar Germany). To quantify lipid vacuoles, images of Nile Red positive areas on aligned ECM structures or the corresponding control area (5 mm1mm) were taken using a confocal laser scanning microscope (TCS SP, Leica, Wetzlar, Germany). A threshold value of the fluorescent intensity was defined to isolate lipidrich vacuoles from background and the total Nile Red positive area was calculated.

2.7.3 Myogenic differentiation

C2C12s were plated on ECM substrates and respective controls at an initial plating density of 5 x 10^3 cells/cm^2. To induce myogenic differentiation of C2C12s, cells were switched to DMEM supplemented with 10% horse serum when they were ∼95% confluent (i.e. within 3 days of initial plating). After 1 week, C2C12 cells were fixed in ethanol:formaldehyde:acetic acid (20:2:1, v/v/v) at -20°C for 10 min. The cells were rehydrated with PBS and incubated for 2 h at 37°C with a monoclonal antibody against myosin heavy chain (MHC) (MF20, Developmental Studies Hybridoma Bank, University of Iowa, IA) at a final concentration of 10 μg/ml in PBS supplemented with 1% goat serum. The cells were then washed twice with PBS and incubated with goat anti-mouse IgG 2b (1:400, Invitrogen Molecular Probes, Eugene). Subsequently cell nuclei were stained with DAPI for 15 min at room temperature. Cells were rinsed and then mounted onto microscope slides using an antifade mounting medium. Images were captured using a

confocal laser scanning microscope (TCS SP, Leica, Bensheim, Germany) and epi-fluorescent microscope (Leica DM IRE2, Leica Microsystems, Wetzlar Germany).

2.8 Statistical analyses

Data were analyzed using GraphPad Instat 3.06 (GraphPad Software, La Jolla USA). Multiple samples were analyzed by one-way analysis of variance (ANOVA) followed by Tukey-Kramer's post hoc test to evaluate the statistical differences (p 0.05) among all samples.

3 Results

3.1 Reconstituted ECM structures

Aligned collagen matrices were generated by employing a novel microfluidic system that has been carefully characterized [8]. In the current study, a 0.8 mg/ml collagen solution was used to generate aligned matrices containing long fibrils at high density (Fig. 1A). In contrast, static fibril formation by a 0.4 mg/ml collagen solution produced randomly oriented collagen fibrils (Fig. 1B). This collagen concentration was chosen for the static system to yield fibril densities comparable to those observed using the microfluidic setup (data not shown). In an effort to mimic native ECM structures more closely and to study the impact of selected GAGs on cell behavior, we functionalized the aligned collagen matrices with heparin. The aligned collagen matrices were first reconstituted (Fig. 1C), then a heparin/PBS solution (2 mg/ml) was subsequently streamed across. CRM and fluorescent micrographs revealed that FITC-labeled heparin co-localized with the corresponding fibrillar matrices, indicating that this 1-step functionalization process decorated most of the collagen fibrils with heparin (Fig. 1C–F). Isotropic collagen/heparin networks were achieved by static incubation of a random network of collagen (Fig.1D) with a heparin/PBS solution (2 mg/ml) (Fig. 1F). Heparin immobilization was subsequently shown to be stable for 3 days when incubated with culture medium (data not shown).

3.2 Cell orientation and viability on reconstituted ECM structures

MSCs were cultured on reconstituted ECM structures (aligned collagen; aligned collagen/heparin; random collagen; random collagen/heparin) and imaged using laser scanning microscopy to examine the effect of fibril alignment on cell orientation and proliferation at days 1, 4 and 7. To simultaneously examine both cell viability and shape, cells were treated with FDA. On all studied substrates, the vast majority of the cells were viable over the study period. Note, dead cells are not captured in the representative images here due to their low abundance (Fig. 2). MSCs seeded on non-aligned ECM structures showed no preferential orientation at any time (Fig. 2A–C). In contrast, cells on aligned collagen and collagen/heparin matrices exhibited an elongated morphology in the direction of the underlying fibrils (Fig. 2G–I,M–O). The addition of heparin did not affect cell viability or alter the cell orientation or morphology. The extent of cell

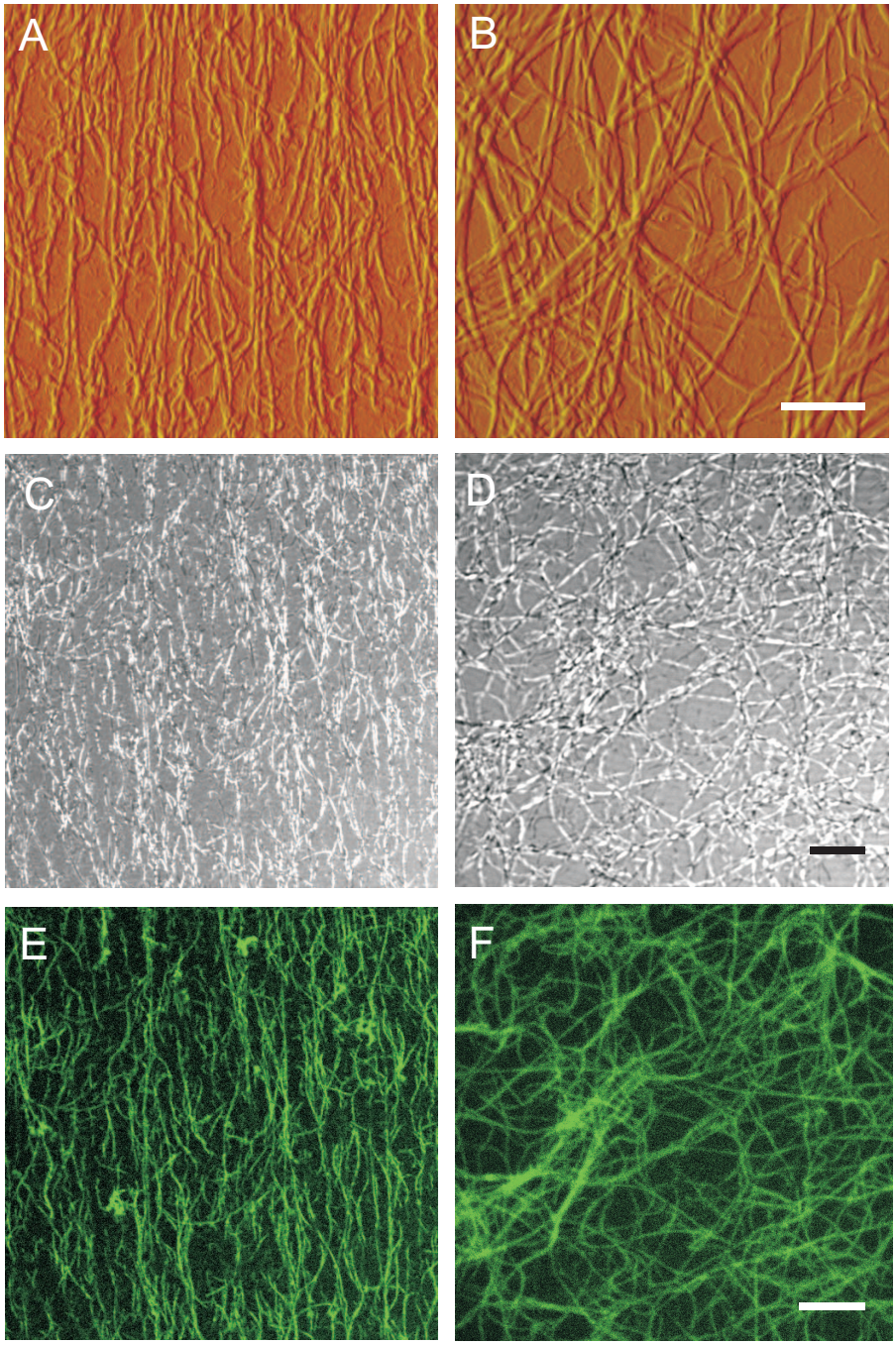

Figure 1: Micrographs of aligned and randomly aligned ECM structures. Atomic force micrographs of (A) aligned collagen matrices and (B) randomly oriented collagen matrices produced by shear flow deposition and static fibril formation, respectively. Scale bar 2 μm. CRM images of heparin-FITC-coated (C) aligned collagen matrices and (D) non-aligned matrices and corresponding fluorescent LSM images visualizing FITC-labeled heparin (green) on (E) aligned and (F) non-aligned collagen. Scale bar 5 μm.

orientation was quantified by determining the orientation angle of each cell with regard to the direction of the aligned fibrils, which was set at 0 as a reference angle. A histogram of orientation angle distribution is shown for each fluorescent micrograph (Fig. 2). This quantitative analysis confirmed our qualitative observations (Fig. 2 A–C, G–I, M–O). Image analysis also indicated that the rate of MSC proliferation on all reconstituted ECM substrates was similar and there were no statistical differences between functionalized and/or aligned matrices (Supplementary Fig. 1).

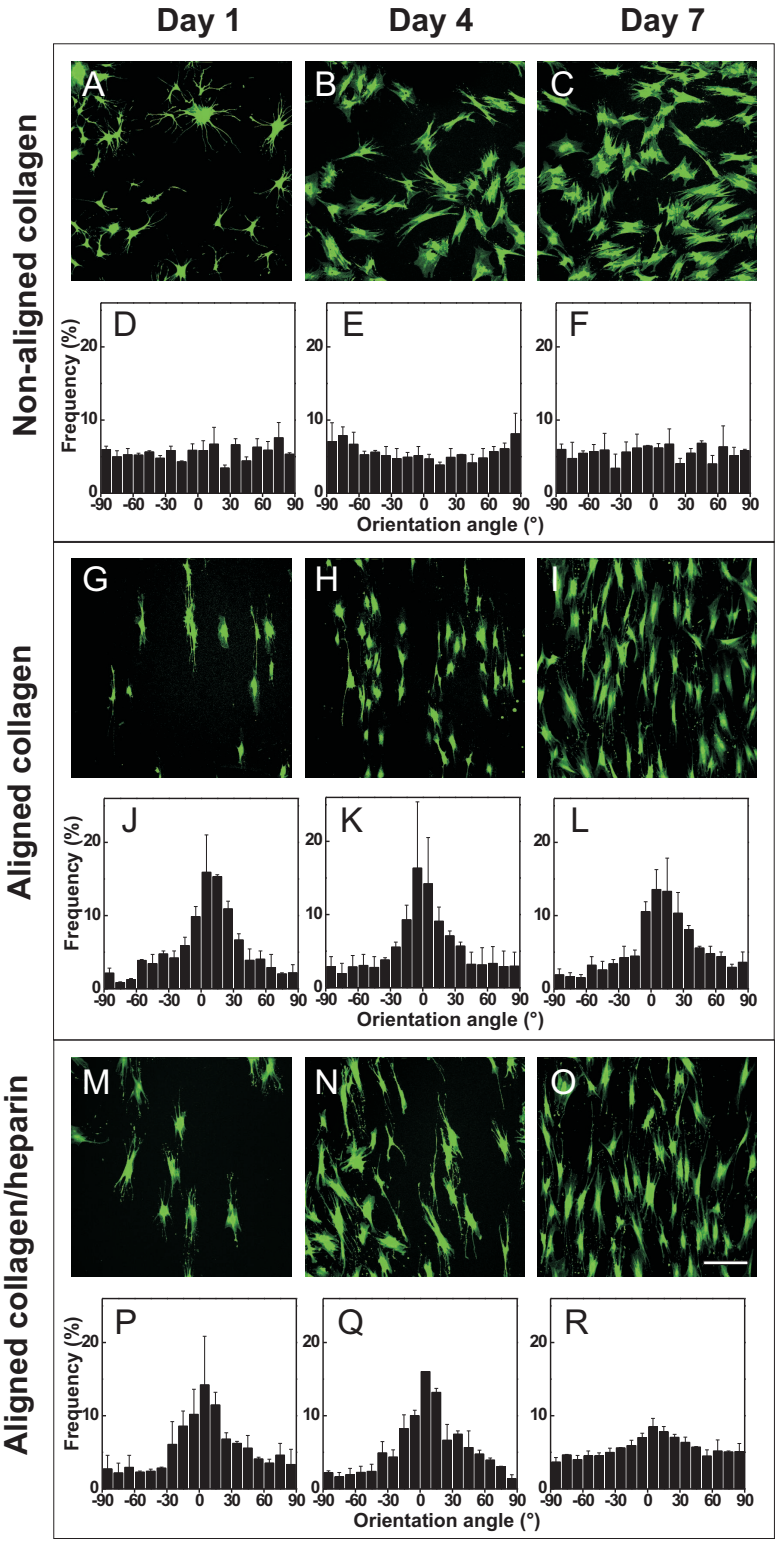

Figure 2: Influence of aligned and randomly aligned ECM structures on cell morphology and orientation. Viable MSCs (green) adopting random and oriented morphologies on non-aligned (A–C) and aligned collagen (G–I) at days 1, 4 and 7. Quantification of cell orientation angles with the corresponding images is shown in the panels below (D–F, J–L). Analogues images (M–O) and quantification (P–O) for cells cultured on heparin functionalized aligned collagen substrates. (Scale bar 200 μm;±s.d., n = 4 replicates from 2 different donors).

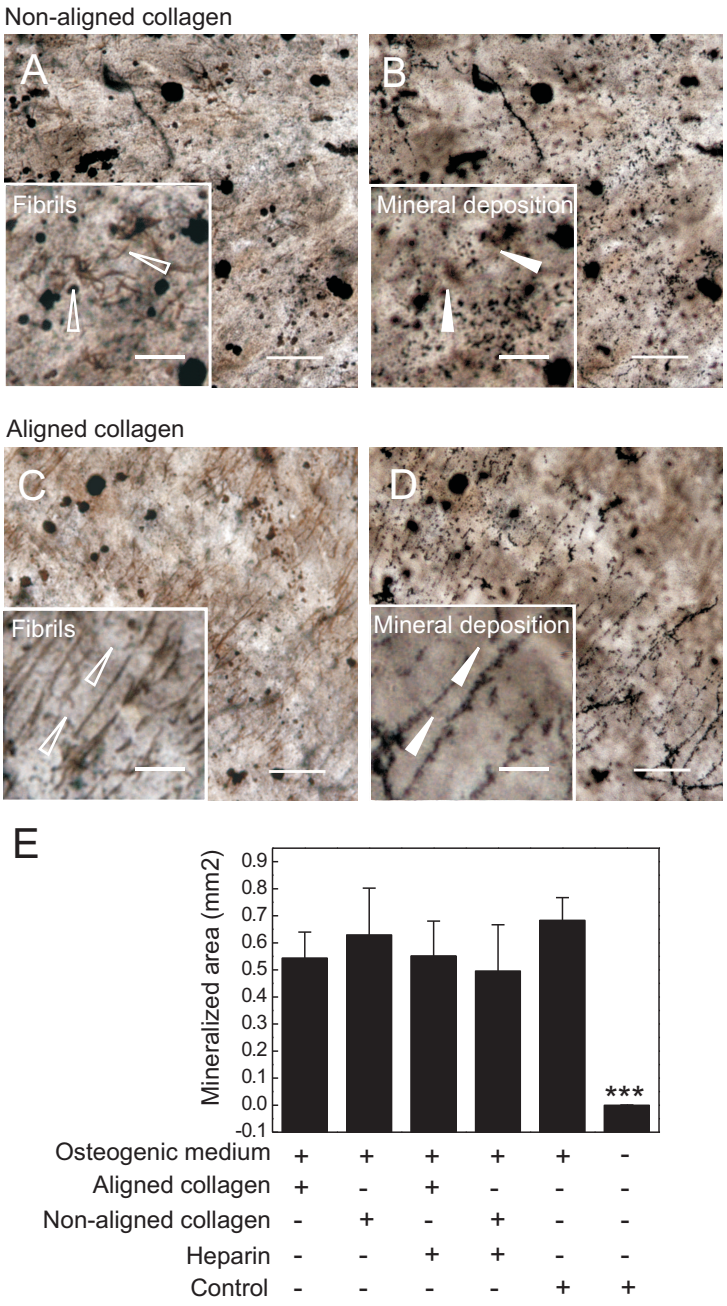

Figure 3: Osteogenesis of MSCs on non-aligned and aligned collagen. MSCs were plated on the substrates and allowed to establish themselves for 7 days. Cultures were then switched to osteogenic medium where indicated and matrix mineralization was detected with von Kossa staining after 2 weeks. At the lower focal plane (A) non-aligned fibrillar structures (open arrows) are visible and above this plane (B) non-aligned mineralized nodules (closed arrows) are visible. At the lower focal plane (C) aligned fibrillar structures (open arrows) are visible and above this plane (D) aligned mineralized nodules (closed arrows) are visible. Scale bar 30 μm, insets 15 μm. (E) Quantitative assessment of mineralization area on the reconstituted ECM structures. Glass served as control surface. Statistical differences between samples were determined using one-way ANOVA and Tukey-Kramer multiple comparison post hoc test (*$p < 0.05$, $\pm$s.d., $n = 4$ replicates from 2 different donors). Note that the mineralized area for non-induced glass control is representative for all aligned and non-aligned ECM substrates in standard medium.

3.3 Osteogenic differentiation of MSCs

A reliable and functional readout for the formation of mature osteoblasts is matrix mineralization [29]. This can be verified by von Kossa staining, which stains areas of mineralization black [26, 27]. MSCs induced with osteogenic medium showed abundant mineralized nodules (i.e. positive von Kossa staining) when cultured on all substrates (Fig. 3A–D). On non-aligned ECM, POMAcoated glass and glass, these calcium accumulations were isotropically distributed (Fig. 3B). However, on aligned ECM structures, mineralized nodules were lined up in an ordered fashion (Fig. 3D). Underneath the mineralized nodules, fibrillar structures were found on both non-aligned and aligned substrates (Fig. 3A,B), indicating that these fibrillar structures provide a framework for the deposition of mineralized nodules. On POMA and glass substrates, no such fibrillar structures were observed. The extent of mineral deposition on the different substrates was quantified by determining the total mineralization area for each substrate. There was a significant increase in mineralization for stimulated cells compared to controls. However, the absolute amount of mineralization on POMA and aligned collagen appeared to be lower than for the other treated groups (Fig. 3E). Cells cultured on reconstituted ECMs did not show spontaneous differentiation and yielded levels of von Kossa staining comparable to the controls shown in Fig. 3.

3.4 Adipogenic differentiation of MSCs

The potential of MSCs to differentiate into adipocytes on aligned ECM was evaluated by culturing MSCs in lineage-specific differentiation medium. After 3 weeks in differentiation medium, the cells were stained with Nile Red to detect the lipid-rich vacuoles of adipocytes that may have developed (Fig. 4A). Adipogenesis was quantified by determining the total Nile Red positive area for each sample (Fig. 4B). Quantitative data showed that adipogenic differentiation successfully occurred on all substrates since a significantly higher amount of lipid vacuoles/Nile Red positive area was observed for stimulated cells compared to controls (Fig. 4B). Alignment of ECM substrates and functionalization with heparin did not significantly change the adipogenic differentiation behavior (Fig. 4B). Cells cultured on reconstituted ECMs did not show spontaneous adipogenesis and yielded levels of Nile red staining comparable to the controls shown in Fig. 4.

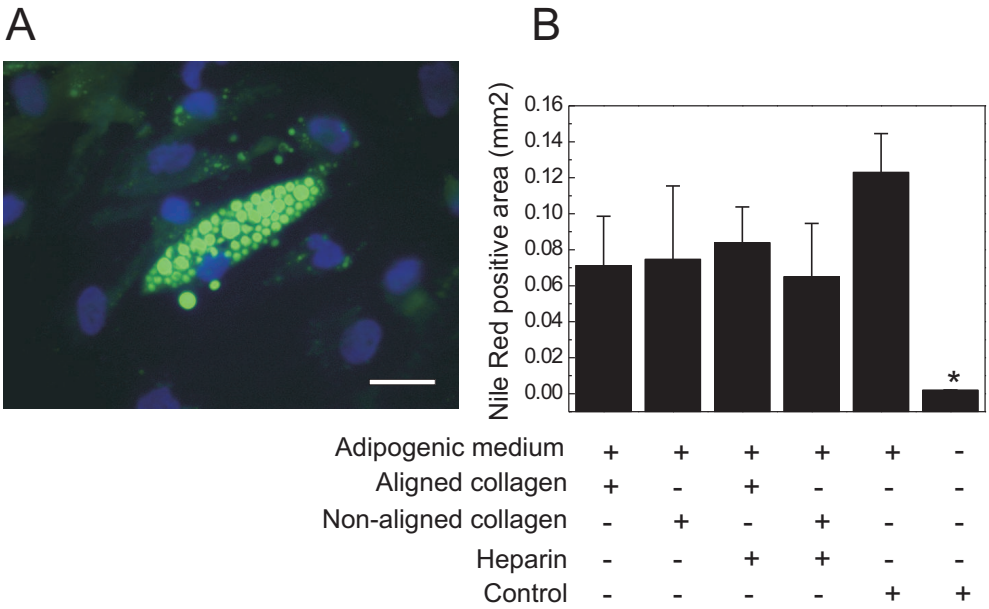

Figure 4: Adipogenesis of MSCs cultured on aligned and non-aligned ECM structures. Glass served as control surface. (A) After a 3-week incubation with adipogenic differentiation medium, cells were stained with Nile Red (green) to mark typical lipid-rich vacuoles within cells; nuclei were stained with DAPI (blue). Scale bar 30 μm. (B) Quantification of Nile Red positive areas on the different substrates to assess adipogenesis. Statistical differences between samples were determined using one-way ANOVA and Tukey-Kramer multiple comparison post hoc test (*$p < 0.05$, $\pm$s.d., $n = 4$ replicates from 2 different donors). Note that Nile Red positive areas for the non-induced glass control are representative for all aligned and non-aligned ECM substrates in standard medium.

3.5 Myogenic differentiation of C2C12 cells

We studied the ability of aligned collagen structures to both guide and support morphogenesis of skeletal muscle tissue using C2C12 myoblasts as a model system. To visualize myotubes formed by fused myoblasts, the samples were stained for myosin heavy chain (MHC), a marker of differentiatedmyofibers. Myotubes on the aligned matrices were highly organized and globally aligned (Fig. 5A,B,D). In contrast, myotubes on non-aligned collagen were oriented in a wide range of directions (Fig. 5C). In some areas myotubes showed local alignment, however, they were not aligned globally. The effect of aligned collagen matrices on myotube orientation was quantified by measuring the myotube orientation angle on each substrate. The observation that myotubes were organized isotropically on random matrices was confirmed by the random distribution of orientation angles in the corresponding histogram (Fig. 5E). In contrast, aligned collagen matrices promoted skeletal muscle morphogenesis into parallel-oriented myotubes as revealed by the corresponding histograms with a peak of angular distribution at 0° (Fig. 5F).

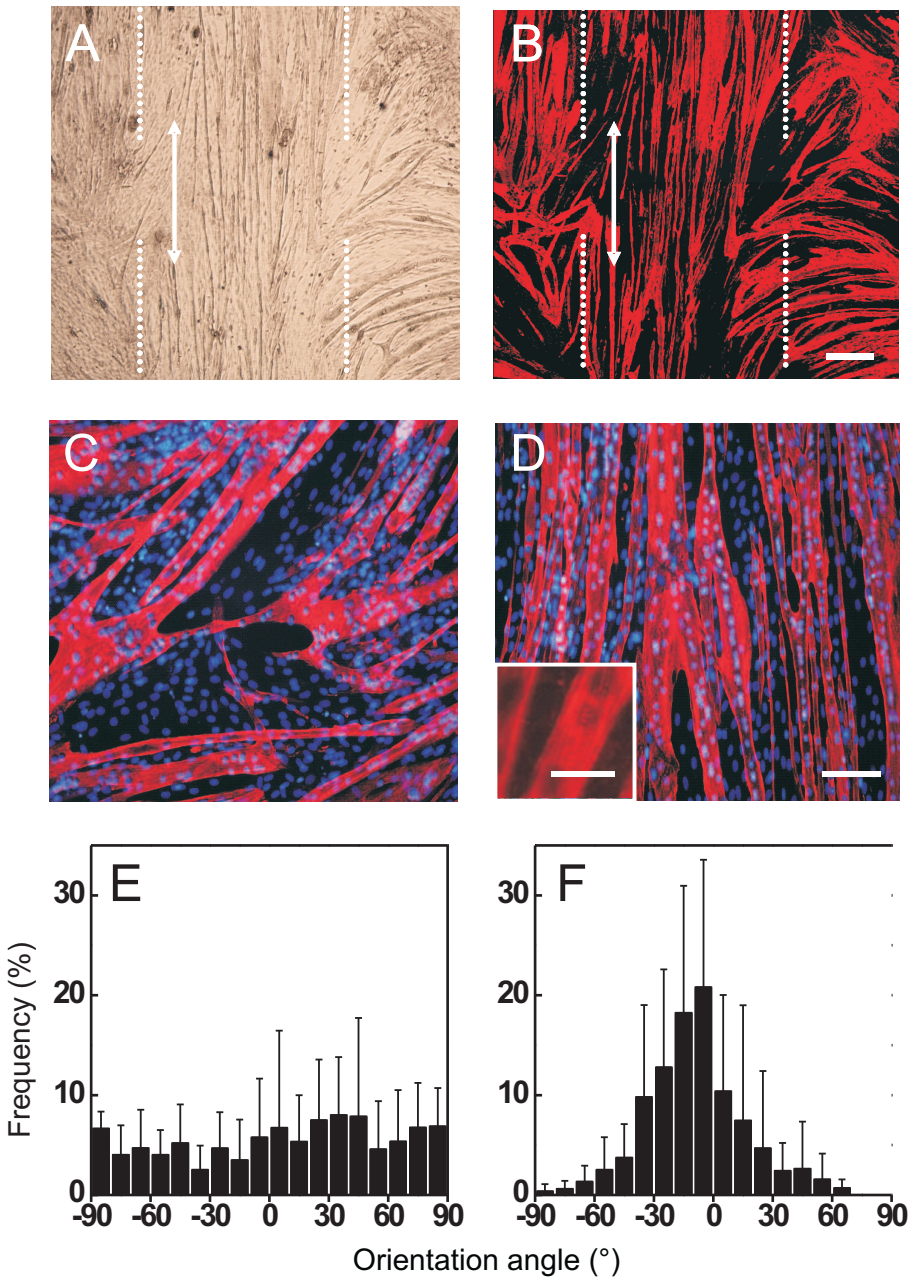

Figure 5: C2C12 myotube orientation is influenced by aligned collagen matrices. Immunofluorescence staining of skeletal MHC and nuclei was performed to visualize myotubes. (A,B) Phase contrast and the corresponding fluorescent image of C2C12s on aligned collagen after 7 days in culture. Arrows and dotted line mark direction and position of aligned ECM, respectively. Scale bar 250 μm. Myotubes are randomly distributed on (C) random matrices, whereas on (D) aligned collagen myotubes adopt highly ordered structures. Scale bar 120 μm, inset 30 μm. (E,F) Cell orientation for cells cultured on (E) non-aligned and (F) aligned collagen matrices ($\pm$s.d.; n = 4 replicates).

4 Discussion

Several *in vitro* studies have demonstrated the importance of aligned topographical cues on cell behavior, employing either aligned electrospun fibers [30, 31] or micro/nanogrooves/patterns [21, 22, 32, 33, 34]. In particular, structures in the nanometer range are known to be crucial for cell proliferation and migration, and act as potent effectors of differentiation [35]. Here we used reconstituted, aligned collagen type I fibrils that resemble collagen fibrils in their native ECM conformation, with diameters ranging from 20 nm to 70 nm and typical banding patterns of 67 nm [36] (Fig. 1). In an effort to go beyond single component ECM systems, we developed an approach allowing rapid functionalization of reconstituted ECM structures. As a demonstration, we locally immobilized heparin, an abundant GAG in ECM, onto aligned and non-aligned collagen fibrils (Fig. 1C–F). This is especially relevant for future applications as heparin is known to bind growth factors and mediate protein binding *in vitro* and *in vivo* [37]. Thus, our method enables the study of multiple biochemical and physical cues in a single set-up and provides a versatile cell culture platform that can be tailored as needed.

Because most tissues and organs are multiphasic in nature and contain multiple cell types, one of our goals was to support multilineage cell types. MSCs differentiate into a variety of connective tissue lineages, including bone, cartilage and adipose [13], making them promising candidates for regenerative medicine. However, to fully exploit MSCs, our understanding of how biochemical– biophysical (ECM) cues impact cell behavior must be increased. None of the ECM substrates used here decreased cell viability within the study period, indicating that our coatings are biocompatible and suitable for culturing primary stem cells. Moreover, the MSCs reacted to the physical signals from the substrates as their cell morphology altered to resemble the anisotropic topographies of the aligned ECM structures (Fig. 2). The aligned structures promoted an elongated cell shape oriented in direction of the underlying collagen or collagen/heparin fibrils, whereas cells were randomly distributed on non-aligned matrices. MSCs can thus 'sense' the aligned topography of the ECM through contact guidance [6, 38]. Cell proliferation was not influenced.

As physical cues are known to play a role in MSC differentiation [22, 39, 40], we additionally addressed the effect of aligned and nonaligned ECM structures on differentiation. We found that aligned ECM structures dictate cell orientation and directly impact differentiation outcome. In the case of osteogenesis, mineralization was highly organized and orchestrated by the underlying ECM, which served as a nucleation network [41, 42]. This was clearly demonstrated by aligned ECM structures that resulted in aligned mineralized nodules, indicating that cell-matrix interactions are precisely controlled by the topographical features of the ECM substrate. Considering the hierarchical structure of bone, i.e. ordered mineralization and oriented collagen type I fibrils, directed mineralization is an important prerequisite for mimicking *in vivo* bone formation. Thus, our results are important for bone tissue engineering and emphasize that cells reciprocally interact with surrounding ECM by adapting cell behavior and function to changes in ECM structure and topography [43]. The extent of osteogenic differentiation however was not significantly affected by aligned and functionalized substrates (Fig. 3E). Considering that collagen type I gels (2.4 mg/ml) are reported to accelerate mineralization *in vitro* [41], it is likely that a certain

critical collagen amount is necessary to achieve this effect. We also found that under adipogenic differentiation conditions MSCs developed into mature adipocytes. Although there are indications in the literature that heparin enhances adipogenesis [44, 45], no such effect was observed in the present study. It is currently not clear if the presence of collagen is responsible for this discrepancy. The standard *in vitro* pellet culture [46] for chondrogenic differentiation of MSCs was not feasible in our system due to technical limitations. However, we did perform a 3-week monolayer culture of MSCs in chondrogenic differentiation medium to examine the ability of the substrates to support chondrogenesis. Stimulation of the cells increased sulfated GAG (sGAG) content (Supplementary Fig. 2) on both non-aligned and aligned substrates. This increase in sGAG content might be due to increasing proteoglycan synthesis, a marker of early chondrogenesis [47]. However, considering that cellular condensation is a prerequisite for chondrogenesis, a monolayer culture has its obvious limitations [48].

Differentiation of human MSCs along the myogenic lineage has previously been controversial. While it was reported that murine MSCs were successfully differentiated into skeletal myoblasts and cardiomyocytes [49, 50], conflicting results have been published with respect to MSCs from other species including human [51, 52]. We therefore chose the C2C12 model system to assess the influence of topographical features on myoblast differentiation and myotube fusion. Only recently have research efforts been made to engineer cardiac anisotropy [53] and C2C12 myoblasts have been shown to align into parallel arrays that fuse to form oriented myotubes in response to aligned topographies [35, 54]. We demonstrated that aligned collagen matrices give rise to aligned and highly organized myotubes, choreographed by the underlying fibrillar structures. These fibrillar structures closely mimic physiological conditions in skeletal muscle and thus prove to be a suitable *in vitro* model system. Although we could not quantify the length of the myotubes due to technical limitations, it appeared that longer myotubes formed on aligned matrices than on randomly aligned ones. This observation is consistent with a recent study reporting enhanced myotube length by an aligned poly(L-lactide) nanofiber scaffold [35].

5 Conclusions

We demonstrated that aligned ECM matrices generated by a novel technique using shear flow deposition directed, supported, and maintained multilineage differentiation of mesenchymal stem and progenitor cells. We showed that myotube assembly of C2C12s was profoundly influenced by topographic features and that aligned collagen could enhance myotube organization and length. Furthermore, aligned collagen culture substrates were found to orchestrate and direct ordered matrix mineralization during osteogenesis of human MSCs. This work not only sheds light on the regulation of mesenchymal stem and progenitor cell alignment and differentiation through directional ECM structures, but also shows the versatility of our novel cell culture platforms in which aligned ECM structures are readily functionalized. Importantly, our system has the potential to guide morphogenesis of other tissue types with anisotropic structure, e.g., cardiac muscle, blood vessel, tendon, and ligament. In such efforts, the immobilization of heparin could provide a means for growth factor presentation.

References

[1] M.P. Lutolf and J.A. Hubbell. Synthetic biomaterials as instructive extracellular microenvironments for morphogenesis in tissue engineering. *Nat Biotechnol*, 23(1):47–55, January 2005.

[2] D.H. ELLIOTT. Structure and function of mammalian tendon. *Biological Reviews of the Cambridge Philosophical Society*, 40(3):392–&, 1965.

[3] S. Weiner and W. Traub. Bone structure: from angstroms to microns. *FASEB J*, 6(3):879–885, February 1992.

[4] J.S. Temenoff and A.G. Mikos. Review: tissue engineering for regeneration of articular cartilage. *Biomaterials*, 21(5):431–440, March 2000.

[5] R. Vanderby and P.P. Provenzano. Collagen in connective tissue: from tendon to bone. *J Biomech.*, 36(10):1523–1527, October 2003.

[6] G.A. Dunn and T. Ebendal. Contact guidance on oriented collagen gels. *Exp Cell Res*, 111(2):475–479, February 1978.

[7] D. Ceballos, X. Navarro, N. Dubey, G. Wendelschafer-Crabb, W.R. Kennedy, and R.T. Tranquillo. Magnetically aligned collagen gel filling a collagen nerve guide improves peripheral nerve regeneration. *Exp Neurol.*, 158(2):290–300, August 1999.

[8] B. Lanfer, U. Freudenberg, R. Zimmermann, D. Stamov, V. Korber, and C. Werner. Aligned fibrillar collagen matrices obtained by shear flow deposition. *Biomaterials*, 29(28):3888–3895, October 2008.

[9] T. Elsdale and J. Bard. Collagen substrata for studies on cell behavior. *J Cell Biol*, 54(3):626–637, September 1972.

[10] D.A. Cisneros, J. Friedrichs, A. Taubenberger, C.M. Franz, and D.J. Muller. Creating ultrathin nanoscopic collagen matrices for biological and biotechnological applications. *Small*, 3(6):956–963, June 2007.

[11] J. Torbet and M.C. Ronziere. Magnetic alignment of collagen during self-assembly. *Biochem J*, 219(3):1057–1059, May 1984.

[12] C. Guo and L.J. Kaufman. Flow and magnetic field induced collagen alignment. *Biomaterials*, 28(6):1105–1114, February 2007.

[13] M.F. Pittenger, A.M. Mackay, S.C. Beck, R.K. Jaiswal, R. Douglas, J.D. Mosca, M.A. Moorman, D.W. Simonetti, S. Craig, and D.R. Marshak. Multilineage potential of adult human mesenchymal stem cells. *Science*, 284(5411):143–147, April 1999.

[14] Y. Jiang, B.N. Jahagirdar, R.L. Reinhardt, R.E. Schwartz, C.D. Keene, X.R. Ortiz-Gonzalez, M. Reyes, T. Lenvik, T. Lund, M. Blackstad, J. Du, S. Aldrich, A. Lisberg, W.C. Low, D.A. Largaespada, and C.M. Verfaillie. Pluripotency of mesenchymal stem cells derived from adult marrow. *Nature*, 418(6893):41–49, July 2002.

[15] D.J. Prockop. Marrow stromal cells as stem cells for nonhematopoietic tissues. *Science*, 276(5309):71–74, April 1997.

[16] J.R. Mauney, V. Volloch, and D.L. Kaplan. Role of adult mesenchymal stem cells in bone tissue engineering applications: current status and future prospects. *Tissue Eng*, 11(5-6):787–802, May 2005.

[17] J.B. Recknor, D.S. Sakaguchi, and S.K. Mallapragada. Directed growth and selective differentiation of neural progenitor cells on micropatterned polymer substrates. *Biomaterials*, 27(22):4098–4108, August 2006.

[18] E. Schnell, K. Klinkhammer, S. Balzer, G. Brook, D. Klee, P. Dalton, and J. Mey. Guidance of glial cell migration and axonal growth on electrospun nanofibers of poly-epsilon-caprolactone and a collagen/poly-epsilon-caprolactone blend. *Biomaterials*, 28(19):3012–3025, July 2007.

[19] T.R. Elsdale. Parallel orientation of fibroblasts in vitro. *Exp Cell Res*, 51(2-3):439–450, August 1968.

[20] K. Shimizu, H. Fujita, and E. Nagamori. Alignment of skeletal muscle myoblasts and myotubes using linear micropatterned surfaces ground with abrasives. *Biotechnol.Bioeng.*, 103(3):631–638, June 2009.

[21] M.J. Dalby, N. Gadegaard, R. Tare, A. Andar, M.O. Riehle, P. Herzyk, C.D. Wilkinson, and R.O. Oreffo. The control of human mesenchymal cell differentiation using nanoscale symmetry and disorder. *Nat.Mater.*, 6(12):997–1003, December 2007.

[22] S. Oh, K.S. Brammer, Y.S. Li, D. Teng, A.J. Engler, S. Chien, and S. Jin. Stem cell fate dictated solely by altered nanotube dimension. *Proc.Natl.Acad.Sci U.S.A*, 106(7):2130–2135, February 2009.

[23] J.K. Wise, A.L. Yarin, C.M. Megaridis, and M. Cho. Chondrogenic differentiation of human mesenchymal stem cells on oriented nanofibrous scaffolds: Engineering the superficial zone of articular cartilage. *Tissue Engineering Part A*, 15(4):913–921, April 2009.

[24] T. Pompe, S. Zschoche, N. Herold, K. Salchert, M.F. Gouzy, C. Sperling, and C. Werner. Maleic anhydride copolymers–a versatile platform for molecular biosurface engineering. *Biomacromolecules*, 4(4):1072–1079, July 2003.

[25] S.L. Voytik-Harbin, B. Rajwa, and J.P. Robinson. Three-dimensional imaging of extracellular matrix and extracellular matrix-cell interactions. *Methods in Cell Biology, Vol 63*, 63:583–+, 2001.

[26] J. Oswald, S. Boxberger, B. Jorgensen, S. Feldmann, G. Ehninger, M. Bornhauser, and C. Werner. Mesenchymal stem cells can be differentiated into endothelial cells in vitro. *Stem Cells*, 22(3):377–384, 2004.

[27] F.P. Seib, M. Franke, D. Jing, C. Werner, and M. Bornhauser. Endogenous bone morphogenetic proteins in human bone marrow-derived multipotent mesenchymal stromal cells. *Eur.J.Cell Biol.*, 88(5):257–271, May 2009.

[28] P. Greenspan, E.P. Mayer, and S.D. Fowler. Nile red - a selective fluorescent stain for intracellular lipid droplets. *Journal of Cell Biology*, 100(3):965–973, 1985.

[29] G.S. Stein and J.B. Lian. Molecular mechanisms mediating proliferation/differentiation

interrelationships during progressive development of the osteoblast phenotype. *Endocr.Rev.*, 14(4):424–442, August 1993.

[30] R. Murugan and S. Ramakrishna. Design strategies of tissue engineering scaffolds with controlled fiber orientation. *Tissue Engineering*, 13(8):1845–1866, August 2007.

[31] A.J. Meinel, K.E. Kubow, E. Klotzsch, M. Garcia-Fuentes, M.L. Smith, V. Vogel, H.P. Merkle, and L. Meinel. Optimization strategies for electrospun silk fibroin tissue engineering scaffolds. *Biomaterials*, 30(17):3058–3067, June 2009.

[32] B.S. Zhu, Q.H. Lu, J. Yin, J. Hu, and Z.G. Wang. Alignment of osteoblast-like cells and cell-produced collagen matrix induced by nanogrooves. *Tissue Engineering*, 11(5-6):825–834, May 2005.

[33] S. Martino, F. D'Angelo, I. Armentano, R. Tiribuzi, M. Pennacchi, M. Dottori, M. Samantha, A. Caraffa, G.G. Cerulli, J.M. Kenny, and A. Orlacchio. a-c:h nanopatterned film designs drive human bone marrow mesenchymal stem cell cytoskeleton architecture. *Tissue Eng Part A*, pages –, April 2009.

[34] D.Y. Wang, Y.C. Huang, H.S. Chiang, A.M. Wo, and Y.Y. Huang. Microcontact printing of laminin on oxygen plasma activated substrates for the alignment and growth of schwann cells. *Journal of Biomedical Materials Research Part B-Applied Biomaterials*, 80B(2):447–453, February 2007.

[35] N.F. Huang, S. Patel, R.G. Thakar, J. Wu, B.S. Hsiao, B. Chu, R.J. Lee, and S. Li. Myotube assembly on nanofibrous and micropatterned polymers. *Nano Letters*, 6(3):537–542, March 2006.

[36] V. Ottani, D. Martini, M. Franchi, A. Ruggeri, and M. Raspanti. Hierarchical structures in fibrillar collagens. *Micron.*, 33(7-8):587–596, 2002.

[37] B. Casu and U. Lindahl. Structure and biological interactions of heparin and heparan sulfate. *Adv.Carbohydr.Chem.Biochem.*, 57:159–206, 2001.

[38] G.A. Dunn and J.P. Heath. A new hypothesis of contact guidance in tissue cells. *Exp.Cell Res.*, 101(1):1–14, August 1976.

[39] A.J. Engler, S. Sen, H.L. Sweeney, and D.E. Discher. Matrix elasticity directs stem cell lineage specification. *Cell*, 126(4):677–689, August 2006.

[40] R. McBeath, D.M. Pirone, C.M. Nelson, K. Bhadriraju, and C.S. Chen. Cell shape, cytoskeletal tension, and rhoa regulate stem cell lineage commitment. *Dev.Cell*, 6(4):483–495, April 2004.

[41] M.P. Lynch, J.L. Stein, G.S. Stein, and J.B. Lian. The influence of type i collagen on the development and maintenance of the osteoblast phenotype in primary and passaged rat calvarial osteoblasts: modification of expression of genes supporting cell growth, adhesion, and extracellular matrix mineralization. *Exp.Cell Res.*, 216(1):35–45, January 1995.

[42] B. Zimmermann, H.C. Wachtel, and C. Noppe. Patterns of mineralization in vitro. *Cell Tissue Res.*, 263(3):483–493, March 1991.

[43] S. Liao, C.K. Chan, and S. Ramakrishna. Stem cells and biomimetic materials strategies

for tissue engineering. *Materials Science & Engineering C-Biomimetic and Supramolecular Systems*, 28(8):1189–1202, December 2008.

[44] W.J. Luo, H. Shitaye, M. Friedman, C.N. Bennett, J. Miller, O.A. MacDougald, and K.D. Hankenson. Disruption of cell-matrix interactions by heparin enhances mesenchymal progenitor adipocyte differentiation. *Experimental Cell Research*, 314(18):3382–3391, November 2008.

[45] S.L. Osip, M. Butcher, E. Young, L. Yang, and S.G. Shaughnessy. Differential effects of heparin and low molecular weight heparin on osteoblastogenesis and adipogenesis in vitro. *Thromb.Haemost.*, 92(4):803–810, October 2004.

[46] B. Johnstone, T.M. Hering, A.I. Caplan, V.M. Goldberg, and J.U. Yoo. In vitro chondrogenesis of bone marrow-derived mesenchymal progenitor cells. *Experimental Cell Research*, 238(1):265–272, January 1998.

[47] N. Kamiya, H. Watanabe, H. Habuchi, H. Takagi, T. Shinomura, K. Shimizu, and K. Kimata. Versican/pg-m regulates chondrogenesis as an extracellular matrix molecule crucial for mesenchymal condensation. *J.Biol.Chem.*, 281(4):2390–2400, January 2006.

[48] L. Quintana, zur Nieden N.I., and C.E. Semino. Morphogenetic and regulatory mechanisms during developmental chondrogenesis: new paradigms for cartilage tissue engineering. *Tissue Engineering Part B*, 15(1):29–41, 2009.

[49] S. Makino, K. Fukuda, S. Miyoshi, F. Konishi, H. Kodama, J. Pan, M. Sano, T. Takahashi, S. Hori, H. Abe, J. Hata, A. Umezawa, and S. Ogawa. Cardiomyocytes can be generated from marrow stromal cells in vitro. *J Clin Invest*, 103(5):697–705, Mar 1999.

[50] S. F. Konieczny and C. P. Emerson. 5-azacytidine induction of stable mesodermal stem cell lineages from 10t1/2 cells: evidence for regulatory genes controlling determination. *Cell*, 38(3):791–800, Oct 1984.

[51] B. Balana, C. Nicoletti, I. Zahanich, E.M. Graf, T. Christ, S. Boxberger, and U. Ravens. 5-azacytidine induces changes in electrophysiological properties of human mesenchymal stem cells. *Cell Research*, 16(12):949–960, December 2006.

[52] Y. Liu, J.A. Song, W.X. Liu, Y. Wan, X.C. Chen, and C.J. Hu. Growth and differentiation of rat bone marrow stromal cells: does 5-azacytidine trigger their cardiomyogenic differentiation? *Cardiovascular Research*, 58(2):460–468, May 2003.

[53] Jr. Engelmayr, G.C., M. Cheng, C.J. Bettinger, J.T. Borenstein, R. Langer, and L.E. Freed. Accordion-like honeycombs for tissue engineering of cardiac anisotropy. *Nat.Mater.*, 7(12):1003–1010, December 2008.

[54] M.T. Lam, S. Sim, X.Y. Zhu, and S. Takayama. The effect of continuous wavy micropatterns on silicone substrates on the alignment of skeletal muscle myoblasts and myotubes. *Biomaterials*, 27(24):4340–4347, August 2006.

Appendix C:

Directed Growth of Adult Human White Matter Stem Cell - derived Neurons on Aligned Fibrillar Collagen

Lanfer B.[a,b], Hermann A.[a,c], Kirsch M.[a,d], Freudenberg U.[a,b], Reuner U.[c], Werner, C.[a,b], Storch, A.[a,b]

[a]Leibniz Institute of Polymer Research Dresden, Max Bergmann Center of Biomaterials Dresden, Dresden

[b]Technische Universität Dresden, Center for Regenerative Therapies, Dresden

[c]Technische Universität Dresden, Department of Neurology, Dresden

[d]Technische Universität Dresden, Department of Neurochirurgy, Dresden

accepted by *Tissue Engineering.*

Abstract

The nanoscale spatial organization of collagen fibrils as major constituents of extracellular matrices (ECM) is believed to be crucial for neurite guidance in neural development and repair. To systematically study the influence of collagen fibril alignment, length and density on human neuronal cell behavior, we used our novel technology to produce aligned collagen matrices by shear flow deposition using a microfluidic channel system and applied these surfaces to functional human neurons and glia derived from white matter neural stem cell (hNSC) cultures. Neurites on aligned collagen were highly oriented in the direction of the underlying fibrils, while neurites on non-aligned collagen or poly-D-lysine did not exhibit a preferred direction, forming instead a web-like morphology. Although the best alignment of collagen fibres in our study was seen using long fibrils at low density, the best neurite orientation was achieved on long fibrils at high density. Neurite outgrowth was enhanced on aligned collagen compared to non-aligned collagen or poly-D-lysine substrates, while neural differentiation and cell survival were not influenced by the type of substrate. Our data show that size and density of aligned collagen fibrils are crucial for axonal sprouting of human NSC-derived neurons. The flexibility of our technology, allowing collagen matrix qualities to be adapted to the neuronal cell type of interest, is thus a major advantage for therapeutic reconstruction of axonal pathways in the central or peripheral nervous system.

1 Introduction

Recovery of diseased nervous tissue has become a major goal for regenerative therapeutic approaches [1]. Neuronal repair is, however, severely hampered by inappropriate neurite outgrowth and synaptic integration of regenerating or grafted neurons [2, 3]. Even though axonal injury can be repaired by recovery of the injured nerve cells themselves, destruction of the myelin sheet often leads to insufficient re-innervation of distal targets [3]. In the injured spine, a glial scar is believed to be the major factor inhibiting targeted axonal re-growth, whereas in lesioned peripheral nerves the lack of suitable guidance material is responsible for the failure to reconnect to the distal targets. The current gold standard for providing guidance cues in peripheral nerve surgery is an autologuous nerve graft [3, 4]. Since this procedure is insufficient with respect to nerve cell regeneration and results in the loss of sensory and/or motor function or pain in the place of removal [3], there is an urgent need for bioartificial materials to improve nerve cell repair in central and peripheral nervous tissue [3, 5]. These materials must serve three major functions: (i) Provision of guidance cues, (ii) passivation of inhibitory signals, and (iii) prevention of glial scar formation [3, 5]. Synthetic tubular nerve guides were designed to replace the need for nerve autografts [6, 7]. Nerve guidance channels/tubes provide global direction to regenerating axons and prevent their escape into neighbouring tissue, however, they do not ensure local direction of axons and cells within the tube. Hence, so-called guidance channels or fibres aligned along the longitudinal axis within the tube were introduced to improve axon regeneration [8]. In this context, extracellular matrix (ECM) components are of great importance, mainly collagen, laminin, and fibronectin, as well as matrix-bound trophic factors [9, 10]. Collagen type I is of special interest since it has been shown to favor neuronal rather than glial cell growth [3, 5]. Transplantation of a collagen matrix into the transected cortico-spinal tract of adult rats induced neuronal fiber ingrowth while inhibiting invasion of reactive astrocytes or microglial cells, which are thought to cause glial scar formation [11]. In a self-assembly process, the triple-helical collagen I forms fibrils 20-70 nm in diameter that in turn associate into fibers and fiber bundles [12, 13]. In many tissues collagen fibrils/fibers are organized in parallel arrays. In peripheral nerves, for instance, the endoneurium surrounding the axons with Schwann cell sheets is predominately composed of orientated collagen fibers [3]. Oriented collagen fibrils aligned within gels by magnetic fields *in vitro* are known to increase neurite extensions in comparison to randomly oriented collagen fibrils [8]. In addition, aligned electrospun fibres or grooves profoundly effect the direction and guidance of cells and their processes [14, 15, 16, 17, 18]. It is now clear from a growing body of evidence that neurite growth strongly depends on substrate topography, including dimension and density of guidance cues [19, 20, 21]. Although it is straightforward to prepare randomly oriented collagen networks *in vitro*, creating aligned structures is more challenging. Several groups have introduced methods to align collagen matrices *in vitro* [22, 23, 24, 25, 26, 27, 28], however these do not allow for systematic adjustment of fibril alignment, density and morphology. Therefore, we have recently developed a new method using a microfluidic system to create well-aligned "native" collagen fibril matrices of variable density and morphology [29]. To assess the potential of these aligned collagen fibrils as bioartificial scaffolds for biomedical applications in humans, we studied the behavior of primary human adult neuronal cells cultured on aligned collagen with

differing fibril alignment, length and density. Since primary human neurons are not available for obvious reasons, we used adult human neural stem cells (hNSCs) as a source for functional human neurons and glia. In detailed analyses of adult hNSCs from various brain regions including subcortical white matter, it has recently been shown that these adult human NSCs behave very similar compared to their murine counterparts both during expansion and differentiation, and differentiate into functional nerve cells with similar neurite outgrowth [30, 31, 32, 33]. We show that aligned collagen matrices with tunable structural characteristics have a great potential to guide and enhance neurite outgrowth.

2 Materials and Methods

2.1 Cell culture

Adult human subcortical white matter tissue was obtained from routine epilepsy surgery (anterior temporal lobectomy or resection of focal cortical dysplasias; 6 samples; individuals 28-49 years old; 5 females and 1 male) following informed consent of the patients. All procedures were in accordance with the Helsinki convention and approved by the Ethical Committee of the Dresden University of Technology (EK 47032006). Specimens were taken from the removed tissue and stored in ice-cold Hank's balanced salt solution (HBSS) supplemented with 11 mM glucose and 1% penicillin/streptomycin while being transported from the operating theatre. All patients underwent high-resolution magnetic resonance imaging to exclude tumors and were screened for the presence of infectious disease. In all cases, tissue and neuropathological examination did not reveal evidence of tumor formation. For expansion of neurospheres consisting of hNSCs, white matter was isolated from tissue samples and then cut into small pieces with a scalpel, incubated in 0.1% trypsin (Sigma Aldrich, St Louis, USA) for 30min at RT, incubated in DNase (40 mg/ml; Sigma) for 10 min at 37°C and homogenized to a quasi single cell suspension by gentle triturating [30, 31, 34]. The cells were added to 25 cm^2 flasks (2×3 $10^6$6 viable cells per flask) in knock-out DMEM (Gibco BRL, Life Technologies; Tulsa, OK), supplemented with 10% serum replacement (Gibco); 0.5 mM glutamine; 1% penicillin/streptomycin and 20 ng/ml of both EGF and FGF- 2 (both from Sigma) at 5% CO_2, 92% N_2 and 3% O_2 using an incubator equipped with an O_2- sensitive electrode system (Haereus, Germany). After 10-20 days, neurosphere formation was observed and these spheres were expanded for additional 5-8 weeks (in total 7 to 12 weeks) before differentiation was initiated. The medium was changed once a week and the growth factors were added twice a week.

2.2 Differentiation conditions

Induction of neural differentiation was initiated by plating the cells on poly-D-lysine (PDL) (5mg/100ml aqua dest.; Sigma) coated glass cover-slips in knock-out-DMEM, 10% serum replacement, 0.5 mM glutamine, 1% penicillin/streptomycin, 10 ng/ml rh-BDNF (Promega, Madison, WI) and 100 µM di-butyryl-(db) cAMP (from Sigma). Three days later, 5% fetal calf serum (Gibco) was added. Cells were differentiated for 7 days. Identical conditions were used to plate

cells on the various collagen matrices.

2.3 Preparation of glass substrates

For experiments with glass substrates coated with PDL and poly(octadecene-alt-maleic acid) (POMA; from Polysciences, Warrington, PA), freshly cleaned 22×22 mm glass cover-slips (Menzel Gläser, Braunschweig, Germany) were oxidized in a 1:1 mixture of aqueous ammonia solution (Acros Organics, Geel, Belgium) and hydrogen peroxide (Merck). PDL solution was pipetted onto the glass substrate, kept at room temperature for 30 min, and rinsed with PBS. For POMA coating, cover-slips were functionalized by a reaction with 3-aminopropyl-dimethylethoxy-silane (ABCR, Karlsruhe, Germany). POMA was dissolved in tetrahydrofuran (THF, Fluka, Deisenhofen, Germany) in a concentration of 0.08 wt% and spin coated (RC 5 Suess Microtec, Garching, Germany) onto the amine-modified cover-slips at 4000 rpm for 30 s. Stable covalent binding of the polymer films was achieved by annealing at 120 °C to form imide bonds with the amino-silane on the glass substrate.

2.4 Microfluidic system and flow conditions

Aligned collagen matrices were prepared by a novel approach using a microfluidic set-up [for further information about the microfluidic system, please refer to [29, 35]. The flow conditions were performed under conditions of laminar flow. In all experiments, the Reynolds number (as a criterion for laminar flow) was smaller than 1 and a flow rate of 11 µl/min corresponding to a wall shear rate of 203.1 s-1 was applied.

2.5 Collagen solution

Bovine dermal collagen I solution (purified and pepsin-solubilized in 0.012 N HCl, PureCol, Inamed, Milmont Drive, USA) was brought to physiological pH by mixing eight parts of acidic collagen solution (3.0 mg/ml) with one part of 10-fold concentrated phosphate buffered saline (PBS, Sigma, Steinheim, Germany) and one part 0.1 M NaOH. All components were kept in an ice bath before and after mixing. Appropriate volumes of chilled 1×PBS were added to adjust the final concentration of the collagen solution.

2.6 Non-aligned collagen matrices

POMA-coated glass slides were coated by contacting the substrates to the collagen solution then subsequently raising the temperature [36]. To precisely apply collagen coating in designated areas, a silicone-based culture insert (Ibidi GmbH, Martinsried, Germany) consisting of two wells was placed onto a POMA-coated glass slide. A 100 µl drop of chilled non-fibrillar collagen solution (0.4 mg/ml) was pipetted into each well and kept in a CO_2-free incubator at 37 °C to initiate fibril formation. After 90 min the resulting fibrillar collagen gel and the culture inset was removed from the surface, leaving two 0.22 cm^2 rectangular areas covered with a thin collagen

layer on the substrate. The modified surface was rinsed with PBS at least three times and subsequently with Milli-Q water (Millipore Corporation, Molsheim, France).

2.7 Aligned collagen matrices

To produce collagen matrices containing long fibrils at a low density, a low concentration collagen solution (3µg/ml) was used as described previously [29]. Briefly, collagen solution (0.8 mg/ml) was prepared at 4°C in a centrifuge tube (Roth, Karlsruhe, Germany), placed in a CO2-free incubator (Sanyo, Bensenville, USA) at 37°C, and allowed to form fibrils for 24 h. The resulting gel was homogenized for 4 min (T-8 Ultra Turrax) and centrifuged (Heraeus) at 1000×g for 6 min. The supernatant (2 ml, 3µg/ml) was drawn into a syringe that was subsequently installed into the syringe pump. The solution was then pumped for 1 h with a flow rate of 11 µl/min through the microfluidic channel. Afterwards the channel was rinsed with PBS for 20 min to flush away loose fibrils and the coated cover-slip was removed from the PDMS channel plate and kept in PBS for cell culture. Aligned collagen matrices containing short fibrils at low density were prepared with a solution concentration of 0.2 mg/ml [29]. Briefly, the microfluidic system was placed in a CO2-free incubator (Sanyo, Bensenville, USA) at 37°C. The collagen solution was prepared at 4°C and drawn into a chilled syringe (Roth, Karlsruhe, Germany), which was quickly installed into the syringe pump to avoid early fibrillogenesis. The streaming process was started immediately by pumping the chilled collagen solution from the cooled storage reservoir through heated tubing followed by streaming through the microfluidic channel for 1 h. The sample was then rinsed with PBS as described above. Aligned collagen matrices containing long fibrils at high density were prepared according to the same protocol for collagen matrices containing short fibrils at a low density using a solution concentration of 0.8mg/ml. Samples were sterilized under UV light for 5 min.

2.8 Confocal reflection microscopy (CRM)

Confocal reflection microscopy (TCS SP, Leica, Bensheim, Germany) was performed at a wavelength of 488 nm (Ar laser) to visualize unstained collagen fibrils as described elsewhere [37]. CRM pictures of fibril matrices were obtained using a 40× oil immersion objective.

2.9 Atomic force microscopy (AFM)

Surface topography of air-dried collagen matrices was investigated via intermittent contact scanning force microscopy with a PicoSPM (Molecular Imaging, Phoenix, AZ, United States) using silicon cantilevers (Tap300, BudgetSensors, Bulgaria) with a 300±100 kHz resonant frequency, 40 N/m force constant and tip radius< 10 nm.

2.10 Scanning electron microscopy (SEM)

Samples for SEM analysis were fixed with 2% glutaraldehyde, dehydrated and critical point dried (CPD 030, Baltec, Schalksmühle, Germany). The samples were gold coated with a sputter

coater (SCD 050, Baltec, Schalksmühle, Germany) to allow sample analysis under high vacuum in an SEM (XL 30 ESEM FEG, FEI-Phillips, Eindhoven, Netherlands) equipped with an SE detector, and operating at 7.5–10 kV, Spot Size 3. Micrographs of hNSCs on the area covered with aligned collagen fibrils or the corresponding area (5 mm×1 mm) on the controls were taken. For each condition (long or short fibrils at high or low density) three independent donors were analysed.

2.11 Image analysis to quantify collagen fibril alignment

Quantification of fibril alignment was performed as described previously [29]. Briefly, CRM images of three samples containing two channels with collagen fibrils were analyzed for each condition and quantified using the NIH ImageJ 1.37v software. One sample contained a minimum of 200 collagen fibrils. A threshold value of the reflection intensity was defined to isolate fibrils from background. By fitting an ellipse to the major axis of each collagen fibril, the angle of the fibrils to the flow direction was determined. The orientation of fibrils parallel to the alignment direction corresponded to an angle of 0°. The angular distribution of collagen fibrils was determined based on the relative frequency of orientation angles (classified into bins of 10°angles) and by a fit to a Gaussian the full width at half maximum (FWHM).

2.12 Image analysis to quantify hNSC extension alignment and length

SEM images were analysed to quantify the extent of alignment and length of cell extensions. Software and quantification of extension alignment was performed as described for quantification of collagen fibril alignment. The angular distribution of extensions was determined based on the relative frequency of extension angles (classified into bins of 10° angles) of three donors. Only cells/extensions on the area covered with aligned collagen fibrils or the corresponding area (5 mm×1 mm) on the controls were measured. The length of each extension extending from neurospheres was measured using NIH ImageJ 1.37v (plugin NeuronJ) software. Each extension was measured from its origin at the edge of the neurosphere to its end. Changes in direction along its course were taken into account by tracing along the entire length of each extension. Extensions which were solitary and clearly isolated were measured only to exclude the possibility of mix-up with other extensions.

2.13 Immunocytochemistry

Cell cultures were fixed with Accustain (Sigma). Immunocytochemistry was carried out using standard protocols described previously [30, 38]. Cell nuclei were counter stained with 4,6-diamidino-2-phenylindole (DAPI). The following primary antibodies were used: Mouse anti-GalC 1:750 (Chemicon International, Temecula, USA), rabbit anti-Tuj1 1:2000, mouse anti-Tuj1 1:500 (both from Covance, Richmond, CA), chicken anti-GFAP 1:1000 (Abcam, Cambridge, UK), rabbit anti-activated caspase3 1µg/ml (BD Pharmingen, San Diego, CA), and secondary antibodies conjugated to Alexa 488, 568 or 647 1:500 (all from Invitrogen-Molecular Probes, Carlsbad, California). Images were captured using a fluorescence microscope (Leica DM IRE2,

Wetzlar, Germany). Living cells were marked for analysis using fluorescein diacetate (FDA) while dead cells were stained with propidiumiodid (PI; Sigma Aldrich). A solution of 100 µg/ml FDA was prepared by dissolving in acetone. A working stock solution containing 100 ng/ml of FDA was prepared in PBS that was added directly to the cell cultures (i.e. no change of culture medium) at a 1:1 volume ratio and PI was added at a concentration of 1:50 (1µg/ml). Samples were incubated for ˜ 5 min and visualised using epi-fluorescent microscopy (Leica DM IRE2, Leica Microsystems, Wetzlar, Germany) with excitation filters at 490/20 nm and emission at 527/30 nm for fluorescein. Since neither PI staining nor activated caspase3 staining worked on the hNSCs on the substrates, dead cells were quantified by counting condensed DNA using DAPI staining correlated to all nuclei.

2.14 Cell counting and statistics

To quantify the percentage of cells producing a given marker in a given experiment, the number of positive cells on the coated well surface was determined relative to the total number of DAPI-labeled nuclei. In a typical experiment, a total of 500-1000 cells were counted per marker. Statistical comparisons were made by ANOVA with post-hoc t-test and Bonferroni adjustment or Dunnett's t-test as appropriate. All data are presented as mean values ± s.e.m. All quantifications were done by an independent blinded investigator.

3 Results

3.1 Alignment of collagen fibrils

As part of neuronal tissue regeneration in both central and peripheral nervous tissue, targeted axo-dendritic outgrowth is a major challenge for reconstructing neuronal tracts and circuitries. We thus tested the ability of aligned collagen fibrils, generated using a microfluidic system [29], to guide neurites during the differentiation process of adult white matter hNSCs (see Fig. 1 for schematic representation of the technology). Collagen fibrils were deposited on planar POMA-coated substrates from collagen solutions streaming through a microfluidic channel. By varying collagen solution concentrations and gelation times, fibril length and density were tuned and varied. In brief, lower concentrations generated shorter fibrils at lower density; higher concentrations resulted in aligned matrices containing long fibrils at high density. AFM was used to observe the resultant aligned collagen matrices: Long fibrils at high density (Figs. 1A), long fibrils at low density (Fig. 1B) and short collagen fibrils at low density (Fig. 1C).

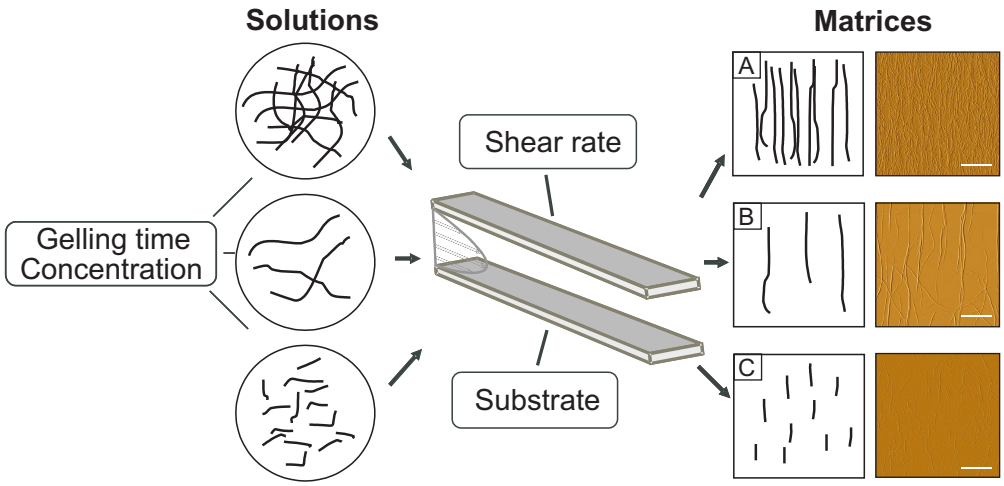

Figure 1: Scheme of the approach to prepare collagen type I fibril matrices that are adjustable in orientation, density and morphology by varying collagen solution concentration, gelling time, shear rate, and substrate. AFM images show the resultant aligned collagen matrices with long fibrils at high density (A), long fibrils at low density (B), and short fibrils at low density (C). Scale bar, 2 µm.

3.2 Influence of aligned collagen with varying structural characteristics on extension alignment

To investigate the significance of the newly developed alignment approach for biomedical application, we attempted to prove its potential in a human nerve cell system. Since human neurons are not routinely available without harming the patient or the cells themselves, we used neurons differentiated from adult human NSCs. Adult hNSCs were isolated from cortical white matter tissue obtained from neurosurgery interventions as recently described [30, 32]. Triple immunofluorescence staining of neuroectodermal markers confirmed typical trilineage neuroectodermal differentiation capacity of the adult hNSCs with 30±5% Tuj1$^+$ neurons, 10±4% GFAP$^+$ astrocytes and 4±2% GalC$^+$ oligodendrocytes after 7 days of differentiation on the standard differentiation surface PDL (data from three independent experiments from 3 different donors). Adult hNSCs are thus a valuable human cell model for investigating axodendritic outgrowth of human Tuj1$^+$ neurons. We used cells from at least three different donors for all further experiments. To assess the effect of aligned collagen matrices with varying structural properties on neurite outgrowth and extension alignment (Fig. 1), hNSCs were differentiated for seven days on rectangular areas (1 mm× 6.5 mm) with aligned collagen fibrils (long fibrils at high density, Fig. 2A; long fibrils at low density Fig. 2B; short fibrils at low density, Fig. 2C) deposited on a POMA-coated glass surface. Non-aligned collagen resulting from static fibril formation and immobilisation on a POMA-coated surface served as the control surface (Fig. 2D). SEM and immunocytochemistry were used to analyze hNSC morphology. Fibril and cell alignment was quantified by determining the angular distribution of collagen fibrils and cell extensions. Based on this analysis, the orientation angle distribution was plotted as a histogram and the corresponding FWHM was determined by a Gaussian fit (see also (29)). Fibril alignment was highest on matrices containing long fibrils at low density (FWHM 18±1°; Fig. 2B,F), followed

by long fibrils at high density (FWHM 30±3°; Figs. 2A,E) and short fibrils at low density (FWHM 41±5°; Figs. 2C,G). Non-aligned collagen showed random distribution of fibre angles (Figs. 2D,H). On all substrates, differentiated hNSCs displayed typical unipolar, bipolar, and multipolar neuronal morphologies with axo-dendritic outgrowth (Fig. 2I-L). We measured the orientation of at minimum 166 extensions per independent experiment. On substrates containing aligned fibrils (Figs. 2I-K), aligned extension outgrowth in the direction of the underlying collagen fibrils was observed, whereas extensions on non-aligned collagen exhibited no preferred orientation (Fig. 2L). In contrast to fibril alignment degree, extension alignment was highest on long collagen fibrils at high density (FWHM 38±3°; Figs. 2I,M), then successively decreased on long fibrils at low density (FWHM 50±19°; Figs. 2J,N) and short fibrils at low density (FWHM 53±11°; Figs. 2K,O). No preferred extension alignment direction was observed on non-aligned collagen (Figs. 2L,P). These findings emphasize the importance of both fibril alignment and fibril density for the orientation of axo-dendritic outgrowth of neurons derived from hNSCs. hNSC differentiation was confirmed using immunofluorescence staining for the neuronal marker Tuj1, and the astroglial marker GFAP. On all substrates, hNSCs acquired morphologic and phenotypic characteristics of $Tuj1^+$ neurons and $GFAP^+$ astrocytes (Figs. 2Q-T).

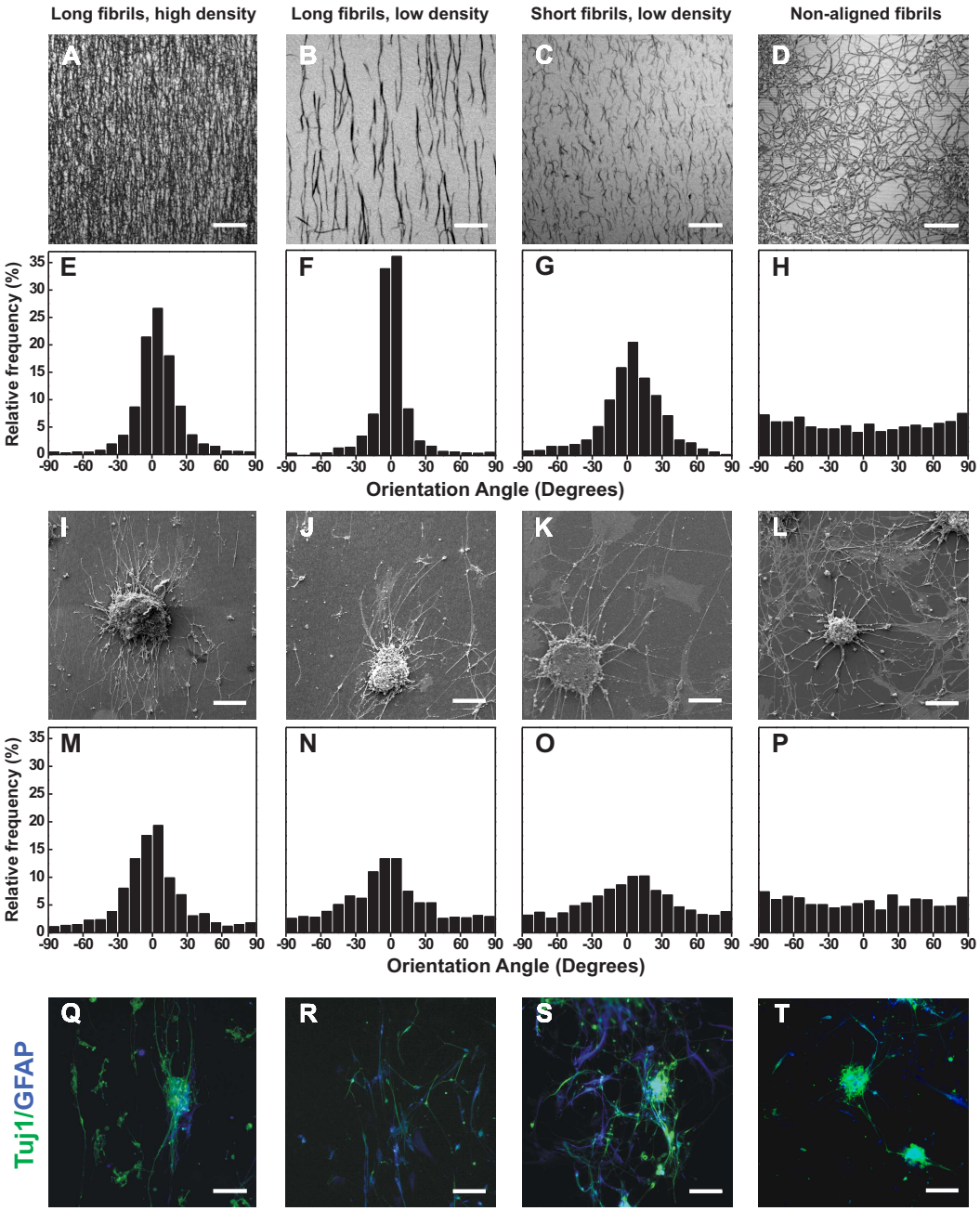

Figure 2: Influence of fibril alignment, length and density on extension alignment of adult white matter-derived hNSCs. (A-D) CRM images of aligned collagen matrices with long fibrils at high density (A), long fibrils at low density (B), short fibrils at low density (C), and randomly oriented fibrils (D). Scale bar, 10 µm. (E-H) Histograms representing the relative frequency of fibril orientation angles with respect to the horizontal axis corresponding to the images shown in A-D. (IL) SEM images of hNSCs grown for seven days on matrices of identical alignment and morphology as depicted in A-D. Scale bar, 100 µm. (M-P) Histograms representing the relative frequency of extension orientation angles with respect to the horizontal axis corresponding to the images shown in I-L. (Q-T) Microphotographs of immunofluorescence staining of differentiated hNSCs showing $Tuj1^+$ neurons (green) and $GFAP^+$ astrocytes (blue) grown for seven days on matrices of identical alignment and morphology as depicted in A-D. Scale bar 100 µm.

3.3 Directional outgrowth of hNSC extensions on aligned collagen matrices

Quantification of cell alignment revealed the highest extension alignment occurs on matrices containing long collagen fibrils at high density. More detailed SEM studies were performed on these substrates to investigate extension morphology and cell-matrix interactions. Extensions on aligned collagen matrices containing long fibrils at high density were highly oriented and extension alignment was consistent along the whole width and length of the collagen-coated area (Figs. 3A-C,E, dotted lines mark the collagen matrix border). In contrast, on the adjacent POMA-coated glass surface, extensions showed no preferred direction of orientation, emanating in radial fashion (Figs. 3A,D). Some neurospheres adhered at the boarder of the aligned collagen layer, extending processes on both the collagen surface and the adjacent POMA-coated glass. While extensions in contact with the POMA surface grew without any bias in alignment, those on the side with aligned collagen followed the direction of the underlying fibrils (Fig. 3E). Once in contact with the fibrils, the processes extended parallel to the fibrils, always in the direction of the aligned collagen (Fig. 3F including inset). Immunocytochemistry staining demonstrated that the alignment cues from collagen fibrils acted almost exclusively on $Tuj1^+$ neurites, while $GFAP^+$ astroglial extensions were rather uninfluenced by collagen fibril alignment (Figs. 3G-J).

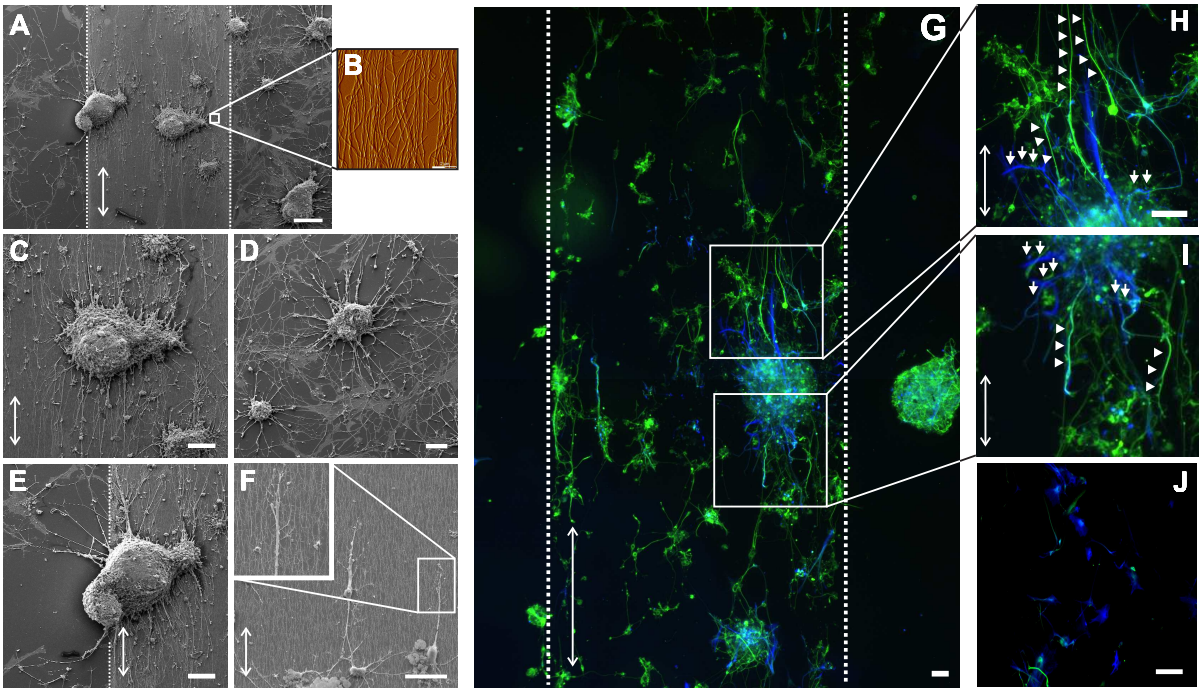

Figure 3: Aligned collagen fibrils guide and direct extensions of adult white matter-derived hNSCs. (A) SEM image displays differentiated hNSCs adhering on top of aligned collagen fibrils (long fibrils at high density) and the surrounding POMA surface (dotted lines mark the boarder between the aligned collagen matrix areas and POMA-coated areas; double-headed arrows show collagen fibril orientation) after 7 days in culture. Differentiated hNSCs adopt characteristics of glial and neuronal cells with axo-dendritic outgrowth. (B) AFM micrograph of aligned collagen with long fibrils at high density. (C-F) Higher magnification SEM microphotographs of hNSCs growing on aligned collagen fibrils (C,F), POMA-coated surface (D), or on both surfaces (E) show that extension outgrowth was highly aligned and guided by the underlying collagen fibrils. On the adjacent POMA surface, extensions grew in radial fashion without a preferred direction of alignment. (F) High-resolution image of single extensions demonstrating that neurites in contact with single collagen fibrils extended their processes parallel to the fibrils (inset). (G-J) Immunocytochemistry staining of Tuj1, a neuronal marker, and GFAP, an astroglial marker, of differentiated hNSCs on aligned collagen fibrils (G-I) and on POMA-coated surfaces (J). The staining clearly shows orientation along the collagen fibrils for most $Tuj1^+$ neurites (arrowheads), but no significant orientation of $GFAP^+$ glial cell processes (arrows). On POMA, no oriented extension growth could be observed. Note the $GFAP^+$ flat cells on POMA-coated surfaces representing astroglial cells (A,D,J). Scale bars, 200 µm (A,G), 80 µm (C-E), 50 µm (F), and 100 µm (H-J).

3.4 Influence of collagen fibril alignment on hNSC behaviour

To further characterize the synergistic influence of topographical and biochemical cues from aligned collagen on hNSC behavior, we compared neuroectodermal differentiation on substrates with the highest cell alignment (long fibrils at high density) to non-aligned collagen and the standard differentiation surface PDL: Trilineage neural differentiation capacity was equivalent

on non-aligned collagen and aligned collagen (long fibrils at high density), and no significant differences were observed compared to PDL (p=0.068, F-value: 4.06 for Tuj1$^+$ cells, p=0.90, F-value: 0.11 for GFAP$^+$ cells, p=0.37, F-value: 1.15 for GalC$^+$ cells; ANOVA; n=3; Figs. 4A,C). Interestingly, on POMA-coated surfaces, we found additional flat GFAP$^+$ astrocytes that were not detectable by immunocytochemistry on PDL, non-aligned or aligned collagen fibrils (Figs. 2,3). The influence of aligned structures on cell survival was quantified by counting condensed and inhomogeneous DNA using DAPI staining correlated to all nuclei. There were no differences in cell survival, with 5±2%, 5±2% and 6±1% pycnotic cell nuclei on PDL, non-aligned and aligned collagen fibrils, respectively (p=0.85, F-value: 0.17; ANOVA; n=3; Figs. 4B,D). Thus both hNSC differentiation and survival showed no difference with respect to the growth surface. This contrasts to the highly specific influence of aligned collagen type I on the direction of neurite outgrowth. To determine the effect of fibril alignment on neurite outgrowth, extension length was quantified in SEM microphotographs by measuring each extension along its entire length from the neurosphere to its end. We measured 109 to 422 extensions per independent experiment. hNSC extension length significantly varied between seeding surfaces (p=0.0014, F-value: 17.01; ANOVA; n=3 independent experiments; Figs. 2,4E). Extensions on aligned collagen fibrils (long fibrils at high density) were significantly longer (145±8 μm) compared to those on PDL (86±8 μm; p=0.0003; post-hoc t-test), POMA (88±4 μm; p=0.0008; post-hoc t-test) and non-aligned collagen (111±3 μm; p=0.0073; post-hoc t-test). On non-aligned collagen, extension outgrowth was significantly higher compared to PDL surfaces (p=0.029). No significant differences were observed between PDL and POMA substrates.

4 Discussion

Biomaterials are especially relevant for biomedical approaches that aid nervous system regeneration. Current interventions are hindered by insufficient or undirected axo-dendritic outgrowth, which leads to a lack of synaptic integration into the host brain circuitries [3, 5]. As we describe here, guidance cues provided by biomaterials may prove essential in repair of central and peripheral nervous system disease/damage. Even though axonal recovery after transection is occasionally observed, this is often hampered by the lack of guidance materials, leading to glial scar formation with subsequent loss of function [3]. As an example, in spinal cord regeneration, the major obstacles to overcome, beyond simply guiding axons in the right direction, are the local inhibitory molecules (e.g. Nogo) and glial scar formation resulting from invasion of reactive astrocytes or microglial cells [3, 5]. Peripheral nerve regeneration pathophysiologically differs from the recovery of central neurons, depending mostly on sufficient guidance cues to direct axonal re-growth to its target. We demonstrate for the first time that neurite outgrowth of adult human nerve cells, derived from white-matter neural stem cells (hNSCs) [3, 30, 31, 32], can be directed by aligned collagen matrices of particular fibril length and density without affecting cell fate decisions or survival. The exact interplay of collagen fibril alignment, density and length was found to be crucial, thus proving the importance of our recently developed shear flow deposition method to produce aligned collagen matrices of varying structural properties [29]. There

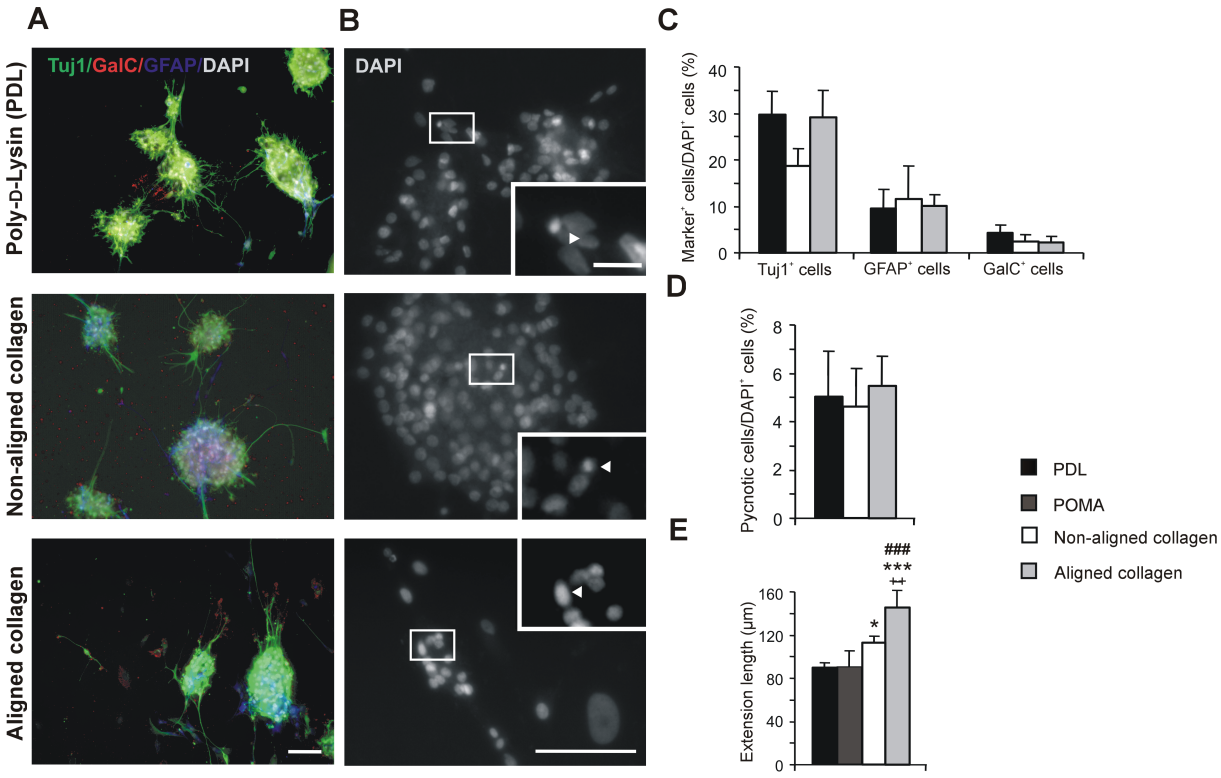

Figure 4: Influence of aligned collagen matrices on hNSC differentiation and survival. (A,C) Representative microphotographs of quadruple immunofluorescence stainings of differentiated hNSCs showing Tuj1$^+$ neurons, GFAP$^+$ astrocytes and GalC$^+$ oligodendrocytes on PDL, on nonaligned and on aligned collagen type I (long fibrils at high density). Cells were allowed to differentiate for seven days. Note that Tuj1$^+$ neurite outgrowth appeared completely randomly and radially on PDL and non-aligned collagen. Nuclei were counter-stained with DAPI. Scale bar, 100 µm. (C) Quantitative measurement of cell fate decision of hNSCs on PDL, non-aligned and aligned (long fibrils at high density) collagen type I by using quadruple immunofluorescence stainings of Tuj1, GFAP and GalC in differentiated hNSCs. Nuclei were counter-stained with DAPI. (B,D) Cell survival of hNSCs measured by counting condensed nuclei in DAPI stainings was unaffected by different substrates (PDL, non-aligned and aligned (long fibrils at high density) collagen type I) after 7 days of differentiation. Higher size images are shown in inserts. Arrowheads indicate fragmented cell nuclei using DAPI staining. Scale bars, 200 µm and 25 µm (insets). Statistical analyses using ANOVA revealed no significant difference in cell types with respect to seeding surfaces. (Data presented are means ± s.e.m. of at least three independent experiments from 3 donors). (E) Extension length of differentiated hNSCs was measured after seven days of culture on PDL, POMA, non-aligned and aligned collagen using SEM pictures and NeuronJ software. Mean values ± s.e.m. of three independent are shown. * represents $p<0.05$ and *** represents $p<0.001$ compared to PDL, ### represents $p<0.001$ compared to POMA, ++ indicates $p<0.01$ compared to non-aligned collagen fibrils (post-hoc t-test with Bonferroni adjustment).

is a general consensus that longitudinally aligned structures improve nerve regeneration and directed neuronal outgrowth [3]. Growth cones at neurite tips respond to aligned structures via contact guidance, resulting in axially directed neurite projections and thus improved structural alignment [39, 40, 41]. Our aligned matrices indeed served as guidance cues to direct neurite outgrowth of human NSCs along aligned collagen fibrils (Fig. 2,3). This was especially true for matrices containing long fibrils at a high density (Fig. 2I,M). Although the best alignment of collagen fibres was seen using long fibrils at low density (Figs. 2A-H), the best neurite orientation was achieved on long fibrils at high density (Figs. 2I-P). It is likely that the close proximity of adjacent fibrils prevents neurites from migrating in all directions when reaching the end of a fibril. Thus, not only the alignment, but the interplay of aligned collagen fibrils of the right size together with the right density is crucial for axonal sprouting of human NSC-derived neuronal extensions. It has been demonstrated in several studies that dimension and size of substrate topography strongly influence neurite guidance and growth. Furthermore, there is substantial evidence from studies on planar substrates using patterned surface chemistry and topography to suggest that feature sizes in the sub-micron range in particular affect cell behaviour. Neurite lengths of C17.2 neural stem cells on nanofibers (700 nm) were significantly higher than on aligned microfibers (3.5 μm) [18]. However, in contrast, it has been reported that neurites extending from chick cerebral neurons do not follow grooves of 130 nm width [42]. Xenopus laevis neurites grew parallel to grooves of 14 nm depth and 1 μm width, but hippocampal neurons grew perpendicular [43]. These examples emphasize the importance of nanoscale topography for guidance of neurites, but substrate topography has to be tuned depending on the cell type as well the species of origin. This might be due to individual growth cone characteristics that impact the remarkable abilities to detect directional cues [44]. These data clearly demonstrate that every bioartificial material applied in human medicine has to be tested in human-derived cell or tissue systems. The second major effect of collagen alignment was enhanced neurite outgrowth, with longer neurites compared to non-aligned collagen or PDL substrates (Fig. 4E). Increased mean extension length on aligned substrates has also been observed for neurites from rat and chick dorsal root ganglia on aligned electrospun nanofibers [14, 17]. Non-oriented surfaces obviously slow down neurite growth, likely due to time spent deciding which path/cue to take [14, 15]. Thus, topographical cues seem to influence axon outgrowth, but additional biochemical cues, here collagen type I, might also affect the speed of axonal outgrowth. In recent studies, the incorporation of porous collagen beads in multi-channel nerve guides enhanced neurite outgrowth and two-dimensional surfaces of collagen type I improved Schwann cell attachment and adhesion [45, 46]. It has also been shown that functionalization of aligned electrospun polycaprolyctone fiber surfaces with collagen type I increases cell adherence, proliferation and process extension [47, 48, 49]. Together, these results suggest that synergistic effects of anisotropic distribution of biochemical and topographical/physical cues enable faster nerve regeneration by exploiting the differential response of growth cones to changes in structural and biochemical features [50]. Interestingly, hNSC differentiation was not affected by aligned or non-aligned collagen (Fig. 4A,C). It has been reported that neuronal differentiation of adult rat hippocampal progenitor cells co-cultured with astrocytes is enhanced on aligned polystyrene microgrooves compared to substrates without a pattern. However, their differentiation is not affected when cultured on

aligned or non-aligned substrates without astrocytes [16]. Neuronal differentiation of C17.2 neural stem cells occurs faster on aligned/non-aligned electrospun nanofibers (300 nm) than on aligned/non-aligned microfibers (1.5 µm). Fiber alignment however does not seem to influence differentiation ([18]. Even though collagen was shown to inhibit glial cell invasion [11], non-aligned and aligned collagen did not favour neuronal differentiation in our study. Collagen matrices have another major advantage for the use in neural repair: They allow axonal growth, but inhibit glial cell invasion, thereby abolishing glial scar formation [11]. Consistently, our immunocytochemistry data showed that collagen fibrils do not change glial cell differentiation of hNSCs (Fig. 4A,C). Finally, the immunocytochemistry studies proved that the guidance cues of the aligned collagen mostly influence the orientation of neurites rather than glial processes (Figs. 2,3). The fibrils in the aligned collagen matrices we used closely resemble those found in nerve ECM structures. For example, the 20-100 nm in diameter fibrils in our matrices are comparable to the 30-110 nm in diameter oriented collagen fibers found in the endoneurium that surrounds axons and thereby guides neurite migration [51, 52, 3].

5 Conclusions

Together our results demonstrate that – by mimicking the size and fashion of endoneurium collagen alignment – the optimal orientation, density and length of collagen fibrils is effective in guiding and promoting human NSC-derived neuronal extensions without hampering cell behaviour and survival. The flexibility of our method to adapt collagen matrices to the nerve type of interest is considered a major prerequisite to mediate these effects. Although the data presented only show the *in vitro* application of aligned collagen matrices, all data were obtained using adult human neurons, providing a proof-of-principle for induction of adult human neurite outgrowth by engineered ECM. Adult nerve cells were chosen rather than fetal or embryonic stem cell-derived neurons to avoid problems posed by the high developmental potential of the fetal/embryonic cells. The use of adult human dorsal root ganglion and/or spinal cord neurons would be highly intriguing in our system; however these cells are unattainable for obvious reasons. Future attempts are warranted to develop three-dimensional scaffolds to apply these aligned collagen matrices *in vivo* to reconstruct axonal pathways in the central or peripheral nervous system.

References

[1] S. A. Goldman. Disease targets and strategies for the therapeutic modulation of endogenous neural stem and progenitor cells. *Clin Pharmacol Ther*, 82(4):453–460, Oct 2007.

[2] Andreas Hermann and Alexander Storch. Endogenous regeneration in parkinson's disease: do we need orthotopic dopaminergic neurogenesis? *Stem Cells*, 26(11):2749–2752, Nov 2008.

[3] C.E. Schmidt and J.B. Leach. Neural tissue engineering: strategies for repair and regeneration. *Annu Rev Biomed Eng*, 5:293–347, 2003.

[4] S. David and A. J. Aguayo. Axonal elongation into peripheral nervous system "bridges" after central nervous system injury in adult rats. *Science*, 214(4523):931–933, Nov 1981.

[5] Ana I Teixeira, Joshua K Duckworth, and Ola Hermanson. Getting the right stuff: controlling neural stem cell state and fate in vivo and in vitro with biomaterials. *Cell Res*, 17(1):56–61, Jan 2007.

[6] T. S. Girton, T. R. Oegema, and R. T. Tranquillo. Exploiting glycation to stiffen and strengthen tissue equivalents for tissue engineering. *J Biomed Mater Res*, 46(1):87–92, Jul 1999.

[7] G. Lundborg, L. B. Dahlin, N. Danielsen, R. H. Gelberman, F. M. Longo, H. C. Powell, and S. Varon. Nerve regeneration in silicone chambers: influence of gap length and of distal stump components. *Exp Neurol*, 76(2):361–375, May 1982.

[8] D. Ceballos, X. Navarro, N. Dubey, G. Wendelschafer-Crabb, W.R. Kennedy, and R.T. Tranquillo. Magnetically aligned collagen gel filling a collagen nerve guide improves peripheral nerve regeneration. *Exp Neurol.*, 158(2):290–300, August 1999.

[9] J. A. Hammarback, J. B. McCarthy, S. L. Palm, L. T. Furcht, and P. C. Letourneau. Growth cone guidance by substrate-bound laminin pathways is correlated with neuron-to-pathway adhesivity. *Dev Biol*, 126(1):29–39, Mar 1988.

[10] P. C. Letourneau, I. V. Pech, S. L. Rogers, S. L. Palm, J. B. McCarthy, and L. T. Furcht. Growth cone migration across extracellular matrix components depends on integrin, but migration across glioma cells does not. *J Neurosci Res*, 21(2-4):286–297, 1988.

[11] E. A. Joosten, P. R. Bär, and W. H. Gispen. Collagen implants and cortico-spinal axonal growth after mid-thoracic spinal cord lesion in the adult rat. *J Neurosci Res*, 41(4):481–490, Jul 1995.

[12] K.E. Kadler, D.F. Holmes, J.A. Trotter, and J.A. Chapman. Collagen fibril formation. *Biochem J*, 316 (Pt 1):1–11, May 1996.

[13] V. Ottani, D. Martini, M. Franchi, A. Ruggeri, and M. Raspanti. Hierarchical structures in fibrillar collagens. *Micron.*, 33(7-8):587–596, 2002.

[14] Joseph M Corey, David Y Lin, Katherine B Mycek, Qiaoran Chen, Stanley Samuel, Eva L Feldman, and David C Martin. Aligned electrospun nanofibers specify the direction of dorsal root ganglia neurite growth. *J Biomed Mater Res A*, 83(3):636–645, Dec 2007.

[15] R. Murugan and S. Ramakrishna. Design strategies of tissue engineering scaffolds with controlled fiber orientation. *Tissue Engineering*, 13(8):1845–1866, August 2007.

[16] J.B. Recknor, D.S. Sakaguchi, and S.K. Mallapragada. Directed growth and selective differentiation of neural progenitor cells on micropatterned polymer substrates. *Biomaterials*, 27(22):4098–4108, August 2006.

[17] E. Schnell, K. Klinkhammer, S. Balzer, G. Brook, D. Klee, P. Dalton, and J. Mey. Guidance of glial cell migration and axonal growth on electrospun nanofibers of poly-epsilon-caprolactone and a collagen/poly-epsilon-caprolactone blend. *Biomaterials*, 28(19):3012–3025, July 2007.

[18] F. Yang, R. Murugan, S. Wang, and S. Ramakrishna. Electrospinning of nano/micro scale poly(l-lactic acid) aligned fibers and their potential in neural tissue engineering. *Biomaterials*, 26(15):2603–2610, May 2005.

[19] Roy M Smeal and Patrick A Tresco. The influence of substrate curvature on neurite outgrowth is cell type dependent. *Exp Neurol*, 213(2):281–292, Oct 2008.

[20] Xuejun Wen and Patrick A Tresco. Effect of filament diameter and extracellular matrix molecule precoating on neurite outgrowth and schwann cell behavior on multifilament entubulation bridging device in vitro. *J Biomed Mater Res A*, 76(3):626–637, Mar 2006.

[21] Roy M Smeal, Richard Rabbitt, Roy Biran, and Patrick A Tresco. Substrate curvature influences the direction of nerve outgrowth. *Ann Biomed Eng*, 33(3):376–382, Mar 2005.

[22] C. Guo and L.J. Kaufman. Flow and magnetic field induced collagen alignment. *Biomaterials*, 28(6):1105–1114, February 2007.

[23] D.A. Cisneros, J. Friedrichs, A. Taubenberger, C.M. Franz, and D.J. Muller. Creating ultrathin nanoscopic collagen matrices for biological and biotechnological applications. *Small*, 3(6):956–963, June 2007.

[24] T. Elsdale and J. Bard. Collagen substrata for studies on cell behavior. *J Cell Biol*, 54(3):626–637, September 1972.

[25] J. Torbet, M. Malbouyres, N. Builles, V. Justin, M. Roulet, O. Damour, A. Oldberg, F. Ruggiero, and D.J. Hulmes. Orthogonal scaffold of magnetically aligned collagen lamellae for corneal stroma reconstruction. *Biomaterials*, 28(29):4268–4276, October 2007.

[26] J. Torbet and M.C. Ronziere. Magnetic alignment of collagen during self-assembly. *Biochem J*, 219(3):1057–1059, May 1984.

[27] B.M. Baker and R.L. Mauck. The effect of nanofiber alignment on the maturation of engineered meniscus constructs. *Biomaterials*, 28(11):1967–1977, April 2007.

[28] P. Lee, R. Lin, J. Moon, and L.P. Lee. Microfluidic alignment of collagen fibers for in vitro cell culture. *Biomed Microdevices.*, 8(1):35–41, March 2006.

[29] B. Lanfer, U. Freudenberg, R. Zimmermann, D. Stamov, V. Korber, and C. Werner. Aligned fibrillar collagen matrices obtained by shear flow deposition. *Biomaterials*, 29(28):3888–3895, October 2008.

[30] Andreas Hermann. *In vitro neurogenesis of adult neural stem cells from bone marrow and brain.* PhD thesis, Universität Ulm, 2006.

[31] Martina Maisel, Alexander Herr, Javorina Milosevic, Andreas Hermann, Hans-Jörg Habisch, Sigrid Schwarz, Matthias Kirsch, Gregor Antoniadis, Rolf Brenner, Susanne Hallmeyer-Elgner, Holger Lerche, Johannes Schwarz, and Alexander Storch. Transcription profiling of adult and fetal human neuroprogenitors identifies divergent paths to maintain the neuroprogenitor cell state. *Stem Cells*, 25(5):1231–1240, May 2007.

[32] Marta C Nunes, Neeta Singh Roy, H. Michael Keyoung, Robert R Goodman, Guy McKhann, Li Jiang, Jian Kang, Maiken Nedergaard, and Steven A Goldman. Identification and isolation of multipotential neural progenitor cells from the subcortical white matter of the adult human brain. *Nat Med*, 9(4):439–447, Apr 2003.

[33] Shinghua Ding, Conrad A Messam, Peiying Li, Michael E Selzer, Marc A Dichter, and Philip G Haydon. Murine brain progenitor cells have the ability to differentiate into functional neurons and integrate into the cns. *Cell Transplant*, 15(8-9):699–710, 2006.

[34] A. Storch, G. Paul, M. Csete, B. O. Boehm, P. M. Carvey, A. Kupsch, and J. Schwarz. Long-term proliferation and dopaminergic differentiation of human mesencephalic neural precursor cells. *Exp Neurol*, 170(2):317–325, Aug 2001.

[35] F.U. Gast, P.S. Dittrich, P. Schwille, M. Weigel, M. Mertig, J. Opitz, U. Queitsch, S. Diez, B. Lincoln, F. Wottawah, S. Schinkinger, J. Guck, J. Kaes, J. Smolinski, K. Salchert, C. Werner, C. Duschl, M.S. Jaeger, K. Uhlig, P. Geggier, and S. Howitz. The microscopy cell (miccell), a versatile modular flowthrough system for cell biology, biomaterial research, and nanotechnology. *Microfluid Nanofluid*, pages 21–36, 2006.

[36] K. Salchert, U. Streller, T. Pompe, N. Herold, M. Grimmer, and C. Werner. In vitro reconstitution of fibrillar collagen type i assemblies at reactive polymer surfaces. *Biomacromolecules*, 5(4):1340–1350, July 2004.

[37] S.L. Voytik-Harbin, B. Rajwa, and J.P. Robinson. Three-dimensional imaging of extracellular matrix and extracellular matrix-cell interactions. *Methods in Cell Biology, Vol 63*, 63:583–+, 2001.

[38] Andreas Hermann, Regina Gastl, Stefan Liebau, M. Oana Popa, Jörg Fiedler, Bernhard O Boehm, Martina Maisel, Holger Lerche, Johannes Schwarz, Rolf Brenner, and Alexander Storch. Efficient generation of neural stem cell-like cells from adult human bone marrow stromal cells. *J Cell Sci*, 117(Pt 19):4411–4422, Sep 2004.

[39] T. Ebendal. The relative roles of contact inhibition and contact guidance in orientation of axons extending on aligned collagen fibrils in vitro. *Exp Cell Res*, 98(1):159–169, Mar 1976.

[40] G.A. Dunn and T. Ebendal. Contact guidance on oriented collagen gels. *Exp Cell Res*, 111(2):475–479, February 1978.

[41] T. Ebendal. Extracellular matrix fibrils and cell contacts in the chick embryo. possible roles in orientation of cell migration and axon extension. *Cell Tissue Res*, 175(4):439–458, Jan 1977.

[42] P. Clark, P. Connolly, A. S. Curtis, J. A. Dow, and C. D. Wilkinson. Cell guidance by ultrafine topography in vitro. *J Cell Sci*, 99 (Pt 1):73–77, May 1991.

[43] A. Rajnicek, S. Britland, and C. McCaig. Contact guidance of cns neurites on grooved

quartz: influence of groove dimensions, neuronal age and cell type. *J.Cell Sci.*, 110 (Pt 23):2905–2913, December 1997.

[44] B. K. Mueller. Growth cone guidance: first steps towards a deeper understanding. *Annu Rev Neurosci*, 22:351–388, 1999.

[45] Matthew D Bender, Jennifer M Bennett, Rebecca L Waddell, John S Doctor, and Kacey G Marra. Multi-channeled biodegradable polymer/cultispher composite nerve guides. *Biomaterials*, 25(7-8):1269–1278, 2004.

[46] Soichiro Itoh, Kazuo Takakuda, Sigenori Kawabata, Yu Aso, Kanae Kasai, Hiroshi Itoh, and Kenichi Shinomiya. Evaluation of cross-linking procedures of collagen tubes used in peripheral nerve repair. *Biomaterials*, 23(23):4475–4481, Dec 2002.

[47] Z. C C Chen, A. K. Ekaputra, K. Gauthaman, P. G. Adaikan, H. Yu, and D. W. Hutmacher. In vitro and in vivo analysis of co-electrospun scaffolds made of medical grade poly(epsilon-caprolactone) and porcine collagen. *J Biomater Sci Polym Ed*, 19(5):693–707, 2008.

[48] N-T. Dai, M. R. Williamson, N. Khammo, E. F. Adams, and A. G A Coombes. Composite cell support membranes based on collagen and polycaprolactone for tissue engineering of skin. *Biomaterials*, 25(18):4263–4271, Aug 2004.

[49] Jose Gerardo-Nava, Tobias Führmann, Kristina Klinkhammer, Nadine Seiler, Jörg Mey, Doris Klee, Martin Möller, Paul D Dalton, and Gary A Brook. Human neural cell interactions with orientated electrospun nanofibers in vitro. *Nanomed*, 4(1):11–30, Jan 2009.

[50] Ravi V Bellamkonda. Peripheral nerve regeneration: an opinion on channels, scaffolds and anisotropy. *Biomaterials*, 27(19):3515–3518, Jul 2006.

[51] H. J. Gamble and R. A. Eames. An electron microscope study of the connective tissues of human peripheral nerve. *J Anat*, 98:655–663, Oct 1964.

[52] P.K. Thomas. *Microscopic anatomy of the peripheral nervous system.* W.B. Sanders, 1993.

Appendix D

Cellulose hollow fiber membranes containing longitudinally aligned collagen for nervous tissue guidance

1 Introduction

Regeneration of nervous tissue is complicated due to the lack of guidance materials to reconnect nerves to the distal targets and inhibitory effects (inflammatory processes/scar formation) impeding targeted cellular re-growth. Regeneration of spinal cord injury is even more complicated and up to now there is no treatment available to restore nerve function [1] Thus, recent bioengineering efforts focus on developing bridging materials and creating permissive environments to support and improve tissue regeneration. It is commonly accepted that physical guidance is an essential element and vital component for regeneration of nerve injury. In the last years tubular scaffolds, the so-called guidance conduits, have been used to bridge gaps at lesion sites and to physically guide tissue repair [1]. These guidance conduits provide global direction to regenerating axons and prevent their escape into neighbouring tissue. However, they do not ensure local direction of axons and cells within the tube. Hence, guidance channels or fibres frequently from synthetic materials have been incorporated that are aligned along the longitudinal axis within the tube to improve tissue regeneration [2]. However, recent research has demonstrated that physical guidance as well as biochemical signals are critical for nerve regeneration [3].

Thus, recent advanced approaches aimed at the incorporation of multiple cues in form of longitudinally aligned fibers and biochemical factors that promote regeneration. For example, tubes containing aligned electrospun fibers that encapsulate human glial cell-derived neurotrophic factor have been fabricated [4]. Alternatively, aligned ECM components have been inserted inside tubular scaffolds such as poly(glycolic acid)-collagen conduits filled with collagen fibers (diameter 50µm) [5] or silicone tubes filled with a magnetically aligned collagen gel (thickness 4mm) [6] to enhance nerve regeneration. However, recent studies emphasized the need to control nanotopographies for optimal nerve repair. Hence combining nanoscale features and the integration of ECM molecules into the conduit design is likely to prove most rewarding.

Here, we introduce a new method to fabricate guidance conduits containing longitudinally aligned collagen fibrils using our recently published shear-flow technique [7]. Cellulose is a widely used biomaterial that has been employed as membrane for hemodialysis, cellulose sponges for cartilage tissue engineering, and temporal skin replacement applications [8]. It was the material of choice for our conduits due to its desirable properties including biocompatibility, sterilizability and their unique mechanical characteristics showing high resistance against mechanical stress allowing for an advanced processing into tubular structures. We used commercially available hollow fiber membranes allowing for nutrient supply /removal of metabolites via the wall of the tubular structure. The interior sides of the membrane tubes were chemically modified to enable covalent attachment of aligned collagen fibrils (for details see methods section). Further, our aligned scaffold was extended to provide also biochemical signals to the incorporated

cells. Therefore we incorporated the highly negative charged glycosaminoglycan heparin [9] well known for its ability to reversible bind and release various growth factors (e.g FGF-2, VEGF). Axolotl tail spinal cord derived neurospheres were cultured inside these tubes in order to verify the applicability of these new conduits to support spinal cord regeneration.

2 Materials and Methods

2.1 Streaming setup

In order to enable a leakage-free and continuous streaming process, cellulose hollow fiber membranes were embedded inside transparent polytetrafluorethylen (PTFE) tubings (Figure 1). Briefly, a dry cellulose hollow fiber membrane (Membrana GmbH, Wuppertal) (length 12 cm; inner diameter 200 µm) was carefully drawn through PTFE tubing (length 8 cm; inner diameter 750 µm) to protrude 2 cm on both sides. For sealing, liquid PDMS was applied to the open spaces between PTFE tube and cellulose capillary at both ends and dried at 120°C for 20 min. Afterwards, the ends were cut with a scalpel to achieve an even cut surface with an embedded open capillary. The PTFE tube with the embedded capillary was then connected to a syringe installed via luer-lock fittings (Nordantec) and installed on a syringe pump (KDS, Holliston, USA) to enable a continuous and controlled streaming process.

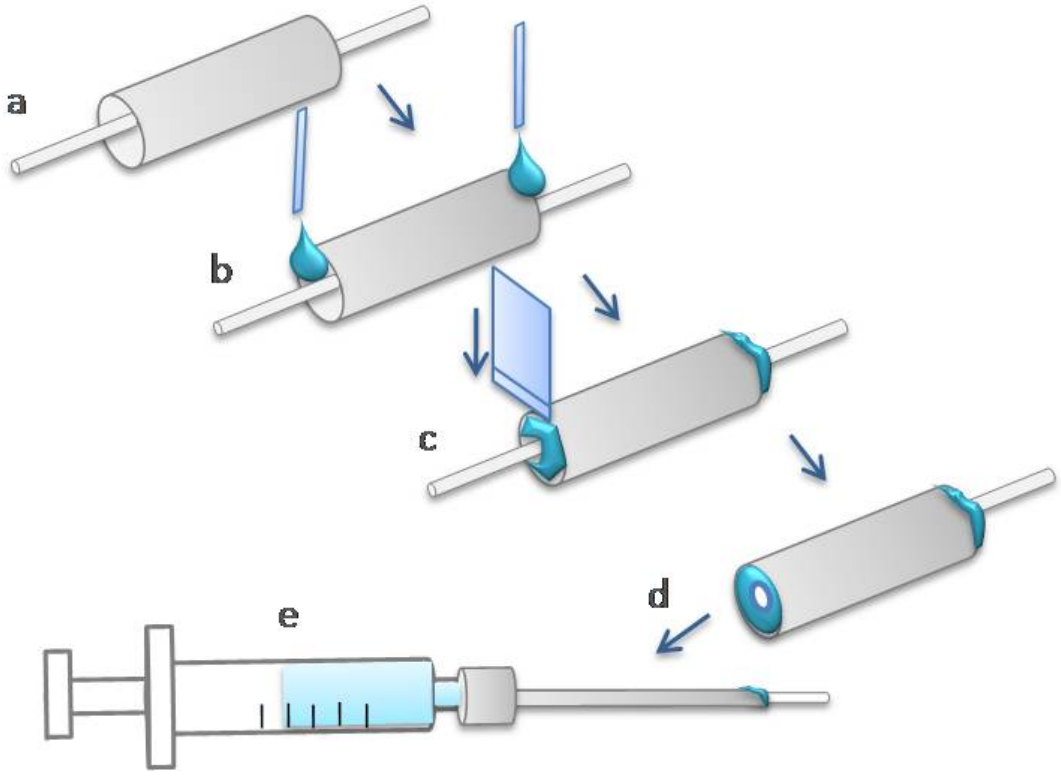

Figure 1: Procedure to embed cellulose hollow fiber membranes in a PTFE tube to enable a controlled and continuous streaming process.

2.2 Flow conditions

Experiments were performed under conditions of laminar flow. In all experiments the Reynolds number (as a criterion for laminar flow) was smaller than 1 and a flow rate of 4 µl/min corresponding to a wall shear rate of 85 s^{-1} was applied.

2.3 Activation of cellulose

To introduce functional groups cellulose was partially oxidized with 2,2,6,6-tetramethylpiperidine-1-oxyl radical (TEMPO) leading to the preferential conversion of the C6-atom of the anhydroglucose unit (AGU) into carboxylic acid groups [10]. The latter will be activated using 1-Ethyl-3-(3-dimethylaminopropyl) carbodiimide (EDC) and N-hydroxysulfosuccinimide (Sulfo NHS) to enable the reaction with amino groups of the collagen molecule (lysin side chains) to form amide bonds. For cellulose oxidation the hollow membranes were filled with water (100 mL) containing TEMPO (0.016 g, 0.1 mmol), sodium bromide (0.1 g, 1 mmol) and NaClO solution (2.5 mmol, 0.19g) for 30 min. The pH was maintained at pH = 10 by adding 0.5 M NaOH controlled by a pH-meter until no NaOH consumption was observed. The sodium carboxylate groups in the TEMPO-oxidized celluloses were subsequently converted to free carboxyl ones by ion-exchange treatment. Therefore the hollow fiber membranes were rinsed with buffer (1/15 M phosphate buffer, pH 5, potassium dihydrogen phosphate, monosodium phosphate) followed by the injection of the activation solution (50mM EDC, 25 mM Sulfo NHS dissolved in buffer (1/15 M phosphate buffer, pH 5, potassium dihydrogen phosphate, monosodium phosphate)). After activation for 45 min at 4°C the membranes were rinsed with PBS followed by immediate streaming of the collagen solution for deposition of aligned fibrils.

2.4 Preparation of collagen solution

To prepare the collagen solution (1.6 mg/ml), bovine dermal collagen I (purified and pepsin-solubilized in 0.012 N HCl, PureCol, Inamed, Milmont Drive, USA,) was brought to physiological pH by mixing eight parts acidified collagen solution (3.0 mg/ml) with one part 10-fold concentrated phosphate buffered saline (PBS, Sigma, Steinheim, Germany) and one part 0.1 M NaOH. To visualize collagen fibrils FITC-labelled collagen was added to yield a portion of 2.5% in the collagen solution. All components were kept on ice before and after mixing. Appropriate volumes of chilled 1x PBS were added to adjust the final concentration of the collagen solution.

2.5 Coating with collagen

Coating of the cellulose capillary with aligned collagen fibrils was performed by placing the experimental setup into an oven at 37°C. The freshly prepared collagen solution was streamed through the cellulose hollow fiber membranes at constant flow rate of 4 µl/min for 45 min. In a subsequent washing step with PBS (5 min, same flow rate) unbound collagen fibrils were flushed away. Functionalized matrices with heparin were produced by subsequent streaming of a heparin/PBS solution (2 mg/ml, FITC labelled heparin was added 1:40). After final PBS

washing the cellulose hollow fiber membranes were carefully withdrawn from the PTFE tubes using tweezers and stored in PBS/Pen Strep. For non-aligned collagen coated hollow fiber membranes, cellulose hollow fiber membranes were filled with a diluted collagen solution (0.1 mg/ml) in HCL for 1h and afterwards rinsed with PBS. Non-treated cellulose hollow fiber membranes served as control.

2.6 Microscopy

The hollow fiber membranes coated with FITC-labelled collagen and heparin were imaged by 3D imaging using a confocal laser scanning microscope (TCS SP 5, Leica, Bensheim, Germany) and by epifluorescence microscopy (Olympus BX 61).

2.7 Cell culture experiments

Cell culture experiments were carried out in collaboration with the Tanaka Group of the Max Planck Institute for Cell biology and Genetics, Dresden following a protocol to culture axolotl spinal cord neurospheres in cellulose hollow fiber membranes. Neurospheres were obtained by dissociation of axolotl tail spinal cord and subsequent cultivation in suspension. Spheroids were drawn inside the hollow fiber membranes via a pipette and cultured for a minimum of 7 days.

3 Results and Discussion

The aim of this study was the formation of longitudinally aligned collagen matrices deposited to the interior side of cellulose hollow fiber membranes. To achieve this, a collagen solution was streamed through the cellulose hollow fiber membranes at a constant flow rate. In order to enable continuous and controlled streaming, cellulose hollow fiber membranes were sealed within PTFE tubes in an embedding procedure (Figure1). Prior to deposition of collagen, cellulose was oxidised and subsequently activated to improve collagen immobilization by reaction of the activated carboxyl groups to the amino groups of collagen. Immediately afterwards the matrices were created by streaming a collagen solution through the embedded cellulose hollow fiber membranes by means of a syringe pump according to the recently published method to align collagen fibrils on planar surfaces (Lanfer 2008). In order to detect the resultant collagen fibrils FITC-labeled collagen was added to the collagen solution. Streaming of a 1.6 mg/ml collagen solution through activated cellulose hollow fiber membranes resulted in a homogenous layer of aligned collagen fibrils longitudinally aligned at the interior side of the cellulose tubes (Figure2 A,B).

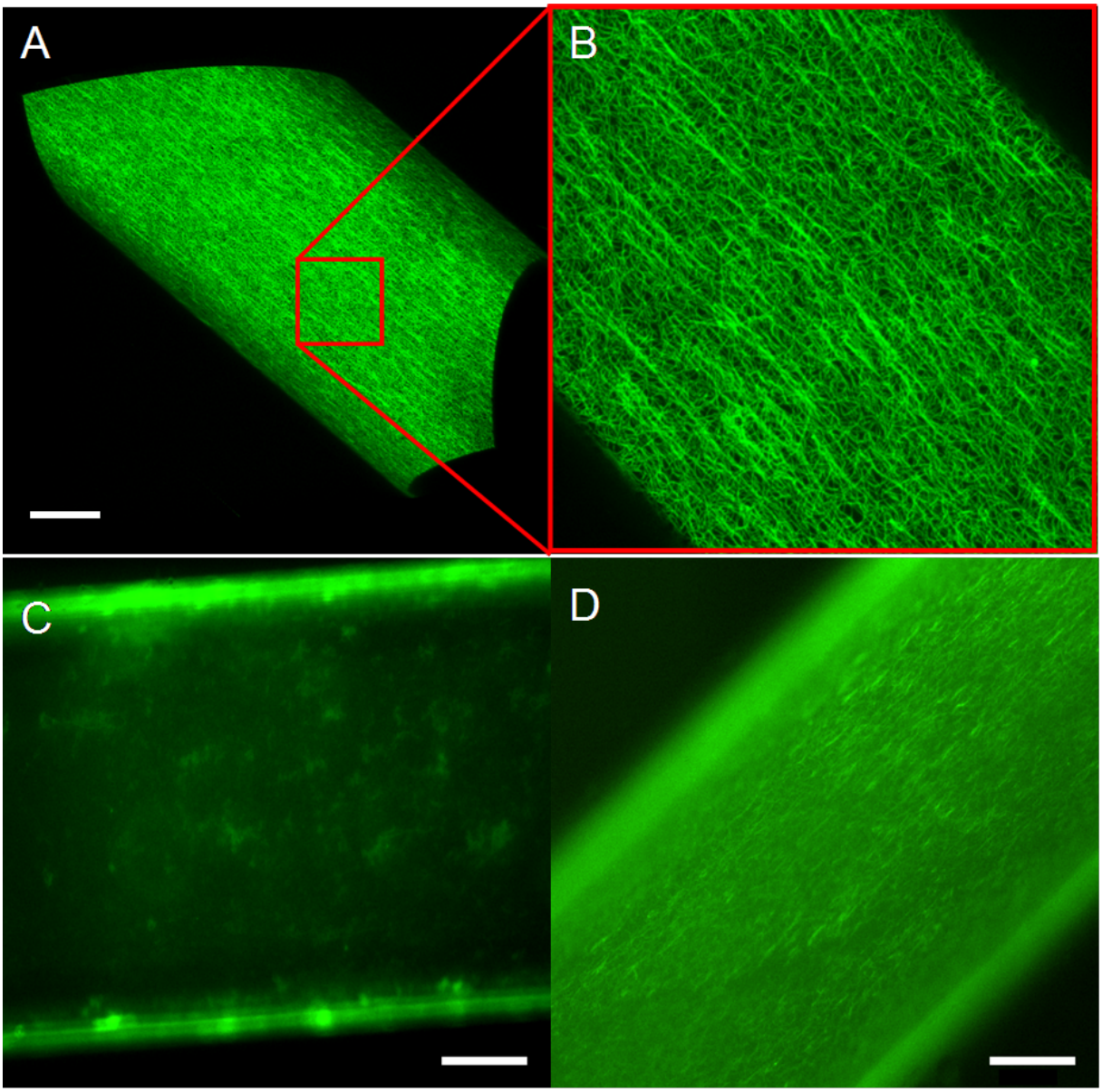

Figure 2: Cellulose hollow fibre membranes coated with collagen. Interior sides of the membranes are coated with (A,B) well-aligned FITC-labelled collagen fibrils consistently aligned along the entire length and width of the hollow fiber membrane (scale bar 50µm), (C) irregular structures of collagen coils; (D) aligned collagen fibrils decorated with FITC-labelled heparin (scale bar 65µm).

In most cases, collagen fibril coverage was constant along the entire length (length 8 cm) and the inner diameter of the cellulose membrane. However, in some membranes, aggregates had formed and collagen deposition was highly reduced (Figure 2C). In order to detect whether the cellulose activation process influenced collagen immobilization, streaming experiments with non-treated cellulose membranes were performed. The quality of the resultant matrices in terms of consistency and fibril alignment varied remarkably from batch to batch ranging from non-coated membranes to well-deposited matrices. Thus, it is currently not clear whether the technical setup or/and the collagen solution as such are responsible for this variation of reproducibility.

The activation process appeared to improve collagen binding however the nature of interaction is yet not fully clarified. Further experiments are necessary to optimize the activation process (e.g. by changing the pH of the activation solution to pH 8 and minimization of PBS rinsing time before collagen streaming) and the technical setup (better homogenization/ pre treatment of the collagen solution) in order to rule out possible artefacts during the streaming process and therefore improve the overall reliability of the process.

The collagen matrices deposited inside the membranes closely resemble those characterized on planar substrates regarding fibril length and density [7]. Thus, it can be expected that fibril length and density can be tuned as described previously [7] by varying process-relevant parameters such as collagen solution concentration. This is highly intriguing for future cell culture experiments since it would allow to modify the matrices according to the cell type of interest. The 20-100 nm diameter fibrils in our matrices are comparable to the 30 – 110 nm fibrils found in the endoneurium that surrounds axons and thereby guides neurite migration [11]. Thus, we established a system that resembles the structural architecture of nerve ECM found *in vivo*. In an effort to mimic native ECM structures more closely and to enable growth factor binding, we functionalized the aligned matrices with heparin. Heparin is known to mediate protein binding and bind growth factors relevant for nervous tissue regeneration. The aligned matrices were first reconstituted, and then a heparin/PBS solution (2mg/ml) was subsequently streamed across. Fluorescent micrographs revealed that FITC-labelled heparin is co-localized with the corresponding fibrillar matrices indicating that this 1-step functionalizing process decorated most of the collagen fibrils with heparin (Figure 2D). Thus, our method enables the study of multiple biochemical and physical cues in a single set-up and provides a versatile cell culture platform that can be tailored as needed.

In order to test the applicability of the novel conduits for neural tissue engineering axolotl spinal cord derived-neurospheres were chosen as cell culture system. The neurospheres were cultured in cellulose membranes (2 hollow fiber membranes for each condition: aligned collagen, non-aligned (tropo-)collagen, non-coated) for 7 days to assess cell viability, adhesion and proliferation. It appeared that in tubes coated with collagen (both aligned and non-aligned) neurospheres adhered immediately after insertion (Figure3AB). When compared to non-coated membranes, cell adhesion occurred more rapidly. Moreover, cells appeared to proliferate faster on collagen-coated tubes than on non-coated ones. These preliminary data show that the presence of collagen seems to have a stimulating effect on spinal cord-derived neurospheres. In further experiments we aim to investigate the influence of aligned fibrils in comparison to non-aligned collagen in more detail.

4 Conclusion

Within this study we showed the fabrication of a guidance conduit containing aligned fibrillar guidance cues that can be used in neural tissue engineering applications. Using our recently developed shear flow method, we demonstrated the deposition of longitudinally aligned collagen to the interior walls of cellulose membranes and the subsequent functionalization with heparin. Our

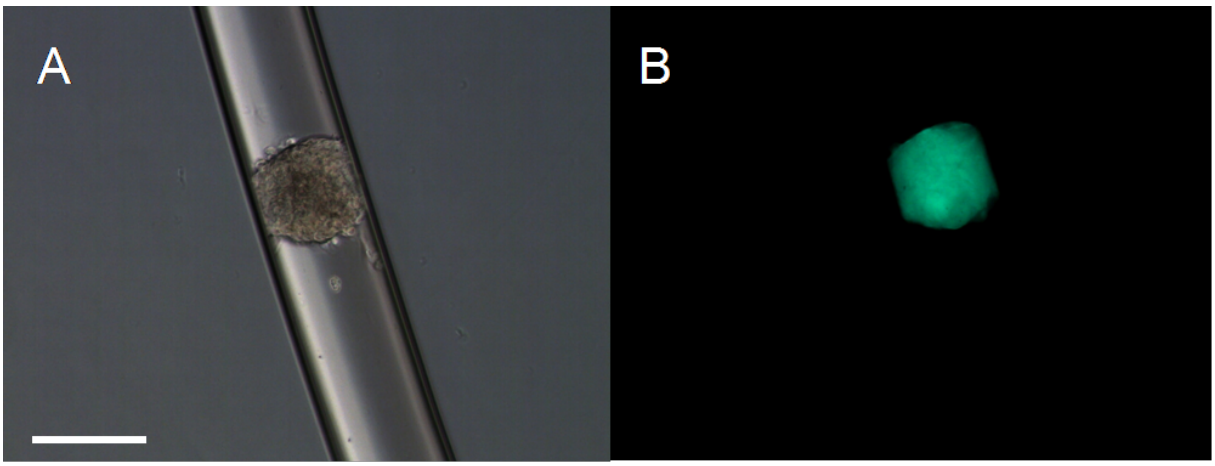

Figure 3: Phase contrast (A) and fluorescent image (B) of GFP-expressing axolotl spinal cord neurospheres cultured in collagen-coated cellulose tubes for 7 days (scale bar 200 µm).

first cell culture experiments showed that the tubes coated with aligned collagen well supported viability and adherence of spinal cord-derived neurospheres. This study provides a strategy to fabricate advanced guidance conduits combining aligned structural and biochemical cues in one system to be utilized for nervous tissue regeneration.

References

[1] C.E. Schmidt and J.B. Leach. Neural tissue engineering: strategies for repair and regeneration. *Annu Rev Biomed Eng*, 5:293–347, 2003.

[2] Li Yao, Norah O'Brien, Anthony Windebank, and Abhay Pandit. Orienting neurite growth in electrospun fibrous neural conduits. *J Biomed Mater Res B Appl Biomater*, 90(2):483–491, Aug 2009.

[3] J.B. Recknor, D.S. Sakaguchi, and S.K. Mallapragada. Directed growth and selective differentiation of neural progenitor cells on micropatterned polymer substrates. *Biomaterials*, 27(22):4098–4108, August 2006.

[4] Sing Yian Chew, Ruifa Mi, Ahmet Hoke, and Kam W Leong. Aligned protein-polymer composite fibers enhance nerve regeneration: A potential tissue-engineering platform. *Adv Funct Mater*, 17(8):1288–1296, 2007.

[5] K. Matsumoto, K. Ohnishi, T. Kiyotani, T. Sekine, H. Ueda, T. Nakamura, K. Endo, and Y. Shimizu. Peripheral nerve regeneration across an 80-mm gap bridged by a polyglycolic acid (pga)-collagen tube filled with laminin-coated collagen fibers: a histological and electrophysiological evaluation of regenerated nerves. *Brain Res*, 868(2):315–328, Jun 2000.

[6] D. Ceballos, X. Navarro, N. Dubey, G. Wendelschafer-Crabb, W.R. Kennedy, and R.T. Tranquillo. Magnetically aligned collagen gel filling a collagen nerve guide improves peripheral nerve regeneration. *Exp Neurol.*, 158(2):290–300, August 1999.

[7] B. Lanfer, U. Freudenberg, R. Zimmermann, D. Stamov, V. Korber, and C. Werner. Aligned fibrillar collagen matrices obtained by shear flow deposition. *Biomaterials*, 29(28):3888–3895, October 2008.

[8] Dieter Klemm, Brigitte Heublein, Hans-Peter Fink, and Andreas Bohn. Cellulose: fascinating biopolymer and sustainable raw material. *Angew Chem Int Ed Engl*, 44(22):3358–3393, May 2005.

[9] Babette Lanfer, Friedrich P Seib, Uwe Freudenberg, Dimitar Stamov, Thomas Bley, Martin Bornhäuser, and Carsten Werner. The growth and differentiation of mesenchymal stem and progenitor cells cultured on aligned collagen matrices. *Biomaterials*, 30(30):5950–5958, Oct 2009.

[10] Tsuguyuki Saito, Satoshi Kimura, Yoshiharu Nishiyama, and Akira Isogai. Cellulose nanofibers prepared by tempo-mediated oxidation of native cellulose. *Biomacromolecules*, 8(8):2485–2491, Aug 2007.

[11] H. J. Gamble and R. A. Eames. An electron microscope study of the connective tissues of human peripheral nerve. *J Anat*, 98:655–663, Oct 1964.

Publikationsliste

Veröffentlichungen in Fachzeitschriften

Lanfer B., Freudenberg U., Zimmermann R., Stamov D., Körber V., Werner C. Aligned fibrillar collagen matrices obtained by shear flow deposition. *Biomaterials.* 2008, 29, 3888-3895.

Lanfer B., Seib F.P., Freudenberg U., Stamov D., Bley T., Bornhäuser M., Werner C. The growth and differentiation of mesenchymal stem and progenitor cells cultured on aligned collagen matrices. *Biomaterials.* 30 (2009) 5950–5958.

Lanfer B., Hermann A., Kirsch M., Freudenberg U., Reuner U., Werner C. and Storch A. Directed Growth of Adult Human White Matter Stem Cell-derived Neurons on Aligned Fibrillar Collagen. Accepted for publication in *Tissue Engineering Part A* 2009.

Seib F.P., **Lanfer B.**, Bornhäuser M., Werner C. Enhanced biological activity of extracellular matrixassociated BMP-2. Accepted for publication in *Journal of Tissue Engineering and Regenerative Medicine* 2009.

Vorträge

Lanfer B.: Orientation and directional movement of stem cells on aligned fibrillar collagen. Max Bergmann Symposium 2008, Max Bergmann Zentrum Dresden, Dresden, 2008.

Poster

Lanfer B., Freudenberg U., Zimmermann R. , Hermann A. , Storch A., Werner C. Aligned Fibrillar Collagen Matrices Produced by Shear Flow Deposition. 8^{th} World Biomaterial Conference, Amsterdam, Netherlands, 2008.

Lanfer B., Freudenberg U., Zimmermann R., Hermann A., Storch A., Werner C. Aligned Fibrillar Collagen Matrices to Guide Neural Stem Cells. 2^{nd} International Congress on Stem Cells and Tissue Formation. Dresden, Germany, 2008.

Lanfer B., Seib F. P., Freudenberg U., Hermann A., Kirsch M., Storch A., Werner C. Stem Cell Behavior on Aligned Extracellular Matrix Structures. $3rd$ CRTD Summer Conference on Regenerative Medicine. Dresden, Germany, 2009.

Lanfer B., Seib F. P, Hermann A., Kirsch M., Freudenberg U., Storch A., Werner C.. Directed Growth of Stem Cells on Aligned Fibrillar Collagen. 22^{nd} European Conference on Biomaterials. Lausanne, Switzerland, 2009.

Selbständigkeitserklärung

Hiermit versichere ich, dass ich die vorliegende Arbeit ohne unzulässige Hilfe Dritter und ohne Benutzung anderer als der angegebenen Hilfsmittel angefertigt habe; die aus fremden Quellen direkt oder indirekt übernommenen Gedanken sind als solche kenntlich gemacht.

Bei der Auswahl und Auswertung des Materials sowie bei der Herstellung des Manuskripts habe ich Unterstützungsleistungen von folgenden Personen erhalten:

- Prof. Dr. Carsten Werner
- Dr. Philipp Seib
- Dr. Uwe Freudenberg

Weitere Personen waren an der geistigen Herstellung der vorliegenden Arbeit nicht beteiligt. Insbesondere habe ich nicht die Hilfe eines kommerziellen Promotionsberaters in Anspruch genommen. Dritte haben von mir keine geldwerten Leistungen für Arbeiten erhalten, die in Zusammenhang mit dem Inhalt der vorgelegten Dissertation stehen. Die Arbeit wurde bisher weder im Inland noch im Ausland in gleicher oder ähnlicher Form einer anderen Prüfungsbehörde vorgelegt und ist auch noch nicht veröffentlicht worden.

Die Promotionsordnung der Fakultät Maschinenwesen der Technischen Universität Dresden vom 1. Juli 2001 erkenne ich hiermit an.

Dresden, den

Babette Lanfer